QUANTUM STATES PREPARATION IN CAVITY OPTOMECHANICS

A Dissertation

by

WENCHAO GE

Submitted to the Office of Graduate and Professional Studies of
Texas A&M University
in partial fulfillment of the requirements for the degree of

DOCTOR OF PHILOSOPHY

Chair of Committee,	M. Suhail Zubairy
Committee Members,	George W. Kattawar
	Alexei Sokolov
	Andreas Klappenecker
Head of Department,	George R. Welch

December 2015

Major Subject: Physics

ABSTRACT

Quantum entanglement and quantum superposition are fundamental properties of quantum mechanics, which underline quantum information and quantum computation. Preparing quantum states in the macroscopic level is both conceptually interesting for extending quantum physics to a broader sense and fundamentally important for testing the validity of quantum mechanics. In this dissertation, schemes of preparing macroscopic entanglement and macroscopic superposition states in cavity optomechanics are studied using the unitary evolution method in the nonlinear regime or Lyapunov equation in the linearized regime. Quantum entanglement and quantum superposition states can be realized using experimentally feasible parameters with the proposals in this dissertation.

Firstly, a scheme of entangling two movable end mirrors in a Fabry-Perot cavity that are coupled to a common single photon superposition state is studied. It is shown that strong entanglement can be obtained either in the single-photon strong coupling regime deterministically or in the single-photon weak coupling regime conditionally.

Secondly, a scheme of entangling two movable end mirrors, that are coupled to two-mode entangled fields generated from a correlated-emission laser is investigated. By tuning the input driving laser frequencies at the Stokes sidebands of the cavity, the radiation-pressure coupling can be linearized as an effective beam-splitter-like interaction. Hence entanglement can be transferred from the two-mode fields to the two mechanical mirrors. Macroscopic entanglement between macroscopic mirrors persists at temperature $\sim$ 1K.

Thirdly, a scheme of creating macroscopic quantum superpositions of a mechanical mirror via periodically flipping a photonic qubit is proposed. Quantum super-

position states of a mechanical mirror can be obtained via the nonlinear radiation coupling with a single-photon superposition state. However, the difference between two superposed mechanical states is very small due to the weak single-photon coupling rate available in experiment. By periodically flipping the photonic qubit state, the difference can be magnified. It is shown in detail that this scheme is experimentally feasible under current technology.

To my wife Jing Xia

ACKNOWLEDGEMENTS

First of all, I would like to express my greatest appreciation to Dr. M. Suhail Zubairy for his patient guidance on my research and on my life. His physics intuition and sharp thinking inspired me throughout my PhD years. I would also like to thank all my committee members, Dr. George W. Kattawar, Dr. Alexei Sokolov, and Dr. Andreas Klappenecker, for their constructive comments on my study.

Second, I would like to thank my colleagues Dr. Sabine Wolk, Dr. Philip R. Hemmer, Dr. M. Al-Amri, and Dr. Hyunchul Nha, for their valuable discussions and fruitful collaborations. It has been a great pleasure to work with them and learn from them. I would like to extend my thanks to the department faculty for their instructions and the staff for their support.

Next, I am very grateful to our former and current group memebers, Dr. Keyu Xia, Dr. Li-gang Wang, Dr. Zhenghong Li, Dr. Xiaodong Zeng, Sheng-li Ma, Dr. Mehmet Emre Tasgin, Dr. Qingqing Sun, Dr. Shuai Yang, Dr. Zeyang Liao, Jabir Hakami, and Longfei fan. I am also very thankful to my friends Dr. Da-wei Wang, Dr. Xin Huang, Dr. Fuxiang Li, Dr. Zhao Wang, Dr. Shun Mao, Dr. Hua Zheng, Dr. Huawei Gao, Dr. Jing-han Chen, Hao Chen, Dingli Hu, Zhenhuan Yi, Han Cai and many more for their help and stimulating discussions during the past years.

Finally, I would like to thank my family for their love, faith, and support. I appreciate especially my wife Jing for her companion in a foreign country during my PhD study.

TABLE OF CONTENTS

Page

LIST OF FIGURES

I. INTRODUCTION

Quantum entanglement and quantum superposition are extraordinary phenomena of quantum mechanics, which have potential applications in quantum metrology [1], quantum information and quantum computation [2]. Entanglement and superposition states of microscopic objects have been demonstrated in systems of photons, atoms, and ions [3, 4, 5, 6, 7, 8]. Entanglement or superposition states of macroscopic objects remains a big challenge due to the fast decoherence of these objects [9]. Bring quantum entanglement or superposition to the macroscopic level [10] is not only of a conceptual interest, but also of a fundamental interest for testing novel decoherence models [11, 12, 13, 14, 15, 16].

Cavity optomechanics [17], which explores the nonlinear radiation-pressure coupling between electromagnetic wave and mechanical motion, provides a promising platform for generating quantum states of macroscopic objects. Quantum effects, such as normal-mode splitting between optical and mechanical modes [18, 19], optomechanically induced transparency [20, 21, 22], and squeezing of light [23, 24, 25], have been studied in cavity optomechanics. Quantum entanglement between a macroscopic mechanical oscillator and a cavity field has also been proposed [26, 27, 28] and demonstrated [29] in cavity optomechanics recently. It is an interesting question whether one can generate entanglement of two macroscopic objects. Schemes of entanglement generation of two micromechanical mirrors have been proposed theoretically, such as in two separate cavities by optomechanical coupling with two entangled output fields [30], in a double cavity driven by squeezed input fields [31], in a classically driven Fabry-Perot cavity [32], and by injecting broadband squeezed vacuum light and laser light into a cavity [33]. More recently, atomic coherence [34]

has been considered for generation of macroscopic entanglement in a doubly-resonant cavity [35].

Macroscopic quantum superposition states have also been studied in optomechanical systems using optically levitated dielectric particles [36, 37] or a massive mechanical mirror [26, 38, 39] recently. In the former, high quality vacuum is required to prepare quantum superposition states with well separated positions. In the latter, a strong single-photon optomechanical coupling rate, comparable to the mechanical oscillation frequency, is required to generate a macroscopic quantum superposition state. To increase the single-photon coupling rate, proposals [40, 41, 42, 43] of using collective optomechanical interactions have been considered. More recently, there have been several proposals to achieve macroscopic quantum superpositions in the single-photon weak coupling regime via conditioned postselection in nested interferometers [44] or strong displaced Fock states [45, 46].

In this dissertation, I will discuss several methods to generate macroscopic quantum states in cavity optomechanics and to overcome some of the difficulties in current technology. In Chapter II, theory of cavity optomechanics is reviewed and a simple scheme is discussed to generate deterministic entanglement between two movable end mirrors in a Fabry-Perot cavity. In Chapter III, a scheme to entangle two mechanical mirrors by their coupling to the two-mode fields of a correlated-emission laser inside a doubly resonant cavity is studied. Entanglement of end mirrors in a doubly resonant cavity is in relevant to the gravitational wave detection [47], such as in the Laser Interferometer Gravitational Wave Observatory (LIGO).

Quantum superposition states of a mechanical mirror can be obtained via the nonlinear radiation coupling with a superposition photonic state. However, the difference between two superposed mechanical states is very small due to the weak single-photon coupling rate available in experiment. To magnify this difference, I

propose a setup in a cavity optomechanical system via periodically flipping the photonic qubit to create macroscopic quantum superpositions of a mechanical mirror, as will be presented in Chapter IV. Finally, Chapter V summarizes the results of this dissertation.

II. ENTANGLEMENT OF TWO MECHANICAL MIRRORS WITH A SINGLE PHOTON SUPERPOSITION STATE*

Quantum entanglement is an important phenomenon in quantum physics, which has potential applications in quantum information and quantum computing [2]. Since the birth of quantum mechanics, the idea of entangling a microscopic object and a macroscopic object, the Schrodinger's cat state, drives people to push the limit of quantum mechanics towards the boundary between the quantum world and the classical world [4, 7, 8, 9]. Entanglement of microscopic objects has been realized experimentally in the systems of photons [3], atoms [5], and ions [6]. Due to fast decoherence of macroscopic objects [9], quantum entanglement of macroscopic objects remains a difficult task.

Cavity optomechanics [17], exploring the effect of radiation-pressure coupling between optical and mechanical elements, provides a platform for realizing quantum effects of macroscopic objects. Optomechanical sideband cooling on a mechanical oscillator [48, 49, 50, 51], normal-mode splitting between optical and mechanical modes [18, 19], optomechanically induced transparency [20, 21, 22], and entanglement between a mechanical oscillator and a cavity field [26, 27, 28, 29] have been proposed theoretically and demonstrated experimentally recently.

Many theoretical proposals have been put forward to generate entanglement between two mechanical oscillators in cavity optomechanics: either with coherent driving or without coherent driving. In the former case, entanglement of two mechanical oscillators can be generated using nonclassical states [30, 31, 33, 35]. Entanglement

*Reprinted with permission from "Entanglement of two movable mirrors with a single photon superposition state" by W. Ge and M. S. Zubairy, 2015. Phys. Scr., vol. 90, pp. 074015, Copyright [2015] by the Institute of Physics

can also be generated with classical driving fields in a cavity with two mechanical oscillators [32, 52, 53, 54], or in two remote optomechanical cavities [55, 56, 57]. More recently, ground-state cooling as well as optomechanical entanglement has been proposed in a double-resonant cavity via a correlated emission laser [34] with classical driving fields [58, 59]. By using coherent driving, optomechanical coupling is affected by the driving laser phase noise [60]. To avoid this problem, one may consider entangling two mechanical oscillators using a single photon without coherent driving. Entanglement of two mechanical mirrors in a two-cavity optomechanical system through the coupling of a single photon between cavities has been proposed [61].

In this chapter, we first review the theory of cavity optomechanics to formulate the relevant Hamiltonian and to obtain the quantum Langevin equations for the system operators. We then propose a simple setup for entangling two movable end mirrors in a Fabry-Perot cavity using a single photon state without any coherent driving. A similar scheme has been proposed [62] recently to generate heralded phonon Bell states with very weak coherent driving conditioned on detection of a single photon. Our proposal can generate deterministic entangled phonon states after measurement on the cavity photon state. A single-photon strong coupling rate [63, 64] may be required for our scheme to generate macroscopic entanglement. Two possible entangled states can be generated depending on the final measurement outcomes. The degree of entanglement of the generated states is quantified by logarithmic negativity and we derive an analytical expression of the negativity for each state. Our results show that the more probable of a state to be generated the smaller the negativity of the state it will be. We also discuss the experimental feasibility of our scheme.

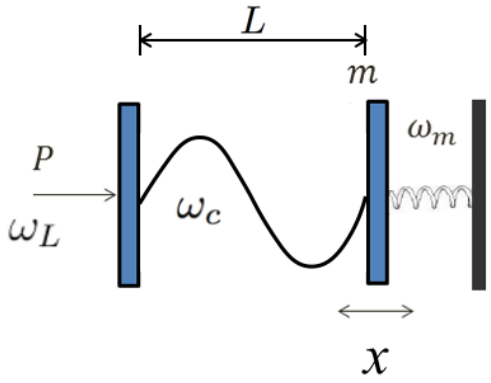

Figure 1: Interaction of a cavity field mode with a mechanical end mirror

II.A Theory of cavity optomechanics

Cavity optomechanics explores the radiation-pressure interaction between electromagnetic radiation and micromechanical motion inside a cavity. There are different types of cavities, such as a Fabry-Perot cavity, a whispering-gallery cavity, and a superconducting microwave circuit, which can interact with different kinds of mechanical objects, such as a suspended end mirror, a microtoroid, and a mechanical membrane. Despite assorted optomechanical systems, their theories are more or less the same.

II.A.1 The basic Hamiltonian

We consider the simplest model of cavity optomechanics, where a single mode optical field ω_c interacts with a suspended end mirror in a Fabry-Perot cavity as shown in Fig. II.A We also restrict our system such that one of the many mechanical modes of the mirror interacts with the single mode field ω_m. Before coupling the

optical field to the end mirror, the free Hamiltonian of the system is represented by

$$\mathcal{H}_0 = \hbar\omega_c c^\dagger c + \hbar\omega_m b^\dagger b, \tag{2.1}$$

where b and c are annihilation operators of the mirror mode and the cavity mode, respectively. When the optical field couples to the mirror, it exerts radiation pressure on the mirror and displaces it from its equilibrium position. Therefore, the cavity frequency, which depends on the cavity length L, is modulated by the mirror's position as $\omega_c(x) \approx \omega_c + \frac{\partial\omega_c}{\partial L}x$. Here $\omega_c = k\frac{\pi c}{L}$, k is the integer mode number, and x is the mirror's position. The interaction Hamiltonian

$$\begin{aligned} \mathcal{H}_1 &\approx \hbar(\omega_c(x) - \omega_c)c^\dagger c \\ &= -\hbar\frac{\omega_c}{L}c^\dagger c x \\ &= -\hbar g c^\dagger c(b^\dagger + b), \end{aligned} \tag{2.2}$$

where $g = (\omega_c/L)x_0$ is the single-photon coupling strength, $x = x_0(b^\dagger + b)$, and $x_0 = \sqrt{\hbar/2m\omega_m}$ is the zero-point fluctuation. Therefore, the basic Hamiltonian of a single-mode optical field interacts with a single-mode mechanical object is described by

$$\mathcal{H}_{\text{un}} = \mathcal{H}_0 + \mathcal{H}_1. \tag{2.3}$$

A more detailed derivation can be found in Ref. [65].

The exact solution of the field-mirror system is described by its unitary evolution operator, which can be obtained exactly using Baker-Campbell-Hausdorff formula as

[66] or using the expansion of time-evolution operator [67] (see Appendix A),

$$U_{\rm fm}(t) = e^{-i\omega_c t c^\dagger c} e^{i\phi(t)(c^\dagger c)^2} \mathcal{D}\left(\eta(t) c^\dagger c\right) e^{-i\omega_m t b^\dagger b}, \tag{2.4}$$

where $\phi(t) = \beta^2\left(\omega_m t - \sin(\omega_m t)\right)$, the displacement operator $\mathcal{D}(\alpha) = e^{\alpha b^\dagger - \alpha^* b}$, $\eta(t) = \beta(1 - e^{-i\omega_m t})$, and $\beta = g/\omega_m$. The first and the last terms in the product are the free evolution of the field and the mirror, respectively. The second term describes a Kerr-like effect of the cavity in the single-photon strong coupling regime [63, 64]. Due to the coupling between the mechanical mirror and the cavity field, the mirror is displaced by the operator $\mathcal{D}$ and the displacement is proportional to $\beta c^\dagger c$.

Now we consider the case when the cavity is driven by a strong external field. With the driving field, the total Hamiltonian of the system is described by

$$\mathcal{H} = \mathcal{H}_0 + \mathcal{H}_1 + \mathcal{H}_{\rm dr}, \tag{2.5}$$

where $\mathcal{H}_{\rm dr} = i\hbar E c^\dagger e^{-i\omega_L t} - i\hbar E^* c e^{i\omega_L t}$. Here $|E| = \sqrt{\frac{2P\kappa}{\hbar\omega_L}}$ is the driving strength with input power P, laser frequency ω_L, and cavity mode decay rate κ. In the rotating frame of the driving field frequency, the Hamiltonian is given by

$$\mathcal{H} = \hbar\Delta_c c^\dagger c + \hbar\omega_m b^\dagger b - \hbar g c^\dagger c(b^\dagger + b) + i\hbar E c^\dagger - i\hbar E^* c \tag{2.6}$$

In the presence of the strong driving field, the cavity field is displaced to a mean value $\alpha_s = \frac{E}{i\Delta_c - 2igq_s + \kappa}$ and the end mirror is displaced with a mean position $q_s = \beta|\alpha|^2$ (details of calculating the mean values are given the following section). Then we shift the operators $c \to \delta c + \alpha_s$ and $b \to \delta b + q_s$, and the Hamiltonian transforms

into

$$\mathcal{H}_{\text{lin}} = \hbar\Delta_c \delta c^\dagger \delta c + \hbar\omega_m \delta b^\dagger \delta b - \hbar g(\delta c^\dagger \delta c + \alpha_s \delta c^\dagger + \alpha_s^* \delta c)(\delta b^\dagger + \delta b), \tag{2.7}$$

where δb and δc are the fluctuation operators around the mean values in the shifted coordinates. For $|\alpha_s| \gg 1$, the second-order term $\delta c^\dagger \delta c$ can be neglected and the system is linearized under the strong driving field to a Jaynes-Cummings model as

$$\mathcal{H}_{\text{lin}} = \hbar\Delta_c \delta c^\dagger \delta c + \hbar\omega_m \delta b^\dagger \delta b - \hbar g(\alpha_s \delta c^\dagger + \alpha_s^* \delta c)(\delta b^\dagger + \delta b). \tag{2.8}$$

In the rotating-wave approximation [67], the interaction term in the above Hamiltonian can be written as $-\hbar g(\alpha_s \delta c^\dagger \delta b + \alpha_s^* \delta b^\dagger \delta c)$ or $-\hbar g(\alpha_s \delta b^\dagger \delta c^\dagger + \alpha_s^* \delta b \delta c)$ for red-detuned driving frequency ($\Delta_c = \omega_m$) or blue-detuned driving frequency ($\Delta_c = -\omega_m$), respectively. Examples will be shown in the following chapters.

II.A.2 Quantum Langevin equations

We have formed the basic Hamiltonian of field-mirror interaction in cavity optomechanics under an external driving field. Now we describe the system dynamics using quantum Langevin equations. The prototype of Langevin equation describes Brownian motion of a particle in a fluid in the form of

$$m\ddot{x} = -\gamma \dot{x} + \sqrt{2\gamma k_B T}\xi(t), \tag{2.9}$$

where γ is the damping rate, k_B is the Boltzmann constant, T is the temperature of the fluid, and $\xi(t)$ is the Brownian noise. The apparently random movement of the particle gives a steadily increasing mean deviation. The quantum Langevin equation is derived using Heisenberg equation with the assumption that a system is

linearly coupled a heat bath consisting of an assembly of harmonic oscillators. By substituting the variables of the heat bath, the quantum Langevin equation is given by the Heisenberg equation involving the system Hamiltonian plus a noise term from the heat bath. Considering the Hamiltonian $\mathcal{H}$ of the cavity optomechanical system described above, the quantum Langevin equations are obtained as

$$\begin{aligned} \dot{b} &= -(i\omega_m + \gamma_m)b + igc^\dagger c + \xi_b(t), \\ \dot{c} &= -(\kappa + i\Delta_c)c + igc(b^\dagger + b) + E + \xi_c(t), \end{aligned} \tag{2.10}$$

where $\xi_b(t)$ and $\xi_c(t)$ are quantum Brownian noises of the mirror's mode and the cavity mode, respectively, due to their coupling to their own heat bathes with $\langle \xi_b(t) \rangle = \langle \xi_c(t) \rangle = 0$. Here γ_m is the decay rate of the mirror's mode. In the limit of large mechanical quality-factor $Q_m = \omega_m/\gamma_m \gg 1$ [68], the noise of the mirror's mode is delta-correlated as

$$\langle \xi_b(t)\xi_b^\dagger(t') + \xi_b^\dagger(t')\xi_b(t) \rangle /2 \approx \gamma_m(2n+1)\delta(t-t'), \tag{2.11}$$

where $n_m = [\exp(\hbar\omega_m/k_BT) - 1]^{-1}$ denotes the average thermal phonon number. The quantum noise correlation of the cavity field mode depends on the property of the heat bath the cavity mode is coupled with.When the cavity mode is coupled to a thermal reservoir, the quantum noise of $\xi_c(t)$ is also a δ function in the Markovian limit, i. e.

$$\begin{aligned} \langle \xi_c^\dagger(t)\xi_c(t') \rangle &= \kappa n_c \delta(t-t'), \\ \langle \xi_c(t)\xi_c^\dagger(t') \rangle &= \kappa(n_c+1)\delta(t-t'), \end{aligned} \tag{2.12}$$

where $n_c = [\exp(\hbar\omega_c/k_BT) - 1]^{-1} \ll 1$ for optical frequency. With a strong driving field, the system is shifted to some mean values and the system dynamics is governed by the fluctuation operators around these mean values. The mean values α_s and q_s are obtained by averaging on Eq. (2.10) and taking the time derivative to be zero. The fluctuation operators satisfy the following quantum Langevin equations

$$\begin{aligned} \dot{\delta b} &= -(i\omega_m + \gamma_m)\delta b + ig(\alpha_s \delta c^\dagger + \alpha_s^* \delta c) + \xi_b(t), \\ \dot{\delta c} &= -(\kappa + i\Delta_c - 2igq_s)\delta c + ig\alpha_s(\delta b^\dagger + \delta b) + \xi_c(t). \end{aligned} \tag{2.13}$$

In the linearized quantum Langevin equations, we observe that with the help of external driving laser, the optomechanical coupling strength is multiplied by the number of mean photons α_s inside the cavity. The equations are coupled harmonic equations with extra noise terms coming from their own heat bathes. The fluctuation operators can be solved formally and their correlation values can be calculated accordingly. I will come up with an example in Chapter IV on calculating the correlation values.

II.B The scheme for entangling two end mirrors

Now we study a simple scheme to entangle two end mirrors in a cavity without a coherent driving field. We consider a Fabry-Perot cavity with two mechanical end mirrors of masses m_1, m_2 and mechanical frequencies $\omega_{m_1}, \omega_{m_2}$ as shown in Fig. 2. These mirrors can be suspended from the ground or attached to cantilevers [17] and we assume only single mode of each mirror is involved in the field-mirror interaction. According to the theory of cavity optomechanics introduced in the previous section, the cavity frequency, which depends on the cavity length L, is modulated by both the mirrors positions, x_1 and x_2, as $\omega_c(\delta x) \approx \omega_c + \frac{\partial \omega_c}{\partial L}(x_1 - x_2)$. The Hamiltonian of

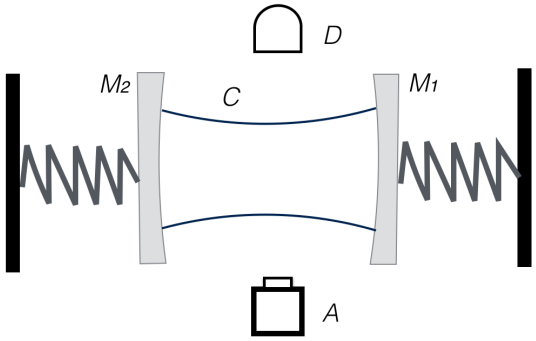

Figure 2: Experimental setup for entangling two macroscopic mechanical end mirrors M_1 and M_2. Single-photon superposition state is prepared in the cavity C by sending a superposition atomic state from the single-atom source A. After the evolution of the field and the mirrors, another atom in the ground state is sent from A to the cavity. The atomic state is then rotated with a fast $\pi/2$ pulse before detected at the detector D. The state of the mirrors then collapses into an entangled state after the detection of the atomic state.

the system is then given by

$$\mathcal{H} = \hbar\omega_c c^\dagger c + \sum_{j=1,2} \hbar\omega_{m_j} b_j^\dagger b_j + \hbar\frac{\omega_c}{L} c^\dagger c(x_2 - x_1), \tag{2.14}$$

where b_j and c are annihilation operators of the j's mirror and the cavity mode, respectively, $x_j = x_{0_j}(b_j^\dagger + b_j)$ and $x_{0_j} = \sqrt{\hbar/2m_j\omega_{m_j}}$ is the zero-point fluctuation of the j's mirror. This scheme is simpler than that in Ref. [61] where two coupled cavities are considered.

Similarly to the case of a cavity mode coupled to a single mechanical mode, it is straightforward to derive the unitary evolution operator of the system consisting of one cavity field coupled to two mechanical modes individually. The unitary operator

of the system is then given by

$$\begin{aligned} U(t) &= e^{-i\omega_c t c^\dagger c} e^{i\phi_1(t)(c^\dagger c)^2} \mathcal{D}_1\left(\eta_1(t) c^\dagger c\right) e^{-i\omega_{m_1} t b_1^\dagger b_1} \\ &\quad \times e^{i\phi_2(t)(c^\dagger c)^2} \mathcal{D}_2\left(-\eta_2(t) c^\dagger c\right) e^{-i\omega_{m_2} t b_2^\dagger b_2}, \end{aligned} \tag{2.15}$$

where $\phi_j(t) = \beta_j^2\left(\omega_{m_j} t - \sin(\omega_{m_j} t)\right)$, the displacement operator for the j's mirror $\mathcal{D}_j(\alpha) = e^{\alpha b_j^\dagger - \alpha^* b_j}$, and $\eta_j(t) = \beta_j(1 - e^{-i\omega_{m_j} t})$. Here $\beta_j = \frac{x_{0_j}\omega_c}{L\omega_{m_j}}$ which characterizes the ratio of the displacement of a single photon due to radiation pressure comparing to that of the mirror's zero-point fluctuation. The terms proportional to $(c^\dagger c)^2$ are effective Kerr-like terms of the cavity in the presence of mechanical mirrors. In the single-photon strong coupling regime when $\beta_j \gtrsim 1$, photon blockade effect can happen due to the Kerr-like terms [63, 64]. The argument $\eta_j(t) c^\dagger c$ in the displacement operator means that the displacement on each mirror is proportional to the photon number $c^\dagger c$ if the cavity field is initially prepared in a Fock state. Therefore, a superposition state of the cavity photon number can result in a superposition of displacement of the mechanical mirror [66].

II.C Entanglement generation

II.C.1 System evolution

We consider initially the mirrors are cooled to their ground states $|0\rangle_{m_j}$ via optomechanical cooling. A superposition state $|\psi_c\rangle = \frac{1}{\sqrt{2}}(|0\rangle_c + |1\rangle_c)$ is prepared inside the cavity. Due to the radiation pressure, the cavity photon state evolves together with the mechanical mirrors. The state of the system is given by

$$\begin{aligned} |\psi_s(t)\rangle &= U(t)|\psi_c\rangle|0\rangle_{m_1}|0\rangle_{m_2} \\ &= \frac{1}{\sqrt{2}}|0\rangle_c|0\rangle_{m_1}|0\rangle_{m_2} + \frac{1}{\sqrt{2}} e^{i2\phi(t)}|1\rangle_c|\eta(t)\rangle_{m_1}|-\eta(t)\rangle_{m_2}, \end{aligned} \tag{2.16}$$

where the mirrors' states $|\eta(t)\rangle_{m_1}$ and $|-\eta(t)\rangle_{m_2}$ are coherent states due to the radiation pressure of the single photon. Here we consider, for simplicity, $m_1 = m_2 = m$, $\omega_{m_1} = \omega_{m_2} = \omega_m$, $\phi_1(t) = \phi_2(t) = \phi(t)$ and $\eta_1(t) = \eta_2(t) = \eta(t)$. From the expression of $|\psi_s(t)\rangle$, the system of one cavity field and two-mechanical mirrors are entangled in general.

After integer number of the mirrors' oscillations $\tau_n = 2n\pi/\omega_m$, the system evolves to its initial state, namely $|\psi_s(\tau_n)\rangle = |\psi_s(0)\rangle$. There is no entanglement among the field and the mirrors. After half integer number of the mirrors' oscillation $\tau_{n+\frac{1}{2}} = (2n+1)\pi/\omega_m$, the displacement of the mirrors are largest where $|\psi_s(\tau_{n+\frac{1}{2}})\rangle = \frac{1}{\sqrt{2}}(|0\rangle_c|0\rangle_{m_1}|0\rangle_{m_2} + e^{i\theta_n}|1\rangle_c|2\beta\rangle_{m_1}|-2\beta\rangle_{m_2})$ with $\beta = \beta_1 = \beta_2$ and $\theta_n = 2\pi(2n+1)\beta^2$. In this case, the entanglement among the tripartite is the maximum.

To see whether there is entanglement between the mirrors due to radiation pressure only, we trace over the cavity field state. We obtain the mirrors' state as

$$\begin{aligned} \rho_m(t) &= \mathrm{Tr}\langle|\psi_s(t)\rangle\langle\psi_s(t)||\rangle \\ &= \frac{1}{2}\left(|0\rangle_{m_1}|0\rangle_{m_2}\langle 0|_{m_2}\langle 0|_{m_1}\right. \\ &+ \left.|\eta(t)\rangle_{m_1}|-\eta(t)\rangle_{m_2}\langle-\eta(t)|_{m_2}\langle\eta(t)|_{m_1}\right), \end{aligned} \tag{2.17}$$

which is a mixed and separable state.

II.C.2 Entanglement via measurement

Generation of entanglement of quantum objects, such as atoms [69] and superconducting qubits [70], have been considered by continuously monitoring the cavity field that interacts with these quantum objects. If no photon is detected outside the cavity, the system of the quantum objects is prepared in an entangled state. Here we show that by measuring the state of the field inside the cavity, the mirrors

collapse to an entangled state. Depending on the measurement result, there are two possible entangled states of the mirrors. We study the properties of each state in the following.

To measure the photon number state of the cavity, we first map the cavity field state to a flying two-level atom by interacting with each other for a π Rabi oscillation U_π. Then we apply a fast $\pi/2$ pulse $R_{\frac{\pi}{2}}$ on the atomic state such that $R_{\frac{\pi}{2}}|g\rangle_a = (|g\rangle_a + |e\rangle_a)/\sqrt{2}$ and $R_{\frac{\pi}{2}}|e\rangle_a = (-|g\rangle_a + |e\rangle_a)/\sqrt{2}$, where $|g\rangle_a$ ($|e\rangle_a$) is the ground (excited) state of the atom. This process is assumed to be much faster than the mirrors' oscillation frequency ω_m and the interaction time can be neglected. The system becomes

$$R_{\frac{\pi}{2}}U_\pi|\psi_s(\tau_{n+\frac{1}{2}})\rangle|g\rangle_a = \left(\sqrt{\mathcal{P}_-}|g\rangle_a|\psi_{m-}\rangle + \sqrt{\mathcal{P}_+}|e\rangle_a|\psi_{m+}\rangle\right)|0\rangle_c, \tag{2.18}$$

where

$$|\psi_{m\pm}\rangle = \frac{1}{\sqrt{4\mathcal{P}_\pm}}\left(|0\rangle_{m_1}|0\rangle_{m_2} \pm e^{i\theta_n}|2\beta\rangle_{m_1}|-2\beta\rangle_{m_2}\right), \tag{2.19}$$

and $\mathcal{P}_\pm = \frac{1}{2} \pm \frac{1}{2}\cos(\theta_n)e^{-4\beta^2}$. The state of the mirrors then collapse to the state $|\psi_{m_+}\rangle$ ($|\psi_{m_-}\rangle$) with probability $\mathcal{P}_+$ ($\mathcal{P}_-$) after we make a measurement on the atomic state and find the atom in the state $|e\rangle_a$ ($|g\rangle_a$). After the measurement the mirrors are disentangled with the atom and the cavity is in vacuum, therefore the entangled state of the mirrors is under free evolution.

For a single-photon strong coupling rate, i. e., $\beta \gtrsim 1$, ${}_{m_1}\langle 0|2\beta\rangle_{m_1} = {}_{m_2}\langle 0| - 2\beta\rangle_{m_2} = e^{-2\beta^2} \ll 1$. The two parts of the entangled states, $|0\rangle_{m_1}|0\rangle_{m_2}$ and $|2\beta\rangle_{m_1}|-2\beta\rangle_{m_2}$, are almost orthogonal to each other. Therefore, the entanglement is strong in this regime.

For a single-photon weak coupling rate, i. e., $\beta \ll 1$, $|\psi_{m+}\rangle \approx |0\rangle_{m_1}|0\rangle_{m_2} +$

$\beta(|1\rangle_{m_1}|0\rangle_{m_2} - |0\rangle_{m_1}|1\rangle_{m_2})$ with $\mathcal{P}_+ \approx 1 - 2\beta^2$ while $|\psi_{m-}\rangle \approx \frac{1}{\sqrt{2}}(|1\rangle_{m_1}|0\rangle_{m_2} - |0\rangle_{m_1}|1\rangle_{m_2})$ with $\mathcal{P}_- \approx 2\beta^2$. The two states $|\psi_{m_\pm}\rangle$ are almost orthogonal to each other. Although $\mathcal{P}_- \ll 1$, the state $|\psi_{m-}\rangle$ is a phonon Bell state [62] which is a strong entanglement state. Therefore, to realize the state $|\psi_{m-}\rangle$ in the weak single-photon coupling regime, one needs to repeat the experiment many times to get one measurement result of $|g\rangle_a$.

II.C.3 Entanglement quantification

II.C.3.1 Entanglement measure

We have shown for $\beta \gtrsim 1$, the entanglement for both states $|\psi_{m_\pm}\rangle$ is strong since the two parts in each state are nearly orthogonal. For $\beta \ll 1$, we have a low probability of $2\beta^2$ to obtain a strong entanglement. Now we quantify the degree of entanglement of our system in general using the logarithmic negativity [71]. A quantum state ρ of a bipartite system with two subsystems A and B is defined to be separable if and only if ρ can be written as

$$\rho = \sum_j p_j \rho_{jA} \otimes \rho_{jB}, \tag{2.20}$$

with $\sum_j p_j = 1$ and $0 \leq p_j \leq 1$. A number of entanglement measures [71, 72, 73, 74, 75, 76, 77] have been proposed based on the physicality of the partial transposed density operator ρ^{T_A}. The logarithmic negativity for a continuous variable bipartite system is defined as [71]

$$E_{\mathcal{N}}(\rho) \equiv \log_2 ||\rho^{T_A}||_1, \tag{2.21}$$

where $||\rho^{T_A}||_1$ is the trace norm of the partial transposed density operator ρ^{T_A}. The general expression of logarithmic negativity is cumbersome to calculate since the

density matrix has an infinite dimension as can be seen from Eq. (2.19). However, for any pure state $\rho = |\Phi\rangle\langle\Phi|$, the logarithmic negativity can be readily calculated as

$$E_{\mathcal{N}}(\rho) = \log_2\Big(\sum_k c_k\Big)^2, \tag{2.22}$$

where c_k are coefficients of the Schmidt decomposed state $|\Phi\rangle = \sum_k c_k |e_k\rangle_A \otimes |e_k\rangle_B$. Here $|e_k\rangle_A$ and $|e_k\rangle_B$ are orthonormal basis of the two subsystems after the Schmidt decomposition. As will be shown in the following, the state of Eq. (2.19) can be Schmidt decomposed into a state of two dimensions whose logarithmic negativity is straightforward to calculate.

II.C.3.2 Zero phase

We consider, for simplicity, that $e^{i\theta_n} \approx 1$ for both strong and weak single-photon coupling regimes, therefore we neglect this phase term in the expression of $|\psi_{m_\pm}\rangle$. This condition can be satisfied by varying the number of oscillations n for different values of β. First, we decompose the state $|\psi_{m_-}\rangle$ as

$$|\psi_{m-}\rangle = \frac{1}{\sqrt{2}} \sum_{k=1,2} |A_k\rangle_{m_1} |A_k\rangle_{m_2}, \tag{2.23}$$

where $|A_1\rangle_{m_j} = (-1)^j (c_1^- |0\rangle + c_2^- \widetilde{|2\beta\rangle})_{m_j}$, and $|A_2\rangle_{m_j} = (c_2^- |0\rangle - c_1^- \widetilde{|2\beta\rangle})_{m_j}$. Here

$$\begin{aligned} c_k^- &= \sqrt{\big(1 + (-1)^k \sqrt{1 - e^{-4\beta^2}}\big)/2}, \\ \widetilde{|2\beta\rangle}_{m_j} &= \frac{1}{\sqrt{1 - e^{-4\beta^2}}} (|(-1)^{j+1} 2\beta\rangle_{m_j} - e^{-2\beta^2} |0\rangle_{m_j}). \end{aligned} \tag{2.24}$$

The negativity of the state $|\psi_{m_-}\rangle$ is $E_{\mathcal{N}}^- = 1$ which equals to the maximum value of the logarithmic negativity of 2×2 system, i. e. the logarithmic negativity of a

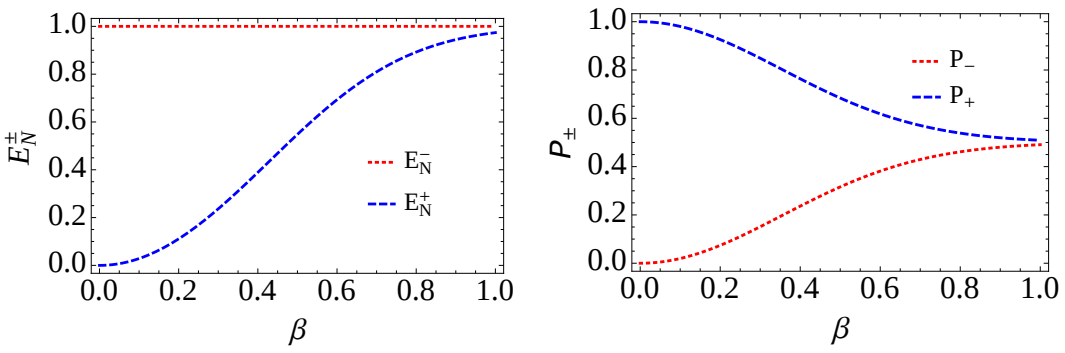

Figure 3: Degree of entanglement and generation probability for zero phase. (a) Logarithmic negativity $E_{\mathcal{N}}^{\pm}$ and (b) the corresponding probability $\mathcal{P}_{\pm}$ of entangled states $|\psi_{m\pm}\rangle$ versus the single-photon coupling rate β.

Bell state. The property of strong entanglement for this state holds for all values of β even if $\beta \ll 1$, albeit it happens with a small probability for small β. $|\psi_{m_+}\rangle$ can be decomposed as

$$|\psi_{m_+}\rangle = \frac{1}{\sqrt{4\mathcal{P}_+}} \sum_{k=1,2} c_k^+ |B_k\rangle_{m_1} |B_k\rangle_{m_2}, \tag{2.25}$$

where $c_j^+ = 1 + (-1)^j e^{-2\beta^2}$, $|B_1\rangle_{m_j} = (\sqrt{c_1^+/2}|0\rangle - \sqrt{c_2^+/2}|\widetilde{2\beta}\rangle)_{m_j}$, and $|B_2\rangle_{m_j} = (\sqrt{c_2^+/2}|0\rangle + \sqrt{c_1^+/2}|\widetilde{2\beta}\rangle)_{m_j}$. The negativity of this state is then given by $E_{\mathcal{N}}^+ = 1 - \log_2(1 + e^{-4\beta^2})$, which shows weak entanglement for $\beta \ll 1$ and strong entanglement for $\beta \gg 1$. We plot the results $E_{\mathcal{N}}^{\pm}$ of the two states in Fig. 3 (a) and the probabilities $\mathcal{P}_{\pm}$ to obtain these states in Fig. 3 (b). We observe from both figures that $E_{\mathcal{N}}^- > E_{\mathcal{N}}^+$ while the relation of the probabilities $\mathcal{P}_{\pm}$ is the inverse.

II.C.3.3 Non-zero phase

Now we calculate the general case of the logarithmic negativity of the two states $|\psi_{m\pm}\rangle$ including the phase term $e^{i\theta_n}$. The generated states $|\psi_{m\pm}\rangle$ can be decomposed into $\sum_{k=1,2} d_k^{\pm} |C_k^{\pm}\rangle_{m_1} |D_k^{\pm}\rangle_{m_2}$, where $|C_k^{\pm}\rangle_{m_1}$ and $|D_k^{\pm}\rangle_{m_2}$ are the mirrors' states under

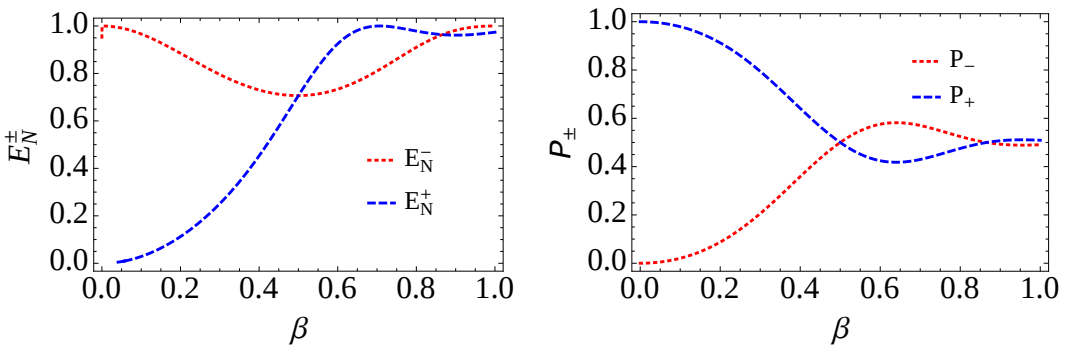

(a) (b)

Figure 4: Degree of entanglement and generation probability with the phase factor $e^{i\theta_0}$. (a) Logarithmic negativity $E_{\mathcal{N}}^{\pm}$ and (b) the corresponding probability $\mathcal{P}_{\pm}$ of entangled states $|\psi_{m\pm}\rangle$ versus the single-photon coupling rate β.

Schmidt decomposition and

$$d_k^{\pm} = \sqrt{\frac{1}{2} + (-1)^k \frac{1}{2}\sqrt{1 - \left[\frac{1 - e^{-4\beta^2}}{1 \pm e^{-4\beta^2}\cos(\theta_n)}\right]^2}}. \tag{2.26}$$

We do not provide the explicit expressions of $|C_k^{\pm}\rangle_{m_1}$ and $|D_k^{\pm}\rangle_{m_2}$ since they are not important in calculating the negativity. The logarithmic negativity is the given by $E_{\mathcal{N}}^{\pm} = 2\log_2(d_1^{\pm} + d_2^{\pm})$. We plot the degree of entanglement and the corresponding probability in this case for $\theta_0 = 2\pi\beta^2$ in Fig. 4. We observe from the figure that the degree of entanglement as well as the probability oscillates back and forth with increasing single-photon coupling rate due to the $\cos(\theta_n)$ term. It is not difficult to see from the expression of $\cos(\theta_n)$ that for greater number n these curves will have more frequent oscillations. By comparing the results of the two states $|\psi_{m\pm}\rangle$, we also observe that the greater the negativity the smaller the probability.

For a finite temperature T, the mirrors are initially prepared in thermal states given by $\rho_m^0(n_{th}) = \frac{1}{(\pi n_{th})^2}\int d^2\alpha_1 e^{-|\alpha_1|^2/n_{th}}(|\alpha_1\rangle\langle\alpha_1|)_{m_1} \otimes \int d^2\alpha_2 e^{-|\alpha_2|^2/n_{th}}(|\alpha_2\rangle\langle\alpha_2|)_{m_2}$

with thermal phonon number $n_{th} = (e^{\hbar\omega_m/k_BT} - 1)^{-1}$ for both mirrors and k_B the Boltzmann constant. After the interaction steps described above, the final state of the mirror will be given by the density operator

$$\begin{aligned}\rho_{m\pm}(n_{th}) &= \frac{1}{(\pi n_{th})^2}\int\int d^2\alpha_1 d^2\alpha_2 e^{-(|\alpha_1|^2+|\alpha_2|^2)/n_{th}} \\ &\times \ |\psi_{m\pm}(\alpha_1,\alpha_2)\rangle\langle\psi_{m\pm}(\alpha_1,\alpha_2)|, \end{aligned} \tag{2.27}$$

where

$$|\psi_{m\pm}(\alpha_1,\alpha_2)\rangle = \frac{1}{\sqrt{4\mathcal{P}_\pm}}\big(|\alpha_1\rangle_{m_1}|\alpha_2\rangle_{m_2} \pm e^{i\theta_n}|\alpha_1+2\beta\rangle_{m_1}|\alpha_2-2\beta\rangle_{m_2}\big). \tag{2.28}$$

The final density operator $\rho_{m\pm}(n_{th})$ represents a mixed state of entangled states. The degree of entanglement of such a state is very complicated to calculate and we do not discuss it here.

II.D Discussion and conclusion

In this paper, we proposed a simple setup to generate deterministic entanglement between two movable end mirrors in a Fabry-Perot cavity using a single photon state. We discussed two single-photon coupling regimes of entanglement generation. In the weak single-photon coupling regime, strong entanglement can be generated with a very small probability. In the strong single-photon coupling regime, strong entanglement can always be generated. Our scheme can be extended to superconducting circuits [78] and nano-resonators coupled to nitrogen-vacancy centers [79] where single-photon strong coupling rate is possible. Another possibility of generating strong entanglement without a strong single-photon coupling rate is to magnify the coherent states of the mirrors via periodic qubit flipping [80, 81]. By comparing the two possible outcomes of the entangled states, we also observed that the

smaller the probability to generate an entangled state the stronger the degree of entanglement of that state.

We now discuss the experimental realization of our scheme. Single-photon superposition state can be generated using a single atom in a superposition state interacting for a period of π Rabi rotation [82]. We require the atom-field coupling strength $g_c \gg \omega_m$ such that the mirrors' motion does not affect the atom-field interaction. This also guarantees the fast mapping between the photonic state and the atomic state during the measurement process. We also assume the decay rate of the photon $\kappa \ll \omega_m$ in order to keep the photon inside the cavity during the interaction. Ground-state cooling of the mirrors has been demonstrated in optomechanics recently [50, 51] in this regime. In summary, our scheme of generating macroscopic entangled states may be realized in experiment.

In the next chapter, we will discuss a different idea of entangling two end mirrors in a doubly-resonant cavity using a correlated emission laser with coherent driving. We will show that steady state entanglement can be obtained without initially cooling the mirrors to their ground states.

III. QUANTUM ENTANGLEMENT OF TWO MECHANICAL MIRRORS IN A CORRELATED EMISSION LASER*

In the previous chapter, we discussed about entanglement generation between two end mirrors without a coherent driving via nonlinear radiation-pressure coupling. In this chapter, we will discuss the idea of steady-state entanglement between two end mirrors in doubly-resonant cavity with coherent driving fields. We will show that steady-state entanglement of mirrors are obtained by transferring entanglement from a correlated emission laser in the linearized optomechanical coupling regime.

Quantum entanglement [83] has received a lot of interest in different areas of physics. Entanglement of microscopic objects such as photons and ions [84] has been demonstrated and it is of fundamental and practical importance whether we can generate entanglement between mesoscopic and even macroscopic objects. Recently, there are many proposals of entangling macroscopic mechanical objects via radiation pressure coupling [65] in optomechanical system. For example, Vitali *et al* [27] have shown that the stationary entanglement can be generated between an optical cavity field mode and a macroscopic vibrating mirror. More recently, schemes of entanglement generation between two micromechanical mirrors have been proposed, such as in two separate cavities by optomechanical coupling with two entangled output fields [30], in a double-cavity driven by squeezed input fields [31], in a classically driven Fabry-Perot cavity [32], and by injecting broadband squeezed vacuum light and laser light into a cavity [33]. Experimentally, strong coupling between micromechanical

*Reprinted with permission from "Entanglement of movable mirrors in a correlated-emission laser" by W. Ge, M. Al-amri, H. Nha and M. S. Zubairy, 2013. Phys. Rev. A, vol. 88, pp. 022338, Copyright [2013] by the American Physical Society, and "Entanglement of movable mirrors in a correlated emission laser via cascade-driven coherence" by W. Ge, M. Al-amri, H. Nha and M. S. Zubairy, 2013. Phys. Rev. A, vol. 88, pp. 052301, Copyright [2013] by the American Physical Society

oscillator and a cavity field has been demonstrated [19], paving the way towards quantum optical control of entanglement in mesoscopic objects.

Recently, atomic coherence has been utilized in a correlated emission laser (CEL) inside a doubly-resonant cavity to generate entanglement source of cavity fields [34, 85, 86, 87, 88, 89], such as in a three-level cascade atomic medium [34], using a four-level single atom [85], and in a four-level Raman-driven quantum beat laser [88]. With the strong entangled fields generated in a doubly-resonant cavity, it is an interesting question whether we can entangle two end mirrors in the cavity via radiation pressure coupling if they are mechanical mirrors that are free to move. From a practical point of view, entanglement between end mirrors in an active Michelson interferometer is relevant in the detection of gravitational waves [47], such as in LIGO [90].

In this regard, Zhou *et al.* [35] recently showed that entanglement between two macroscopic mirrors becomes possible if atoms with initial atomic coherence are injected into the cavity. In view of laser operation, however, one may apply an external driving field to a gain medium in order to establish the atomic coherence, e.g. in a correlated spontaneous emission laser (CEL) [91], rather than preparing an initial state of coherence. In this chapter, we consider a CEL system with an external driving field to generate entanglement between two movable mirrors as well as two-mode fields. We show that in the strong field-mirror coupling regime, the entanglement between the field modes can be transferred to the movable mirrors when the cavity-driving laser frequencies are both detuned at the anti-Stoke sidebands. Remarkably, in contrast to the previous works [31, 33, 35], our scheme can control the degree of entanglement of two movable mirrors and of two field modes with the external field(s) that driving the gain medium.

Moreover, the macroscopic entanglement between the mirrors of our scheme is robust against environmental thermalization. By tuning the input laser frequencies

both at the Stokes sidebands of the cavity, both mirrors can be cooled close to their ground states in the resolved sideband regime [48, 49] through an effective beam-splitter process. Meanwhile, the stationary entanglement between two mirrors are generated via an effective down-conversion process. We show that close to ground-state macroscopic entanglement is possible and persists for experimental temperature above 2K with realistic parameters.

In the following, we will consider two types of gain medium used in the doubly-resonant cavity, i.e. three-level cascade atoms [34] and four-level atoms [88]. By using the first gain medium, the CEL can reduce to a parametric oscillator in the strong driving limit [92]. While in the other medium, the CEL serves as a phase-sensitive amplifier [86]. We will first review the theory of a CEL as an entanglement source with the two types of gain medium as examples. Then we will present the results of steady-state entanglement between the mirrors with the help of the CEL in two different cases.

III.A Theory of a CEL as a source of entanglement

Entanglement of radiation fields receives considerable interest in recent years due to its potential applications in quantum information processing [2]. However, generation of macroscopic entangled states with a large number of photons remains an open question. Recently, a new type of entanglement amplifier based on two-mode CELs[91] of cascade three-level atoms was proposed [34]. The CEL operates in the presence of atomic coherence between the upper level and the lower level which is created by an external driving field. Here we review the basic theory of a CEL as a source of entanglement using both cascade three-level atoms and four-level atoms.

In order to see how does the atomic coherence in cascade three-level atoms leads to an entangled radiation fields, we first consider an example of initially prepared

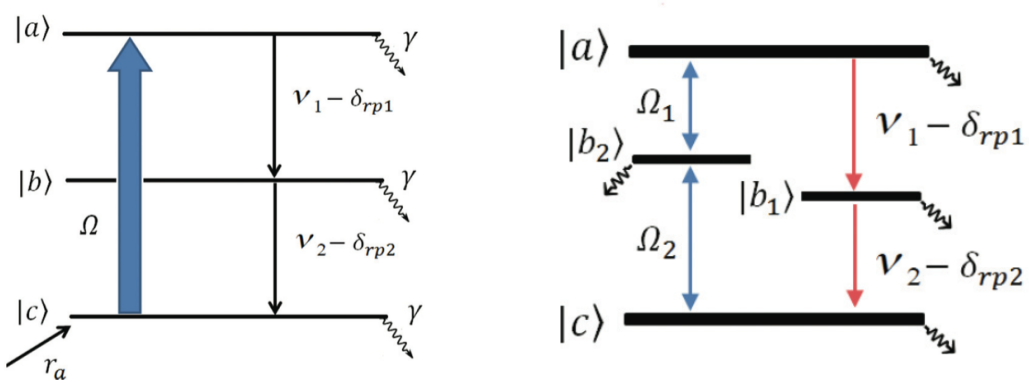

(a) (b)

Figure 5: Level diagrams for (a) three-level cascade atoms and (b) four-level atoms.

atomic coherence. We prepare atomic coherence between the upper and the lower levels $|a\rangle$ and $|c\rangle$ in an initial vacuum doubly-resonant cavity and the state of the atom-field system is $\big(|a\rangle + |c\rangle\big)/\sqrt{2} \otimes |0,0\rangle$. Due to spontaneous emission, the atoms in the excited state will undergo a transition to the intermedia level $|b\rangle$, and another transition from $|b\rangle$ to $|c\rangle$. The state of the atom-field system becomes $|c\rangle \otimes \big(|0,0\rangle + |1,1\rangle\big)/\sqrt{2}$. Clearly, the two-mode radiation fields is in an entangled state. Therefore, the CEL can be used as an entanglement amplifier when a large number of atoms are prepared in a coherent state.

III.A.1 Three-level cascade scheme

We consider first a scheme of using a gain medium consisting of three-level cascade atoms inside a doubly-resonant cavity as shown in Fig. 5 (a). The natural line-width γ is assumed to be equal for all levels and the atoms are pumped to the lowest level $|c\rangle$ at a rate r_a. The atoms have two dipole allowed transitions $|a\rangle - |b\rangle$ and $|b\rangle - |c\rangle$ that are coupled to two nondegenerate cavity modes at frequencies ν_1, ν_2, respectively. They also have a dipole forbidden transition $|a\rangle - |c\rangle$ that can be

induced by a resonant laser field with Rabi frequency Ω and phase ϕ. The dipole forbidden transition can be induced, for example, by applying a strong magnetic field for a magnetic dipole allowed transition. Atomic coherence is generated by the strong driving laser. In the interaction picture, the Hamiltonian of the system under the rotating-wave approximation is given by [34]

$$\mathcal{H}_I^{af} = \hbar g_1(\sigma_{ab}a_1 + a_1^\dagger\sigma_{ba}) + \hbar g_2(\sigma_{bc}a_2 + a_2^\dagger\sigma_{cb}) - \hbar\frac{\Omega}{2}\left(\sigma_{ac}e^{-i\phi} + \sigma_{ca}e^{i\phi}\right). \quad (3.1)$$

Here the first two terms represent the interaction between the atomic medium and the two cavity modes with coupling strengthes g_1 and g_2 respectiely. $\sigma_{ij}(i,j = a,b,c)$ is the Pauli pseudo-spin operator $|i\rangle\langle j|$ of the atoms. a_1, a_2 are the annihilation operators of each cavity mode. The third term in Eq. (3.1) generates an atomic coherence between the levels $|a\rangle$ and $|c\rangle$, which contributes to the correlated lasing operation of the CEL. The master equation of the atom-field system is given by

$$\rho_{af} = -\frac{i}{\hbar}[\mathcal{H}_I^{af}, \rho_{af}]. \quad (3.2)$$

To study the dynamics of the cavity modes, we obtain the reduced master equation for the two-mode fields in the CEL. In the regime of large atomic decay $\gamma \gg \kappa_j$, the atoms reach their steady state much faster than the cavity fields so that the dynamics of the atoms can be eliminated adiabatically. The reduced master equation is obtained from the interaction Hamiltonian H_I^{af} using the standard methods of laser theory [34, 67] as

$$
\begin{aligned}
\dot{\rho}_f &= -\left[\alpha_{11}^* a_1 a_1^\dagger \rho + \alpha_{11}\rho a_1 a_1^\dagger - (\alpha_{11}+\alpha_{11}^*) a_1^\dagger \rho a_1)\right] \\
&\quad -\left[\alpha_{22}^* a_2^\dagger a_2 \rho + \alpha_{22}\rho a_2^\dagger a_2 - (\alpha_{22}+\alpha_{22}^*) a_2 \rho a_2^\dagger\right] \\
&\quad -\left[\alpha_{12}^* a_1 a_2 \rho + \alpha_{21}\rho a_1 a_2 - (\alpha_{12}^*+\alpha_{21}) a_2 \rho a_1\right] \\
&\quad -\left[\alpha_{12}\rho a_1^\dagger a_2^\dagger + \alpha_{21}^* a_1^\dagger a_2^\dagger \rho - (\alpha_{12}+\alpha_{21}^*) a_1^\dagger \rho a_2^\dagger\right] \\
&\quad -\kappa_1(a_1^\dagger a_1 \rho + \rho a_1^\dagger a_1 - 2a_1 \rho a_1^\dagger) - \kappa_2(a_2^\dagger a_2 \rho + \rho a_2^\dagger a_2 - 2a_2 \rho a_2^\dagger). \qquad (3.3)
\end{aligned}
$$

We provide a detailed derivation of the reduced master equation for this scheme in the Appendix B. The first two terms proportional to α_{11} and α_{22} in the above equation describe the emission from level $|a\rangle$ and the absorption from level $|c\rangle$, respectively. The next two terms correspond to the effective coupling of the two cavity modes via atomic coherence generated by the classical field Ω. The last two terms represent the damping of each cavity mode with rate κ_j $(j = 1, 2)$. The system dynamics of the two-mode fields can be obtained from the master equation, see Ref. [89] or the study on the entanglement generation below for example.

In Eq. (3.3), the two quantum fields of the cavity are taken into account to second order in the coupling constants g_1 and g_2 while the classical laser field is considered to all orders in the Rabi frequency Ω. The coefficients $\alpha_{11}, \alpha_{22}, \alpha_{12}$ and α_{21} are then given by

$$
\alpha_{11} = \frac{g_1^2 r_a}{4} \frac{3\Omega^2}{(\Omega^2+\gamma^2)(\Omega^2/4+\gamma^2)}, \qquad (3.4)
$$

$$
\alpha_{22} = g_2^2 r_a \frac{1}{(\Omega^2+\gamma^2)}, \qquad (3.5)
$$

$$\alpha_{12} = -g_1 g_2 r_a \frac{\Omega}{\gamma(\Omega^2 + \gamma^2)}, \tag{3.6}$$

$$\alpha_{21} = \frac{g_1 g_2 r_a}{4} \frac{\Omega(\Omega^2 - 2\gamma^2)}{\gamma(\Omega^2 + \gamma^2)(\Omega^2/4 + \gamma^2)}, \tag{3.7}$$

where the phase of the driving field is assumed to be $\phi = -\frac{\pi}{2}$ for simplicity.

III.A.2 Four-level cascade-driven scheme

Now we consider a gain medium of four-level atoms in a doubly-resonant cavity, as shown in Fig. 5 (b). The atoms are injected into the cavity with a rate r_c in the lower level $|c\rangle$. A coherent superposition of the upper level $|a\rangle$ and the lower level $|c\rangle$ is created by two resonant classical laser fields of Rabi frequencies Ω_1, Ω_2, and phases ϕ_1, ϕ_2 interacting with $|a\rangle$ and $|c\rangle$ through an auxiliary level $|b_2\rangle$. This is one reason we study the four-level cascade-driven scheme because all the relevant transitions are dipole allowed. Two cavity modes are coupled to their respective atomic transitions $|a\rangle \leftrightarrow |b_1\rangle$ and $|b_1\rangle \leftrightarrow |a\rangle$ with coupling strengthes g_1 and g_2 as shown in Fig. 5 (b). The atomic decay rates of all four levels are assumed to be the same as γ for simplicity. The Hamiltonian of the atom-field system is given by

$$\mathcal{H}_I^{af} = \hbar g_1 \sigma_{ab_1} a_1 + \hbar g_2 \sigma_{b_1 c} a_2 - \hbar \frac{\Omega_1}{2} \sigma_{b_2 a} e^{i\phi_1} - \hbar \frac{\Omega_2}{2} \sigma_{cb_2} e^{i\phi_2} + \text{H.c.}. \tag{3.8}$$

Similarly, by adiabatically eliminating the atomic variables, we obtain the exact same master equation as in Eq. 3.3 for the two-mode fields. The only difference is

the different coefficients α_{ij} which are given as, in this case,

$$\alpha_{11} = \frac{g^2 r_c \Omega_1^2 \Omega_2^2}{\gamma^2 \Omega_D^4 \Omega_E^2}(\Omega_1^2 + \Omega_2^2 + 10\gamma^2), \tag{3.9}$$

$$\alpha_{22} = \frac{g^2 r_c}{\gamma^2 \Omega_D^4 \Omega_E^2}\left[\Omega_1^4(\Omega_1^2 + \Omega_2^2) + (9\Omega_1^4 + \Omega_2^4)\gamma^2 + 8(3\Omega_1^2 + \Omega_2^2)\gamma^4 + 16\gamma^6\right], \tag{3.10}$$

$$\alpha_{12} = -\frac{g^2 r_c \Omega_1 \Omega_2}{\gamma^2 \Omega_D^4 \Omega_E^2}\left[\Omega_1^2(\Omega_1^2 + \Omega_2^2) + (13\Omega_1^2 + 3\Omega_2^2)\gamma^2 + 12\gamma^4\right], \tag{3.11}$$

$$\alpha_{21} = -\frac{g^2 r_c \Omega_1 \Omega_2}{\gamma^2 \Omega_D^4 \Omega_E^2}\left[\Omega_1^2(\Omega_1^2 + \Omega_2^2) + 5(\Omega_1^2 - \Omega_2^2)\gamma^2 + 4\gamma^4\right], \tag{3.12}$$

where $\Omega_D^2 \equiv \Omega_1^2 + \Omega_2^2 + 4\gamma^2$, $\Omega_E^2 \equiv \Omega_1^2 + \Omega_2^2 + \gamma^2$, and we have assumed that $\phi_1 + \phi_2 = 0$ for simplicity. In the four-level scheme, there is no parametric limit as that in the three-level cascade configuration in [92]. With very strong driving fields $\Omega_j \gg \gamma$, α_{ij} reach to different constants. By setting $\Omega_1 = \Omega_2 = \Omega$, and $g_1 = g_2 = g$, we find that in this limit, $\alpha_{ij} \approx (-1)^{i+j}\alpha$ with $\alpha \equiv g^2 r_c / 4r^2$. Therefore, strong driving fields are preferable in our scheme since the coupling strength α_{ij} does not vanish for large Ω. This result is different from Refs. [86, 87, 88], where atoms are initially pumped to the auxiliary level, such that at very strong driving fields the coupling strength $\alpha_{ij} \propto 1/\Omega^2$.

III.B Entanglement of movable mirrors in a CEL

We consider a scheme of a doubly-resonant cavity with two movable mirrors M_1 and M_2 in a correlated emission laser using three-level cascade atoms as discussed in Sec. A (see Fig. 6). Each of the mirrors is treated as a quantum mechanical harmonic oscillator with an effective mass m and frequencies ω_{m_j} $(j = 1, 2)$. The annihilation and the creation operator of each vibrational mode are b_j and $b_j^\dagger$ satisfying $[b_j, b_j^\dagger] = 1$.

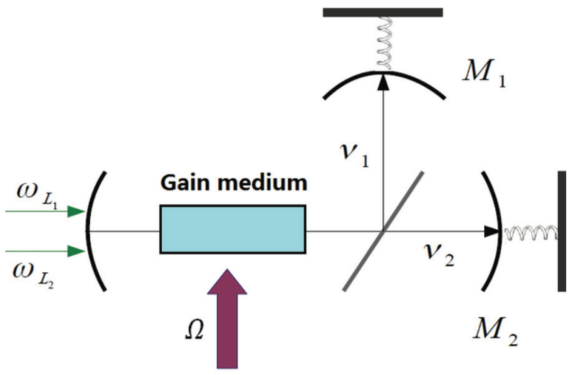

Figure 6: Scheme of entangling movable mirrors in a doubly-resonant cavity using three-level atoms as a gain medium. The gain medium inside the cavity is driven by an external field and also interacts with two cavity modes.

In the interaction picture, the Hamiltonian of the system under the rotating-wave approximation is written as $\mathcal{H}_I = \mathcal{H}_I^{af} + \mathcal{H}_I^{fm}$, where $\mathcal{H}_I^{af}$ given by Eq. (3.1) and

$$\begin{aligned}\mathcal{H}_I^{fm} &= \sum_{j=1}^{2}\left(\hbar\delta_{rp_j}a_j^\dagger a_j + \hbar\omega_{m_j}b_j^\dagger b_j\right) \\ &+ \sum_{j=1}^{2} i\hbar\left(E_j a_j^\dagger e^{i\delta_j t} - E_j^* a_j e^{-i\delta_j t}\right) \\ &- \hbar G_1 q_1 a_1^\dagger a_1 - \hbar G_2 q_2 a_2^\dagger a_2. \end{aligned} \tag{3.13}$$

Here $\mathcal{H}_I^{af}$ and $\mathcal{H}_I^{fm}$ describe the atom-field and the field-mirror interaction, respectively. In Eq. (3.13), the first line represents the energies of the cavity modes and the movable mirrors. Note that δ_{rp_1} and δ_{rp_2} denote the frequency shift of each cavity mode due to radiation pressure, which will be clarified later. We assume a resonant condition on the shifted cavity modes, i.e., $(\nu_1 - \delta_{rp_1}) - (\omega_a - \omega_b) = 0$ and $(\nu_2 - \delta_{rp_2}) - (\omega_b - \omega_c) = 0$. The second line in Eq. (3.13) represents two laser fields

driving the cavity modes, where $|E_j| = \sqrt{\frac{2P_j\kappa_j}{\hbar\omega_{L_j}}}$ with input power P_j, laser frequencies ω_{L_j}, and decay rates κ_j of each mode. Here $\delta_j \equiv \nu_j - \delta_{rp_j} - \omega_{L_j}$ is the effective detuning of each cavity-driving field. The third line in Eq. (3.13) corresponds to the coupling via radiation pressure [65] of mirrors and cavity modes with the coupling rates $G_j \equiv \frac{\nu_j}{L_j}\sqrt{\frac{\hbar}{m\omega_{m_j}}}$ and (cavity lengthes: L_j). We also define dimensionless position and momentum operators $q_j = (b_j + b_j^\dagger)/\sqrt{2}$ and $p_j = (b_j - b_j^\dagger)/i\sqrt{2}$ for the mirrors.

III.B.1 System dynamics

In this section, we use the master equation for the reduced density operator of the cavity field modes in CEL derived in Sec. A and then derive the quantum Langevin equations for the field-mirror subsystem separately. This approach is justified if the atom-field interaction is much stronger than the field-mirror interaction and the atomic medium is here treated as a general reservoir to the two cavity modes.

From the master equation (3.3), the diffusion coefficients for the cavity modes are readily derived using Einstein's relation [67]. For any operators O_1, O_2 and their noise operators F_{O_1}, F_{O_2}, it follows from Einstein's relation

$$\begin{aligned} 2\langle D_{O_1O_2}\rangle &= \frac{d}{dt}\langle O_1O_2\rangle - \left\langle \left(\frac{dO_1}{dt} - F_{O_1}\right) O_2 \right\rangle \\ &- \left\langle O_1 \left(\frac{dO_2}{dt} - F_{O_2}\right)\right\rangle \end{aligned} \tag{3.14}$$

that the nonzero diffusion coefficients are

$$\begin{aligned}
2\left\langle D_{a_1^\dagger a_1}\right\rangle &= 2\alpha_{11}, \\
2\left\langle D_{a_1 a_1^\dagger}\right\rangle &= 2\kappa_1, \\
2\left\langle D_{a_2 a_2^\dagger}\right\rangle &= 2(\kappa_2+\alpha_{22}), \\
2\left\langle D_{a_2 a_1}\right\rangle &= 2\left\langle D_{a_1^\dagger a_2^\dagger}\right\rangle = -(\alpha_{12}+\alpha_{21}).
\end{aligned} \tag{3.15}$$

In the following, we use these diffusion coefficients in specifying the correlation functions of the cavity-mode noise operators.

III.B.1.1 Quantum Langevin equations

Now we derive the quantum Langevin equations for the field-mirror subsystem and obtain their covariance matrix in steady-state. We consider a general analysis for the field-mirror subsystem including cavity decay, mirror damping, cavity modes noise and the Brownian noise of the mirrors. With the help of the master equation (3.3) and the field-mirror interaction Hamiltonian H_I^{fm}, the nonlinear quantum Langevin equations are obtained as

$$\begin{aligned}
\dot{b}_1 &= -i\omega_m b_1 + i\frac{G_1}{\sqrt{2}}a_1^\dagger a_1 - \gamma_m b_1 + \xi_1, \\
\dot{b}_2 &= -i\omega_m b_2 + i\frac{G_2}{\sqrt{2}}a_2^\dagger a_2 - \gamma_m b_2 + \xi_2, \\
\dot{a}_1 &= -(\kappa_1 + i\delta_{rp_1})a_1 + iG_1 a_1 q_1 + E_1 e^{i\delta_1 t} + \alpha_{11}a_1 + \alpha_{12}a_2^\dagger + F_{a_1}, \\
\dot{a}_2 &= -(\kappa_2 + i\delta_{rp_2})a_2 + iG_2 a_2 q_2 + E_2 e^{i\delta_2 t} - \alpha_{22}a_2 - \alpha_{21}a_1^\dagger + F_{a_2}.
\end{aligned} \tag{3.16}$$

We here assume that the two mirrors have the same damping rate γ_m and the same oscillation frequency ω_m. In Eq. (3.34), we have the quantum Brownian noise operators ξ_j and $\xi_j^\dagger$ with their delta-correlated function at temperature T in the limit of

large mechanical quality factor $Q = \omega_m/\gamma_m \gg 1$ [68],

$$\langle \xi_j(t)\xi_k^\dagger(t') + \xi_k^\dagger(t')\xi_j(t)\rangle/2 \approx \gamma_m(2n+1)\delta_{jk}\delta(t-t'), \tag{3.17}$$

where $n = [\exp(\hbar\omega_m/k_BT) - 1]^{-1}$ denotes the average thermal photon number and k_B is the Boltzmann constant. We introduce the nonzero correlation functions of the cavity noise operators $F_{a_1}, F_{a_1^\dagger}, F_{a_2}$ and $F_{a_2^\dagger}$ in the presence of atomic medium as:

$$\langle F_{O_1}(t)F_{O_2}(t')\rangle = 2\langle D_{O_1O_2}\rangle\,\delta(t-t'), \tag{3.18}$$

where $\langle D_{O_1O_2}\rangle$ are given by Eq. (3.15).

The nonlinear Langevin equations can be transformed to linearized Langevin equations of zero-mean fluctuation operators around $c-$number steady values. This is justified if the input power P_j to the cavity modes is very large [93]. That is, we take $b_j = b_{js} + \delta b_j,\ \tilde{a}_j = \alpha_{js} + \delta\tilde{a}_j$, where $\tilde{a}_j \equiv a_j e^{-i\delta_j t}$ are the slowly-varying field modes operators. The steady values are given by

$$\begin{aligned} p_{1s} = p_{2s} = 0, \qquad & q_{js} = \frac{G_j|\alpha_{js}|^2}{\omega_m}, \\ \alpha_{1s} = \frac{E_1}{s_1}, \qquad & \alpha_{2s} = \frac{E_2}{s_2}, \end{aligned} \tag{3.19}$$

with $s_j = i(\nu_j - G_jq_{js} - \omega_{L_j}) + \kappa_j + (-1)^j\alpha_{jj}$ and $p_{js} = (b_{js} - b_{js}^*)/i\sqrt{2},\ q_{js} = (b_{js} + b_{js}^*)/\sqrt{2}$. The term $\nu_j - G_jq_{js} - \omega_{L_j}$ represents the effective detuning of each cavity mode frequency. Thus it follows that the mean frequency shift due to radiation pressure, which is introduced in Eq. (3.13), is given by $\delta_{rp_j} \equiv G_jq_{js}$.

We introduce the slowing varying fluctuation operators, $\delta\tilde{b}_j(t) \equiv \delta b_j(t)e^{i\omega_{m_j}t}$ and

$\delta a_j(t) \equiv \delta\tilde{a}_j(t)e^{i\delta_j t}$ and write the linear quantum Langvin equations for them as

$$\begin{aligned}
\delta\dot{\tilde{b}}_1 &= -\gamma_m\delta\tilde{b}_1 + \sqrt{2\gamma_m}b_{1in} + i\frac{G_1\alpha_{1s}^*}{\sqrt{2}}\delta a_1 e^{i(\omega_m-\delta_1)t} + i\frac{G_1\alpha_{1s}}{\sqrt{2}}\delta a_1^\dagger e^{i(\omega_m+\delta_1)t},\\
\delta\dot{\tilde{b}}_2 &= -\gamma_m\delta\tilde{b}_2 + \sqrt{2\gamma_m}b_{2in} + i\frac{G_2\alpha_{2s}^*}{\sqrt{2}}\delta a_2 e^{i(\omega_m-\delta_2)t} + i\frac{G_2\alpha_{2s}}{\sqrt{2}}\delta a_2^\dagger e^{i(\omega_m+\delta_2)t},\\
\delta\dot{a}_1 &= -\kappa_{11}\delta a_1 + \alpha_{12}\delta a_2^\dagger + F_{a_1} + i\frac{G_1\alpha_{1s}}{\sqrt{2}}(\delta\tilde{b}_1 e^{-i(\omega_m-\delta_1)t} + \delta\tilde{b}_1^\dagger e^{i(\omega_m+\delta_1)t}),\\
\delta\dot{a}_2 &= -\kappa_{22}\delta a_2 - \alpha_{21}\delta a_1^\dagger + F_{a_2} + i\frac{G_2\alpha_{2s}}{\sqrt{2}}(\delta\tilde{b}_2 e^{-i(\omega_m-\delta_2)t} + \delta\tilde{b}_2^\dagger e^{i(\omega_m+\delta_2)t}), \quad (3.20)
\end{aligned}$$

where $\kappa_1 = \kappa_2 = \kappa$ for simplicity and $\kappa_{11} \equiv \kappa - \alpha_{11}$ and $\kappa_{22} \equiv \kappa + \alpha_{22}$. We have introduced the noise operators $b_{jin} \equiv \xi_j e^{i\omega_m t}/\sqrt{\gamma_m}$ for the mirrors' vibrational modes $(j = 1, 2)$, which satisfy the correlation relations [94]

$$\begin{aligned}
\langle b_{jin}^\dagger(t)b_{kin}(t')\rangle &= n\delta_{jk}\delta(t-t')\\
\langle b_{jin}(t)b_{kin}^\dagger(t')\rangle &= (n+1)\delta_{jk}\delta(t-t'). \quad (3.21)
\end{aligned}$$

It has been shown in [28] that the optomechanical interaction and consequently the field-mirror entanglement are enhanced when the cavity-driving light is scattered by the vibrating cavity boundary at the first Stokes $(\omega_{L_j} - \omega_m)$ and the anti-Stokes $(\omega_{L_j} + \omega_m)$ sidebands. Therefore there are two choices of our interest for the detuning of each cavity-driving field, i.e., $\delta_1 = \pm\omega_m$ and $\delta_2 = \pm\omega_m$. It is seen from Eqs. (3.20) that for the anti-Stokes sidebands $\delta_j = +\omega_m$, the field fluctuation operator δa_j are coupled to the movable mirror fluctuation operator $\delta\tilde{b}_j$ effectively in a beam-splitter-like (BSL) process. On the other hand, for the first Stokes sidebands $\delta_j = -\omega_m$, each pair of operators δa_j and $\delta\tilde{b}_j$ is coupled effectively in a parametric down conversion (PDC) process. Due to the symmetric configuration of field-field and mirror-mirror in our setup, we may deal with three different situations, i.e., $\delta_1 = \delta_2 = +\omega_m$,

$\delta_1 = \delta_2 = -\omega_m$ and $\delta_1 = -\delta_2 = \pm\omega_m$.

III.B.1.2 The steady-state covariance matrix

We define the dimensionless position and momentum fluctuation operators $\delta q_j = (\delta\tilde{b}_j + \delta\tilde{b}_j^\dagger)/\sqrt{2},\ \delta p_j = (\delta\tilde{b}_j - \delta\tilde{b}_j^\dagger)/i\sqrt{2},\ \delta x_j = (\delta a_j + \delta a_j^\dagger)/\sqrt{2},\ \delta y_j = (\delta a_j - \delta a_j^\dagger)/i\sqrt{2}$ and their corresponding noise operators $q_{jin},\ p_{jin},\ F_{x_j},\ F_{y_j}\ (j = 1, 2)$. We also define $u = (\delta q_1,\ \delta p_1,\ \delta q_2,\ \delta p_2,\ \delta x_1,\ \delta y_1, \delta x_2,\ \delta y_2)^T$. Then, the linear Langevin equations in the rotating-wave approximation ($\omega_m \gg \kappa,\ G$) can be written in a compact form as

$$\dot{u}(t) = Au(t) + B(t), \tag{3.22}$$

where

$$A = -\begin{pmatrix} \gamma_m & 0 & 0 & 0 & 0 & \left(\frac{\delta_1}{\omega_m}\right)G & 0 & 0 \\ 0 & \gamma_m & 0 & 0 & -G & 0 & 0 & 0 \\ 0 & 0 & \gamma_m & 0 & 0 & 0 & 0 & \left(\frac{\delta_2}{\omega_m}\right)G \\ 0 & 0 & 0 & \gamma_m & 0 & 0 & -G & 0 \\ 0 & \left(\frac{\delta_1}{\omega_m}\right)G & 0 & 0 & \kappa_{11} & 0 & -\alpha_{12} & 0 \\ -G & 0 & 0 & 0 & 0 & \kappa_{11} & 0 & \alpha_{12} \\ 0 & 0 & 0 & \left(\frac{\delta_2}{\omega_m}\right)G & \alpha_{21} & 0 & \kappa_{22} & 0 \\ 0 & 0 & -G & 0 & 0 & -\alpha_{21} & 0 & \kappa_{22} \end{pmatrix}, \tag{3.23}$$

and $B(t) = (\sqrt{\gamma_m}q_{1in}, \sqrt{\gamma_m}p_{1in}, \sqrt{\gamma_m}q_{2in}, \sqrt{2\gamma_m}p_{2in}, F_{x_1}, F_{y_1}, F_{x_2}, F_{y_2})$. For simplicity the parameters of the two field-mirror pairs are chosen such that $G_1\alpha_{1s} = G_2\alpha_{2s} = |G_j\alpha_{js}|$. The effective coupling rate is thus defined as $G \equiv G_j\alpha_{js}/\sqrt{2}$ which is controlled by the cavity-driving input power $P \equiv P_1 = P_2$.

We study the quantum fluctuations of the operators when the system reaches a steady-state. Since the quantum noises $q_{jin},\ p_{jin}$ and $F_{x_j},\ F_{y_j}$ are all zero-mean Gaussian noises and the dynamics has been linearized, the steady state of the system becomes a zero-mean multipartite Gaussian state. We define the covariance matrix (CM) of the system whose elements are $V_{ij} = (\langle u_i(\infty)u_j(\infty)+u_j(\infty)u_i(\infty)\rangle)/2$. The system can reach a stable steady-state when all real parts of the eigenvalues of the drift matrix A are negative. The eigenvalues s are given by the roots of equation $s^4+a_3s^3+a_2s^2+a_1s+a_0=0$ with $a_0 = (\kappa_{11}\gamma_m+\frac{\delta_1}{\omega_m}G^2)(\kappa_{22}\gamma_m+\frac{\delta_2}{\omega_m}G^2)+\alpha_{12}\alpha_{21}\gamma_m^2$, $a_1 = \gamma_m^2(\kappa_{11}+\kappa_{22}) + 2\gamma_m(\kappa_{11}\kappa_{22}+\alpha_{12}\alpha_{21}) + G^2(\frac{\delta_1}{\omega_m}\kappa_{22}+\frac{\delta_2}{\omega_m}\kappa_{11}) + \gamma_m(\frac{\delta_1}{\omega_m}+\frac{\delta_2}{\omega_m})$, $a_2 = 2\gamma_m(\kappa_{11}+\kappa_{22})+(\kappa_{11}\kappa_{22}+\gamma_m^2+\alpha_{12}\alpha_{21})++G^2(\frac{\delta_1}{\omega_m}+\frac{\delta_2}{\omega_m})$ and $a_3 = (\kappa_{11}+\kappa_{22}+2\gamma_m)$ ($\delta_j = \pm\omega_m,\ j=1,2$). We obtain from the Routh-Hurwitz stability criterion [95] the following stability conditions

$$\begin{cases} a_i > 0 & (i=0,1,2,3) \\ a_3a_2a_1 > a_1^2+a_3^2a_0 \end{cases}. \tag{3.24}$$

Now we simply assume that the parameters satisfy the stationary conditions, then the CM in the steady-state satisfies the Lyapunov equation [32]

$$AV+VA^T = -D, \tag{3.25}$$

where

$$D = \begin{pmatrix} D_m & 0 \\ 0 & D_f \end{pmatrix}, \tag{3.26}$$

with $D_m = \mathrm{diag}[\gamma_m(2n+1), \gamma_m(2n+1), \gamma_m(2n+1), \gamma_m(2n+1)]$ and

$$D_f = \begin{pmatrix} \kappa + \alpha_{11} & 0 & -\frac{\alpha_{12}+\alpha_{21}}{2} & 0 \\ 0 & \kappa + \alpha_{11} & 0 & \frac{\alpha_{12}+\alpha_{21}}{2} \\ -\frac{\alpha_{12}+\alpha_{21}}{2} & 0 & \kappa + \alpha_{22} & 0 \\ 0 & \frac{\alpha_{12}+\alpha_{21}}{2} & 0 & \kappa + \alpha_{22} \end{pmatrix}. \tag{3.27}$$

The exact solution of the CM can be obtained from Eq. (3.40) with nontrivial elements under three different situations of our interest. We pick up relevant elements in each case to obtain a two-mode covariance matrix V^s in the steady state with $u = (\delta Q_1, \delta P_1, \delta Q_2, \delta P_2)^T$ where $Q_j = q_j$,x_j and $P_j = p_j$,y_j $(j = 1, 2)$ and test the entanglement conditions for three different pairs of macroscopic objects, namely field-field, field-mirror, and mirror-mirror.

III.B.2 Entanglement measure for a bipartite Gaussian state

In this section, we investigate the degree of entanglement for each bipartite Gaussian state of the field-mirror system under three different detuning conditions leading effectively to the BSL or PDC process for the mirror-field coupling. By definition, a quantum state $\hat{\rho}$ of a bipartite system is said to be separable if and only if $\hat{\rho}$ can be written as a convex combination of product states, i.e.,

$$\hat{\rho} = \sum_j p_j \hat{\rho}_{jA} \otimes \hat{\rho}_{jB}, \tag{3.28}$$

where $\hat{\rho}_{jA}$ and $\hat{\rho}_{jB}$ are density operators of mode A and mode B respectively with the probability sum $\sum_j p_j = 1$ $(0 \leq p_j \leq 1)$. There are many criteria proposed to test the separability for a CV bipartite system [71, 72, 73, 74, 75, 76, 96].

In this paper we employ a quantitative measure of entanglement, i.e., the loga-

rithmic negativity $E_{\mathcal{N}}$ [71] that is based on the negative eigenvalues of the density matrix under partial transposition. In the case of a two-mode Gaussian state, the logarithmic negativity is given by

$$E_{\mathcal{N}} = \max\{0, -\ln 2\eta^{-}\} + \max\{0, -\ln 2\eta^{+}\}, \tag{3.29}$$

where $\eta^{\pm}$ are the two positive roots of characteristic function of the covariance matrix,

$$\eta^4 - (\det V_A + \det V_B - 2\det V_C)\eta^2 + \det V^s = 0. \tag{3.30}$$

In the above we assume a block-matrix form of the covariance matrix as

$$V^s = \begin{pmatrix} V_A & V_C \\ V_C^T & V_B \end{pmatrix}. \tag{3.31}$$

In the following we investigate the effects of various parameters such as the input power P, the driving field Ω and the temperature T of the mirrors on the degree of output entanglement. In turn this analysis shows that the generated entanglement can be controlled by adjusting experimental conditions particularly the external driving field Ω. We consider three different detuning conditions, i.e. $\delta_j = +\omega_m$, $\delta_j = -\omega_m$ and $\delta_1 = -\delta_2 = \omega_m$, to find out an experimental configuration relevant to the output entanglement.

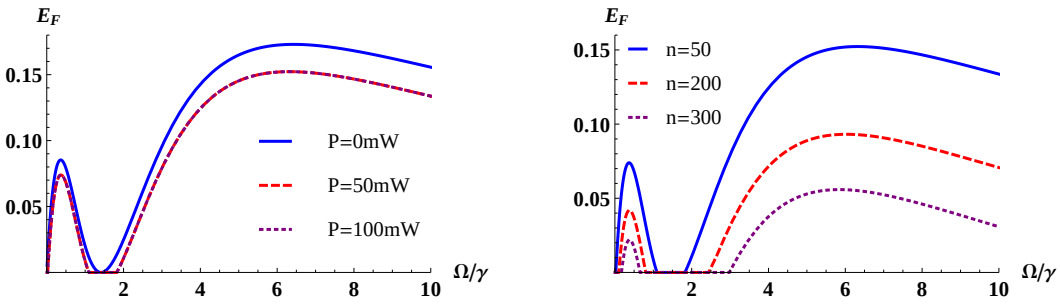

(a) (b)

Figure 7: Logarithmic negativity $E_{\mathcal{F}}$ of the two-mode fields as a function of Ω/γ. (a) Effect of the cavity-driving laser power P on $E_{\mathcal{F}}$ at $n = 50$ for P =0 mW (blue solid curve), P =50 mW (red-dashed curve) and P =100 mW (purple-dotted curve). (b) Effect of thermal noise of the mirrors on $E_{\mathcal{F}}$ at $P = 100$ mW for $n = 50$ (blue solid curve), n =200 (red-dashed curve), n =300 (purple-dotted curve). The optomechanical doubly-resonant cavity parameters are taken as $\gamma_m = 2\pi \times 50$ Hz, $\kappa = 2\pi \times 215$ kHz, $\omega_m = 2\pi \times 3$ MHz, $m = 5$ ng, $L_1 = 1.064$ mm and $L_2 = 0.810$ mm according to recent experiments [19, 97]. The input laser wavelengthes are $\lambda_1 = 810$ nm and $\lambda_2 = 1064$ nm and the input power P varies from 0 to 100 mW so that $0 \leq G/\sqrt{\kappa\gamma_m} \leq 140$. The atom-cavity coupling strength is $g_1 = g_2 = g = 2\pi \times 2.5$ MHz, the injection rate $r_a = 1.6$ MHz and the atomic decay rate $\gamma = 1.7$ MHz.

III.B.3 Entanglement generation of two movable mirrors

III.B.3.1 Both field-mirror pairs coupled in a BSL process

We first discuss the case of $\delta_j = +\omega_m$ $(j = 1, 2)$ so that the field-mirror effective coupling is a BSL process for both pairs. As has been shown in Refs. [28, 48, 97], the effective BSL process for the field-mirror coupling is very stable since this process followed by the cavity photon decay leads to the cooling of movable mirrors [48]. We find from stability conditions (3.24) that the cross-coupling strength α_{12} and α_{21} can not be too large since $\alpha_{12}\alpha_{21}$ becomes negative for $\Omega > \sqrt{2}\gamma_m$. On the other hand, the cavity loss κ and field-mirror coupling strength G are preferable to be large from Eq. (3.24). We study our scheme in the strong radiation-pressure coupling regime,

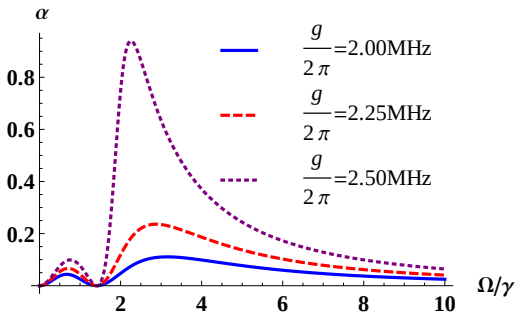

Figure 8: Influence of atom-cavity coupling on the effective two-mode fields coupling strength α as a function of Ω/γ for the coupling $g = 2\pi\times 2.00$, $2\pi\times 2.25$ and $2\pi\times 2.50$ MHz. The other parameters are the same as in Fig. 7.

i.e., $G^2/\gamma_m \gg \kappa$.

Field-Field pair: Let us first look at the entanglement of two-mode fields. In Fig. 7, we plot the logarithmic negativity of the two-mode fields as a function of the driving field strength Ω for different cavity-driving laser powers P and thermal noises n of mirrors. Except for the case of $\Omega = \sqrt{2}\gamma$, we see that there generally arises the entanglement between the two-mode fields by the external driving field, which makes the coherence of the gain medium coupled to the cavity modes.

To understand the behavior of the logarithmic negativity with the driving field Ω, we also plot in Fig. 8 the effective field-field coupling strength $\alpha \equiv \alpha_{21}^2/(\kappa_{11}\kappa_{22} + \alpha_{12}\alpha_{21})$. By comparing Figs. 7 and 8, we see that the effective coupling α and the degree of entanglement behave very similarly as a function of Ω. That is, the driving field Ω controls the effective field-field coupling which in turn determines the shape of the degree of entanglement in Fig. 7. There are two peaks of entanglement $E_{\mathcal{F}}$ in Fig. 7 at $\Omega \approx 0.5\gamma$ and $\Omega \approx 6\gamma$ which correspond to two maxima of the effective field-field coupling strength in Fig. 8.

When the cavity-driving power P changes from 0 to a nonzero value (Fig. 7 (a)),

we see that the degree of entanglement is slightly reduced. This is due to the coupling of the cavity-field mode to a mirror. The effective coupling G of field-mirror pair in Eq. (3.23) is defined as $G \equiv G_j \alpha_{js}/\sqrt{2}$ so that it increases with the input power P in view of Eq. (3.19). Therefore, noting that there is no direct interaction between two mirrors in our setup, the effective coupling G indirectly transfers the entanglement of two fields to that of two mirrors (Fig. 9). We also observe in Fig. 7 (b) that the degree of entanglement decreases with the thermal noise n of the mirrors. Except for two small regions around $\Omega = 0$ and $\Omega = \sqrt{2}\gamma$ where $\alpha_{21} = 0$, we generally obtain the steady-state entanglement for the two-mode fields. The range of those two regions with no entanglement increases as the thermal noise n increases.

Field-Mirror pair: On the other hand, the field-mirror pairs are coupled in a BSL process and it has been proved [98, 99] that a nonclassical input state is required to have an entangled output state in a BSL process. Under this theorem, we readily see that there arises no entanglement between field and mirror due to the classical input states in our scheme.

Mirror-Mirror pair: Although there is no entanglement between cavity fields and movable mirrors, we show that the entanglement between the two-mode fields can be transferred to the entanglement of the mirrors. To be more elaborate, the effective coupling between the two mirrors can be obtained from Eq. (3.20) by eliminating adiabatically the dynamics of field modes δa_j under the condition $\kappa \gg \gamma_m(2n+1)$ and substituting into the mirrors' vibrational modes [30]. It can be shown in the corresponding equations that the two vibrational modes are coupled to each other in a PDC process so that it is possible to generate entanglement between two movable mirrors.

In Fig. 9, the degree of entanglement of the two movable mirrors is plotted against the external field Ω for different cavity-driving laser powers P and thermal

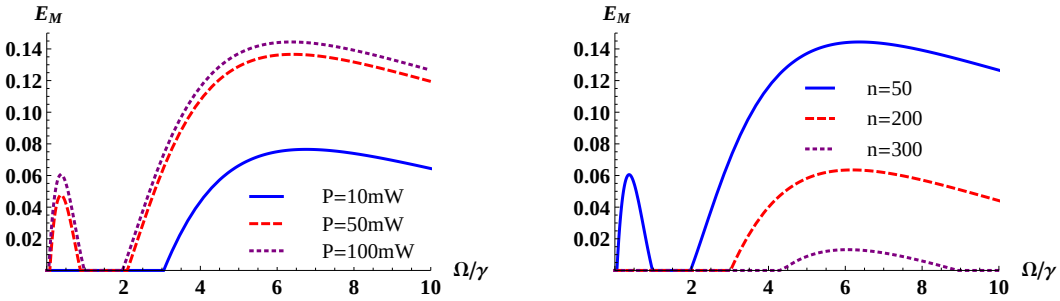

(a) (b)

Figure 9: Logarithmic negativity $E_{\mathcal{M}}$ of the movable mirrors as a function of Ω/γ. (a) Effect of the cavity-driving laser power p on entanglement for $n = 50$ with P =10 mW (blue solid curve), P =50 mW (red-dashed curve) and P =100 mW (purple-dotted curve) (b) Effect of thermal noise on entanglement at $P = 100$ mW for $n = 50$ (blue solid curve), n =200 (red-dashed curve) and n =300 (purple-dotted curve). The other parameters are the same as in Fig. 7.

noises n. We observe in the figures that the degree of entanglement for the movable mirrors has a similar curve to that of the two-mode fields for a large input power P and a small thermal noise n. In our scheme there is no direct interaction between the mirrors so one may say that the entanglement of the two mode fields is transferred to the entanglement of mirrors due to the field-mirror coupling (radiation pressure). In Fig. 9 (a), we observe that in a large cavity-driving power P, the value of $E_{\mathcal{M}}$ is comparable to that of $E_{\mathcal{F}}$ in the strong coupling regime ($G/\sqrt{\kappa\gamma_m} = 140$). In Fig. 9 (b), we also see that the degree of entanglement for the mirrors is reduced with an increasing temperature. From the figure, we see that a macroscopic bipartite entanglement can be realized despite the condition $k_B T > \hbar\omega_m$.

To see the effect of the atom-cavity coupling strength on the output entanglement, we plot $E_{\mathcal{M}}$ versus T for different values of g with $\Omega = 6\gamma$ in Fig. 10. We observe that the degree of entanglement $E_{\mathcal{M}}$ increases with the atom-cavity coupling g. This is consistent with the increasing field-field coupling strength α so that a

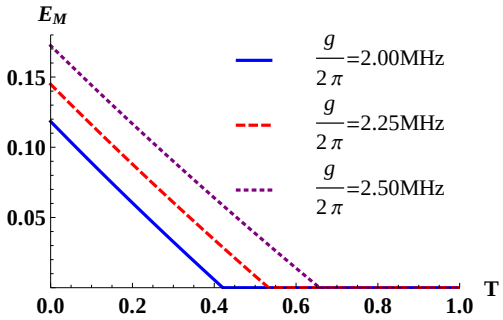

Figure 10: Effect of atom-cavity coupling on the two mirrors' entanglement $E_{\mathcal{M}}$; $E_{\mathcal{M}}$ as a function of mirrors' environment temperature T at $\Omega = 6\gamma$ for the coupling $g = 2\pi \times 2.00$, $2\pi \times 2.25$ and $2\pi \times 2.50$ MHz. The other parameters are the same as in Fig. 7.

higher entanglement from the fields can be transferred to the mirrors. However, g has an upper bound restricted by both the cavity loss κ and the field-mirror coupling strength G such that the stability condition Eq. (3.24) is satisfied.

In Fig. 11, we plot $E_{\mathcal{M}}$ versus T for different values of κ with $\Omega = 6\gamma$ to see the effect of cavity loss on entanglement. This plot shows that the slope of $E_{\mathcal{M}}$ versus T decreases with an increasing cavity loss, however, it is desirable to have a smaller κ in order to obtain a higher entanglement. A larger cavity loss results in a smaller field-field coupling strength α so that the degree of entanglement for both the field-field pair and the mirror-mirror pair is reduced with otherwise the same parameters. We also see that the critical temperature above which the entanglement $E_{\mathcal{M}}$ disappears increases with a decreasing cavity loss.

Therefore, we have demonstrated that a macroscopic bipartite entanglement of both the field-field and the mirror-mirror pair can be obtained with the degree of entanglement controllable by an external driving field that implements the correlated emission laser under experimentally realizable conditions.

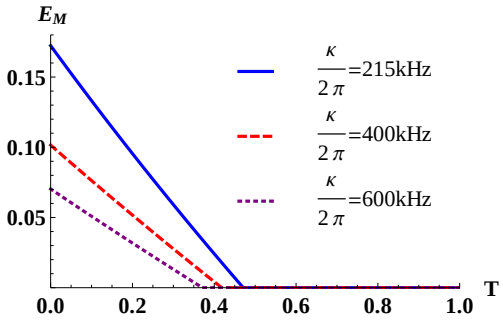

Figure 11: Influence of cavity loss on the two mirrors' entanglement $E_{\mathcal{M}}$; $E_{\mathcal{M}}$ as a function of environment temperature T at $\Omega = 6\gamma$ for cavity loss $g = 2\pi \times 215$, $2\pi \times 400$ and $2\pi \times 600$ kHz. The other parameters are the same as Fig. 7.

III.B.3.2 Field-mirror pairs coupled in different processes

We now study the case of the two field-mirror pairs coupled in two different processes, e.g. field 1 (F1) and mirror 1 (M1) are coupled in a BSL process and field 2 (F1) and mirror 2 (M2) are coupled in a PDC process. We obtain from Eq. (3.24) one necessary condition needed for the steady state solution in this case as

$$\left(\kappa_{11} + \frac{G^2}{\gamma_m}\right)\left(\kappa_{22} - \frac{G^2}{\gamma_m}\right) + \alpha_{12}\alpha_{21} > 0. \tag{3.32}$$

Now the parametric region is restricted to a weak field-mirror coupling regime as one of the field-mirror pairs is coupled in the PDC process which is hindered by the stability condition [100]. This stability region approximates as $\frac{G^2}{\gamma_m} < \alpha_{11} + \alpha_{22}$.

In this case we find there are only three bipartite pairs, i.e. F1F2, F2M2, and F1M2, that are coupled effectively in a PDC process to generate an entangled stationary state. All the other bipartite states are Gaussian states coupled effectively in a BSL process which can not be entangled states due to the classical inputs. Due to the weak radiation-pressure coupling, the field-mirror pair coupled in PDC process

is poorly entangled. Therefore, in this case we only obtain the entangled two-mode fields of a correlated emission laser significantly and its degree of entanglement is slightly reduced by the weak radiation-pressure coupling.

III.B.3.3 Both field-mirror pairs coupled in a PDC process

In this subsection, the field-mirror coupling is considered in a PDC process for both pairs, therefore the system of field-mirror pairs are very unstable. To see this, we derive from Eq. (3.24) two necessary conditions by setting $\delta_j = -\omega_m$:

$$\begin{cases} \left(\kappa_{11} - \frac{G^2}{\gamma_m}\right)\left(\kappa_{22} - \frac{G^2}{\gamma_m}\right) + \alpha_{12}\alpha_{21} > 0 \\ \gamma_m(2\alpha_{12}\alpha_{21} + 2\kappa_{11}\kappa_{22} + \kappa_{11}\gamma_m + \kappa_{22}\gamma_m) \\ -G^2(\kappa_{11} + \kappa_{22} + 2\gamma_m) > 0. \end{cases} \tag{3.33}$$

This condition is more stringent than Eq. (3.32) leaving us very little to play with. Although all the bipartite states (F1M1, F2M2, F1F2, F1M2, F2M1 and M1M2) in this case are Gaussian states coupled effectively in a PDC process, there is no significantly entangled bipartite state except the two-mode fields due to the weak radiation-pressure coupling restricted by the stability condition.

Therefore, we conclude that the seemingly achievable entanglement of movable mirrors coupled effectively in a PDC process can not be practicable due to the stability condition Eq. (3.33). In this case, we only obtain the entangled bipartite Gaussian states of the two-mode fields in the steady-state solution.

In summary, we have studied the gain medium of cascade three-level atoms placed inside the doubly-resonant cavity as a scheme of entangling the two-mode fields whose entanglement can be transferred to two movable mirrors through radiation pressure. We first studied the master equations of the atom-cavity subsystem and the quantum Langevin equations of the mirror-cavity subsystem in order to derive the dynamical

coupling equations among the two cavity fields and the two mirrors. We considered three different cases of tuning the two cavity-driving laser frequencies such that $\delta_j = +\omega_m$, $\delta_1 = -\delta_2 = +\omega_m$ and $\delta_j = -\omega_m$ and generalized the three cases into the Lyapunov equation Eq. (3.40) for stationary covariance matrix V with a generalized drift matrix A in the rotating-wave approximation. In each case, we investigated all six bipartite Gaussian states in steady state and the entanglement conditions quantitatively with the logarithmic negativity $E_{\mathcal{N}}$ as well as the stability conditions obtained from the drift matrix. Among the three cases considered, we obtain the macroscopic entanglement of movable mirrors only in the case of both field-mirror pairs interacting in a BSL process. The two mirrors are coupled effectively in a PDC process in this case and the steady-state of the field-mirror system is stable in the strong field-mirror coupling regime.

Remarkably, the generated entanglement can be controlled by adjusting the external driving field Ω. We have shown that in the strong field-mirror coupling regime ($G^2/\gamma_m \gg \kappa$) the entanglement of two-mode fields entanglement can be transferred to the two movable mirrors. The degree of entanglement $E_{\mathcal{M}}$ is significant for a high atom-cavity coupling g and a low cavity loss κ. With the stability condition Eq. (3.24) and the experimentally accessible parameters [19, 97], the macroscopic entanglement for two movable mirrors can be realized with the current state-of-the-art experiments.

III.C Entanglement of two movable mirrors in a CEL via cascade-driven coherence

Now we consider a scheme, as shown in Fig. 12, consists of two micromechanical mirrors with mass m and a four-level atomic gain medium in a doubly-resonant cavity, as discussed in [88], with lengths L_1, L_2. The two mirrors are considered to have the same vibration frequency ω_m and the same mechanical decay rate γ_m. The

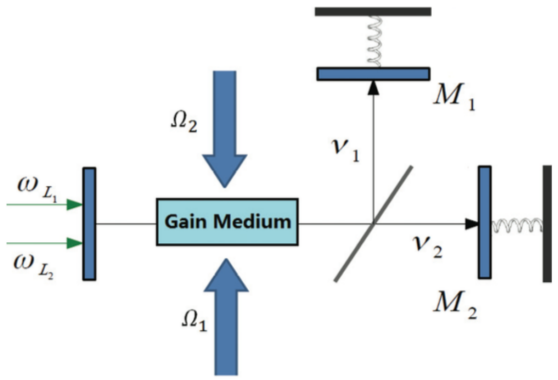

Figure 12: Schematics for entangling two micromechanical mirrors in a doubly-resonant cavity with four-level atoms as a gain medium.

dimensionless position and momentum operators of each mechanical mode q_j and p_j satisfy $[p_j, q_j] = i$ $(j = 1, 2)$. We assume that, in the steady state, two cavity modes ν_1 and ν_2 are shifted by $\delta_{rp_1} = G_1 q_{1s}$ and $\delta_{rp_2} = G_2 q_{2s}$, respectively and the shifted cavity modes $\nu_j - \delta_{rp_j}$ are resonant with their corresponding transitions. Here $G_j \equiv \frac{\nu_j}{L_j}\sqrt{\frac{\hbar}{m\omega_m}}$ represent the radiation pressure coupling rate for each field-mirror pair and q_{js} are the stationary solutions of the dimensionless positions for the mechanical modes which will be given explicitly later. The doubly resonant cavity is driven by two lasers with frequencies $\omega_{L_1}, \omega_{L_2}$. Therefore, the total Hamiltonian of the system in the interaction picture is written as $\mathcal{H} = \mathcal{H}_I^{af} + \mathcal{H}_{fm}$, where $\mathcal{H}_I^{af}$ is given by Eq. (3.8) and $\mathcal{H}_{fm}$ is given by Eq. (3.13). The Hamiltonian of this scheme differs with the previous scheme in the expression of the atom-field interaction which result in different coefficients of the reduced master equation of the field modes.

III.C.1 System dynamics

The stationary solutions of our system can be obtained by solving the master equation for the reduced density operator for the cavity field modes due to the atom-

field interaction $\mathcal{H}_I^{af}$ and quantum Langevin equations for the field-mirror subsystem separately. This is justified if the entanglement of two-mode fields is not reduced significantly after including the radiation-pressure coupling from the micromechanical mirrors. The master equation is given by Eq. (3.3) and the coefficients are given by Eq. (3.12).

Considering the field-mirror interaction H_{fm} and lasing effect of atoms from Eqs. (3.13) and (3.3), the quantum Langevin equations for the field-mirror subsystem are written as

$$\begin{aligned}
\dot{b}_1 &= -i\omega_m b_1 + i\frac{G_1}{\sqrt{2}}a_1^\dagger a_1 - \gamma_m b_1 + \xi_1, \\
\dot{b}_2 &= -i\omega_m b_2 + i\frac{G_2}{\sqrt{2}}a_2^\dagger a_2 - \gamma_m b_2 + \xi_2, \\
\dot{a}_1 &= -(\kappa_1 + i\delta_{rp_1})a_1 + iG_1 a_1 q_1 + E_1 e^{i\delta_1 t} + \alpha_{11}a_1 + \alpha_{12}a_2^\dagger + F_{a_1}, \\
\dot{a}_2 &= -(\kappa_2 + i\delta_{rp_2})a_2 + iG_2 a_2 q_2 + E_2 e^{i\delta_2 t} - \alpha_{22}a_2 - \alpha_{21}a_1^\dagger + F_{a_2}. \qquad (3.34)
\end{aligned}$$

The quantum Brownian noise operators ξ_j and $\xi_j^\dagger$ in the large mechanical quality factor limit $Q = \omega_m/\gamma_m \gg 1$ [68] have δ-correlated function written as:

$$\langle \xi_j(t)\xi_k^\dagger(t') + \xi_k^\dagger(t')\xi_j(t)\rangle/2 \approx \gamma_m(2n+1)\delta_{jk}\delta(t-t'). \qquad (3.35)$$

Here $n \equiv [\exp(\hbar\omega_m/k_B T) - 1]^{-1}$ is the average thermal phonon number for each mirror at temperature T and k_B is the Boltzmann constant. The correlation functions of the cavity modes noise operators $F_{a_1}, F_{a_1^\dagger}, F_{a_2}$ and $F_{a_2^\dagger}$ can be obtained from the master equation (3.3) by using the Einstein's relation [67, 58]:

$$\langle F_{O_1}(t)F_{O_2}(t')\rangle = 2\langle D_{O_1O_2}\rangle \delta(t-t'), \qquad (3.36)$$

where the nonzero values are $\left\langle D_{a_1^\dagger a_1}\right\rangle = \alpha$, $\left\langle D_{a_1 a_1^\dagger}\right\rangle = \kappa_1$, $\left\langle D_{a_2 a_2^\dagger}\right\rangle = (\kappa_2 + \alpha)$, and $\langle D_{a_2 a_1}\rangle = \left\langle D_{a_1^\dagger a_2^\dagger}\right\rangle = -\alpha$ for strong Rabi frequencies.

We assume that the input power P_j are large so that the stationary amplitudes of the intracavity fields α_{1s}, α_{2s} are large. The nonlinear Langevin equations can be decomposed into linearized Langevin equations of zero-mean fluctuation operators around $c-$number steady state values in this approximation [93], i.e., $b_j = b_{js} + \delta b_j$, $\tilde{a}_j = \alpha_{js} + \delta\tilde{a}_j$, where $\tilde{a}_j \equiv a_j e^{-i\delta_j t}$ are the detuned cavity modes operators. We find that the steady state values, in the limit $Q \gg 1$, are $p_{js} \approx 0$, $q_{js} \approx \frac{G_j|\alpha_{js}|^2}{\omega_m}$, and $\alpha_{js} = \frac{E_j}{s_j}$, with $s_j \equiv i\delta_j + \kappa_j + (-1)^j\alpha$ and $p_{js} \equiv (b_{js} - b_{js}^*)/i\sqrt{2}$, $q_{js} \equiv (b_{js} + b_{js}^*)/\sqrt{2}$ $(j = 1, 2)$.

As shown in Ref. [48, 49], a micromechanical mirror is cooled (heated) when input laser field is red-detuned (blue-detuned). The effective coupling between the field and the mirror in the rotating-wave approximation (RWA) is a beam-splitter process followed by the decay of cavity photon for cooling or a down-conversion process for entanglement [98, 99]. Indeed, the beam-spitter process for cooling in the optomechanical system can be understood as a red-detuned photon enters into the cavity, excites a cavity photon by absorbing a phonon from the mirror's motion, and then decays out of the cavity [48]. In the doubly-resonant cavity, the two-mode fields are entangled through a down-conversion process [34, 87]. Therefore, only when both input laser fields are red-detuned at the Stokes sidebands of cavity modes, i.e., $\delta_j = \omega_m$, the two micromechanical mirrors of the cavity can be entangled via an effective down-conversion process. This is also restricted by the stability conditions of the system [28, 48, 97] in reaching strong field-mirror cooperative regime $|G_j\alpha_{js}|^2 \gg \kappa_j\gamma_m$. Therefore, with red-detuned lasers, we can realize both ground-state cooling of the micromechanical mirrors and macroscopic entanglement of the two. This feature makes the steady-state entanglement robust against environmental

thermalization.

It is convenient to define $u = (\delta q_1,\ \delta p_1,\ \delta q_2,\ \delta p_2,\ \delta x_1,\ \delta y_1, \delta x_2,\ \delta y_2)^T$, where the fluctuation operators are defined as $\delta q_j = (\delta\tilde{b}_j + \delta\tilde{b}_j^\dagger)/\sqrt{2}$, $\delta p_j = (\delta\tilde{b}_j - \delta\tilde{b}_j^\dagger)/i\sqrt{2}$, $\delta x_j = (\delta a_j + \delta a_j^\dagger)/\sqrt{2}$, $\delta y_j = (\delta a_j - \delta a_j^\dagger)/i\sqrt{2}$ with the slow varying operators $\delta\tilde{b}_j \equiv \delta b_j e^{i\omega_m t}$ and $\delta a_j \equiv \delta\tilde{a}_j e^{i\delta_j}$. The corresponding noise operators are $q_{jin},\ p_{jin},\ F_{x_j},\ F_{y_j}$ $(j = 1, 2)$. We consider $P_1 = P_2 \equiv P$, $\kappa_1 = \kappa_2 \equiv \kappa$, and $\sqrt{2}G_1\alpha_{1s} \approx \sqrt{2}G_2\alpha_{2s} \equiv G$ for simplicity. The linearized quantum Langevin equations in the RWA $(\omega_m \gg \kappa,\ G)$ are given by [58]

$$\dot{u}(t) = Au(t) + B(t), \tag{3.37}$$

where $A = \begin{pmatrix} A_M & A_I \\ A_I & A_F \end{pmatrix}$ with $A_M = -\gamma_m I$,

$$A_I = \begin{pmatrix} 0 & -G & 0 & 0 \\ G & 0 & 0 & 0 \\ 0 & 0 & 0 & -G \\ 0 & 0 & G & 0 \end{pmatrix}, \tag{3.38}$$

$$A_F = \begin{pmatrix} -\kappa + \alpha_{11} & 0 & \alpha_{12} & 0 \\ 0 & -\kappa + \alpha_{11} & 0 & -\alpha_{12} \\ -\alpha_{21} & 0 & -\kappa - \alpha_{22} & 0 \\ 0 & \alpha_{21} & 0 & -\kappa - \alpha_{22} \end{pmatrix}, \tag{3.39}$$

and $B(t) = (\sqrt{\gamma_m}q_{1in}, \sqrt{\gamma_m}p_{1in}, \sqrt{\gamma_m}q_{2in}, \sqrt{2\gamma_m}p_{2in}, F_{x_1}, F_{y_1}, F_{x_2}, F_{y_2})$. Since the quantum noises are zero-mean quantum Gaussian noises and the dynamics has been lin-

earized, the steady-state of the system is a zero-mean multipartite Gaussian state.

The system is stable when all real parts of the eigenvalues s of the matrix A are negative. The general stability condition of the system can be obtained from Routh-Hurwitz criterion [95]. In our scheme, we are interested in the regime of strong Rabi frequency ($\Omega/\gamma \gg 1$) such that α_{ij} are constants. The eigenvalues s are, therefore, given as $-\frac{1}{2}[\kappa+\gamma_m \pm \sqrt{-4G^2+(\kappa-\gamma_m)^2}]$ and $\mathrm{Re}(s)<0$ is always satisfied in the RWA. We observe from imaginary part of the eigenvalues that normal-mode splitting of micromechanical mirrors in the strong coupling regime $G>\kappa/2$ is the same as in Ref. [18]. This shows that the current type of cascade-driven CEL does not affect the normal-mode splitting in the cavity optomechanics.

In the following, we assume the system is stable within our choices of parameters. In the steady-state, the solution satisfies the Lyapunov equation [32]

$$AV + VA^T = -D, \tag{3.40}$$

where the covariance matrix (CM) $V_{ij} \equiv [\langle u_i(\infty)u_j(\infty) + u_j(\infty)u_i(\infty)\rangle]/2$ and

$$D = \begin{pmatrix} D_M & 0 \\ 0 & D_F \end{pmatrix}, \tag{3.41}$$

with $D_M = \gamma_m(2n+1)I$ and

$$D_F = \begin{pmatrix} \kappa+\alpha_{11} & 0 & -\frac{\alpha_{12}+\alpha_{21}}{2} & 0 \\ 0 & \kappa+\alpha_{11} & 0 & \frac{\alpha_{12}+\alpha_{21}}{2} \\ -\frac{\alpha_{12}+\alpha_{21}}{2} & 0 & \kappa+\alpha_{22} & 0 \\ 0 & \frac{\alpha_{12}+\alpha_{21}}{2} & 0 & \kappa+\alpha_{22} \end{pmatrix}. \tag{3.42}$$

We then solve the CM V from Eq. (3.40) with nontrivial elements and form a two-mode CM V^s with $u = (\delta Q_1, \delta P_1, \delta Q_2, \delta P_2)^T$ for the two-mode fields and two micromechanical mirrors, respectively.

III.C.2 Entanglement criteria

We investigate the degree of entanglement for each bipartite Gaussian state. We consider quantitative measure of entanglement based on the logarithmic negativity $E_{\mathcal{N}}$ in Ref. [71] and Duan-Giedke-Cirac-Zoller (DGCZ) criterion [74] since both criteria are necessary and sufficient conditions for a two-mode Gaussian state.

In the continuous variable case, the logarithmic negativity is defined as

$$E_{\mathcal{N}} = \max\{0, -\ln 2\eta^-\} + \max\{0, -\ln 2\eta^+\}, \tag{3.43}$$

where $\eta^{\pm}$ are the two positive roots of the characteristic function of the CM, $\eta^4 - (\det V_A + \det V_B - 2\det V_C)\eta^2 + \det V^s = 0$ with $V^s = \begin{pmatrix} V_A & V_C \\ V_C^T & V_B \end{pmatrix}$.

The DGCZ criterion states that a two-mode state is considered to be entangled if the quantum fluctuations of the two Einstein-Podolsky-Rosen-like operators, $\hat{u}$ and $\hat{v}$, of the two modes satisfy the inequality

$$\left\langle (\Delta\hat{u})^2 \right\rangle + \left\langle (\Delta\hat{v})^2 \right\rangle < a^2 + \frac{1}{a^2}, \tag{3.44}$$

where $\hat{u} = |a|\hat{X}_1 + \frac{1}{a}\hat{X}_2$ and $\hat{v} = |a|\hat{P}_1 - \frac{1}{a}\hat{P}_2$ with the commutators $[\hat{X}_j, \hat{P}_{j'}] = i\delta_{jj'}$, and a is assumed to an arbitrary (nonzero) real number. However, this criterion is often used in a special case as $\langle (\Delta\hat{u})^2 \rangle + \langle (\Delta\hat{v})^2 \rangle < 2$ ($a = \pm 1$) [30, 33, 34, 35, 85, 87, 88] which can only extract partial information of entanglement for a system. In this paper, we will use the general form in Eq.(3.44) to study the entanglement condition

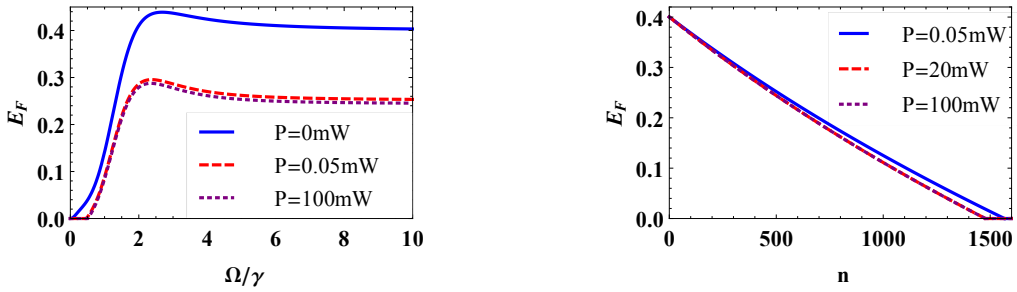

(a) (b)

Figure 13: Logarithmic negativity of the two-mode fields (a) as a function of Ω/γ at constant $n = 500$ for P =0, 0.05, and 100 mW; (b) as a function of n at constant $\Omega = 20\gamma$ for P =0.05, 20, and 100 mW.

for a two-mode state and compare it with that using the logarithmic negativity.

III.C.3 Discussion

In this section, we present the results of entangling two micromechanical mirrors as well as two-mode fields using two different criteria. In all the numerical results, we choose the parameters based on recent experiments [19, 97, 101]: $\gamma_m = 2\pi \times 50$Hz, $\kappa = 2\pi \times 250$ kHz, $\omega_m = 2\pi \times 30$ MHz, $m = 5$ ng, $L_1 = 0.532$ mm and $L_2 = 0.405$ mm. The input laser wavelengths $\lambda_1 = 810$ nm, and $\lambda_2 = 1064$ nm. The cavity coupling $g = 2\pi \times 4$ MHz, the injection rate $r_a = 1.6$ MHz, and the atomic decay rate $\gamma = 2\pi \times 1.4$ MHz.

III.C.3.1 Marcroscopic entanglement generation

Now we discuss the effect of various parameters Ω, P and n on entanglement generation of both two-mode fields and two micromechanical mirrors. In Fig. 13 we plot the degree of entanglement for the two-mode fields versus Ω/γ and n, respectively, at different input laser powers P. We observe in the Fig. 13 (a) that the amount of

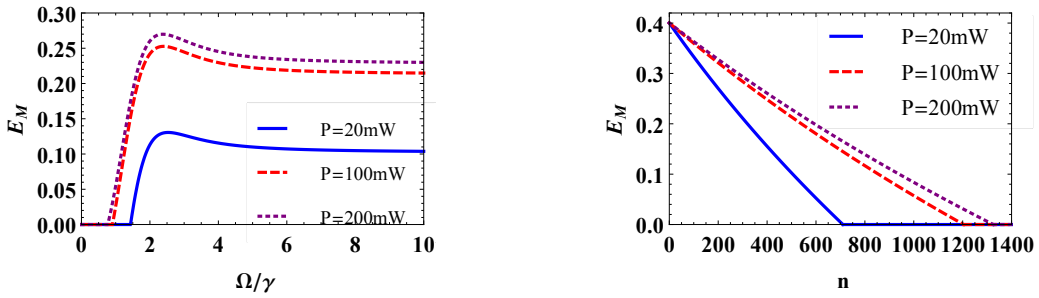

(a) (b)

Figure 14: Logarithmic negativity of the micromechanical mirrors for $P = 20$, 100, and 200mW (a) as a function of Ω/γ at constant $n = 500$; (b) as a function of n at constant $\Omega = 20\gamma$.

entanglement increases sharply with Ω to a maximum then reaches to a constant for $\Omega/\gamma \gg 1$. This is due to the physical behavior of the scheme determined by the coupling strengthes α_{ij} under current pumping method. By comparing Fig. 13 (a) and 13 (b), we observe that $E_{\mathcal{F}}$ is fractionally reduced when interacting with micromechanical mirrors and the reduction increases with n. Particularly, the entanglement of the fields vanishes when $\gamma_m n \approx \kappa$ for $G^2 \gg \kappa\gamma_m$ ($P > 20$mW) as shown in Fig. 13 (b). This justifies our approximation of solving two subsystems, i.e., atom-field and field-mirrors, separately for small thermal noise such that $\kappa \gg \gamma_m(2n+1)$.

In Fig. 14 (a), we plot the degree of entanglement for the mirrors tunable via external Rabi frequency at different P. We observe that $E_{\mathcal{M}}$ has a similar shape as $E_{\mathcal{F}}$ which is due to the transferring effect through radiation pressure coupling. We find that the amount of entanglement increases with P and it is saturated for $P > 100$mW as the system enters the strong-coupling regime ($G \gg \kappa$) [101]. This is also seen in Fig. 14 (b), in which we plot $E_{\mathcal{M}}$ as a function of n for different P. As shown in this figure, $E_{\mathcal{M}}$ decreases with increasing n and the slope of $E_{\mathcal{M}}$ becomes

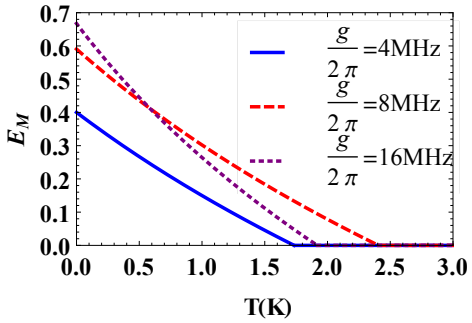

Figure 15: Influence of cavity coupling strength g on $E_{\mathcal{M}}$ versus T at constant $P = 100\text{mW}$, $\Omega = 20\gamma$, and $k = 2\pi \times 250\text{kHz}$ for $g = 2\pi \times 4$, $2\pi \times 8$, and $2\pi \times 16\text{MHz}$.

less sharp as the coupling strength increases.

We mentioned that with strong Rabi frequencies of the driving fields, the field coupling strength $\alpha_{ij} \approx (-1)^{i+j}\alpha$, and the field-mirror subsystem can always reach to a steady state with arbitrary parameters in the RWA. Therefore, we can study the effects of cavity coupling strength α and cavity dissipation rate κ in a large parametric regime, particularly when $\alpha \gg \kappa$.

To see the effect of cavity coupling strength α on the mirrors' entanglement, we plot Fig. 15. We observe that the maximum amount of entanglement increases with g at $T = 0K$. This shows that with larger value of g, the coupling strength α increases and hence $E_{\mathcal{M}}$ increases. We also find that the highest temperature allowed for entanglement increases with g first then drops. This is due to the inverse relation between G and α from the expression $G = G_j|E_j|/\sqrt{\omega_m^2 + [\kappa + (-1)^j\alpha]^2}$ in the regime of $\alpha \gg \kappa$. As g increases, the field-field coupling strength α becomes larger which in turn greatly decreases the field-mirror coupling strength G. Thus, α has to be balanced to realize an optimal T for entanglement when $\alpha \gg \kappa$. This result is different from our previous proposal of three-level cascade system [58]. In

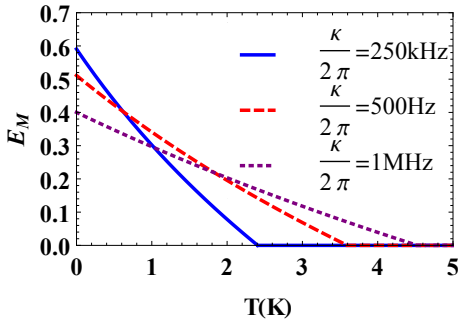

Figure 16: Influence of cavity decay rate κ on $E_{\mathcal{M}}$ versus T at constant $P = 100$mW, $\Omega = 20\gamma$, and $g = 2\pi \times 8$MHz for $\kappa = 2\pi \times 250$, $2\pi \times 500$, and $2\pi \times 10^3$kHz.

that scheme, required by the stability conditions, $\alpha \ll \kappa$, which does not affect G significantly as α increases.

To see the influence of cavity dissipation on the mirrors' entanglement, we plot Fig. 16. We observe that the maximum amount of entanglement decreases with κ at $T = 0K$. The plot also shows that the entanglement is more resistant against temperature for larger κ. Since in our scheme $\alpha \gg \kappa$, change of κ does not affect the field-mirror coupling significantly. With increasing cavity dissipation, the condition $\kappa \gg \gamma_m(2n+1)$ can be satisfied with larger n (The average phonon number $n = 1041$ for $T = 1.5$K.). Remarkably, the entanglement of the two mirrors persists for higher temperature with larger dissipation rate. This is one of the important features distinct from previous cascade scheme [58]. We conclude from these two properties that in order to retain macroscopic entanglement for high temperature, strong-coupling conditions, i.e.,

$$G \sim \alpha \gg \kappa \gg \gamma_m(2n+1), \tag{3.45}$$

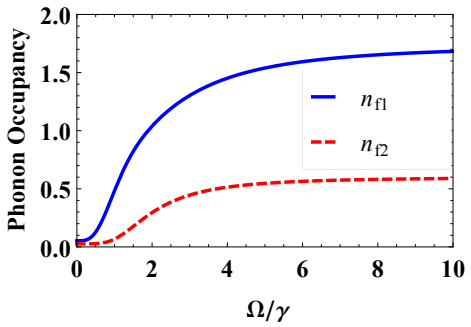

Figure 17: Steady-state phonon numbers of M1 (n_{f1}) and M2 (n_{f2}) versus Ω/γ at constant $P = 100\text{mW}$, $n = 500$, $k = 2\pi \times 1\text{MHz}$, and $g = 2\pi \times 8\text{MHz}$.

should be satisfied.

III.C.3.2 Ground-state cooling

We have already shown that the micromechanical mirrors can be entangled with experimental realistic parameters. Now we show that close to ground-state cooling of both mirrors is possible under the same experimental apparatus. As in our scheme, each mirror is coupled to each field in an effective beam-splitter process in the RWA. Each field serves as a zero-temperature bath to respective mirror. In equilibrium, the phonon occupation of each mirror will be determined by the cooling mechanism from the zero-temperature bath and the heating mechanism from the environmental thermalization. Due to the CEL, additional noise may heat the micromechanical mirrors from the atoms. We neglect the heating from non-RWA term which is negligible when $\kappa/\omega_m \ll 1$. We plot the steady-state phonon occupancies of the mirrors versus Ω/γ at constant P and n in Fig. 17. We observe that when there is no CEL ($\Omega = 0$), the final phonon numbers simply correspond to ground-state cooling in the resolved-sideband regime. When the CEL becomes strong ($\Omega \gg \gamma$), the final phonon

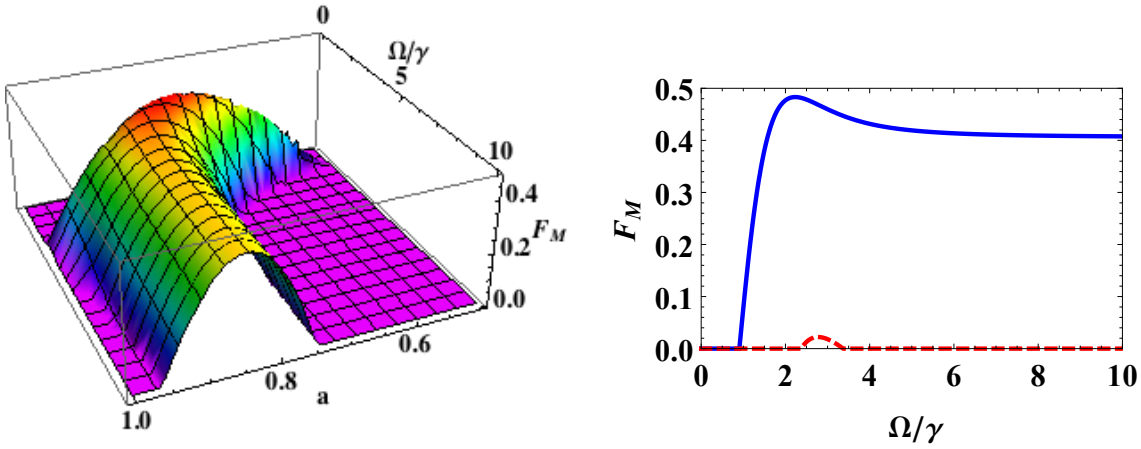

(a) (b)

Figure 18: (a) Entanglement of two micromechanical mirrors F_M as a function of Ω/γ and a at $n = 500$ and $P = 100$mW. (b) Projection of Fig. 18 (a) onto the front plane (blue-solid curve) and cross section of Fig. 18 (a) at $a = 1$ (red-dashed curve).

numbers are still within the ground-state regime, i.e. $n_{f1}, n_{f2} \sim 1$, although they are heated by the extra noise from the atoms. The difference between n_{f1} and n_{f2} when $\Omega \gg \gamma$ comes from emission of field a_1 and absorption of field a_2 in the presence of atoms. Therefore, the micromechanical mirrors are cooled close to their ground states, which makes our scheme more realistic since the macroscopic entanglement is more robust against environmental thermalization.

III.C.3.3 DGCZ criterion for entanglement

As for a comparison, we study the entanglement of the two micromechanical mirrors using DGCZ criterion. We define $\hat{X}_j = \delta q_j$, $\hat{P}_j = \delta p_j$ and

$$\begin{aligned} F_M(a) &\equiv a^2 + \frac{1}{a^2} - \left(\left\langle(\Delta\hat{u})^2\right\rangle_M + \left\langle(\Delta\hat{v})^2\right\rangle_M\right) \\ &= a^2\left(1 - \left\langle\delta q_1^2\right\rangle - \left\langle\delta p_1^2\right\rangle\right) + \frac{1}{a^2}\left(1 - \left\langle\delta q_2^2\right\rangle - \left\langle\delta p_2^2\right\rangle\right) \\ &\quad -2\frac{a}{|a|}\left(\langle\delta q_1\delta q_2\rangle + \langle\delta p_1\delta p_2\rangle\right), \end{aligned} \tag{3.46}$$

where the steady-state quantum fluctuations are given by CM V. We carefully choose the parameter a and plot the entanglement F_M on Ω/γ and a in Fig. 18 (a). We find that for different values of a, entanglement condition $F_M > 0$ is satisfied with different intervals of Ω/γ. To compare with the logarithmic negativity $E_{\mathcal{M}}$, we plot the projection of Fig. 18 (a) in Fig. 18 (b) (blue-solid curve). We observe that the interval of entanglement on Ω/γ is almost the same as that in Fig. 14 (a) (red-dashed curve) and the shapes of the entanglement are similar for the two criteria. To see the difference of Eq. (3.44) and a special form $(\langle(\Delta\hat{u})^2\rangle + \langle(\Delta\hat{v})^2\rangle) < 2$, we also plot the entanglement F_M when $a = 1$ (red-dashed curve) in Fig. 18 (b). It is shown in the figure that $F_M(a = 1) > 0$ is satisfied for a very small region. Therefore, we conclude that to obtain a complete and adequate entanglement condition, the general form of Eq. (3.44) should be considered.

In summary, we have studied the scheme of entanglement generation in a CEL via cascade-driven coherence which avoids the experimental difficulties by using dipole-forbidden transition. Two different entanglement criteria, i.e., the logarithmic negativity and DGCZ, are studied and shown to give the same entanglement condition as long as DGCZ criterion is considered in a general form. We have shown that entanglement can be transferred from two-mode fields to micromechanical mirrors in the regime of strong coupling.

We have considered the case with pumping to the lower level $|c\rangle$, where the field coupling coefficients α_{ij} never vanish even in the strong Rabi frequency limit $\Omega \gg \gamma$ and the field-mirror subsystem can always have a stationary solution with arbitrary parameters under this limit. We have also studied the effects of cavity coupling strength g and cavity dissipation rate κ on the entanglement versus temperature. We recognized a strong-coupling parametric regime in Eq. (3.45) to persist macroscopic entanglement for the mirrors at high temperature. Within this regime, the

macroscopic entanglement is in favor of large dissipation rate. We also achieved close to ground-state cooling of the two mirrors in the resolved side-band limit when the mirrors are entangled. Therefore, our scheme will make a potential candidate for the realization of robust macroscopic entanglement.

III.D Conclusion

In this chapter, we studied entanglement generation of two end mirrors in a doubly-resonant cavity with a CEL using two different types of gain medium, i. e., three-level cascade atoms and four-level cascade-driven coherence atoms. We first showed that the interaction of coherent atoms with two cavity modes generates macroscopic entangled light. Then we showed that by including the radiation-pressure coupling to the end mirrors, the entangled light will transfer entanglement to the two mirrors with coherent driving fields in the linearized regime. Robust macroscopic entanglement between two micromechanical mirrors as well as close to ground-state cooling of the mirrors is possible with realistic experimental parameters.

IV. MACROSCOPIC OPTOMECHANICAL SUPERPOSITION VIA PERIODIC QUBIT FLIPPING*

Quantum superposition, one of the fundamental principles of quantum mechanics, usually appears at the microscopic level [4, 7, 8]. Bringing quantum superposition to the macroscopic level [10], of massive objects, is an intriguing task as it bridges the quantum world to the classical world and macroscopic superposition may be used to test novel decoherence models [11, 12, 13, 14, 15, 16].

Optomechanical systems have been recently studied to reveal quantum effects of macroscopic objects [24, 25, 27, 29, 48, 49, 50, 51, 101, 102, 103]. One scheme uses optically levitated dielectric particles to achieve quantum superpositions with well separated positions [36, 37], which relies on very good cavities and high quality vacuum. Another approach creates a superposition of coherent states of a macroscopic mirror by mapping a single-photon superposition state into the mechanical state [26, 38, 39]. The most demanding requirement of this scheme is a strong coupling rate g comparable to the mechanical oscillation frequency ω_m to displace a position larger than its zero-point fluctuation with a single photon. Recently, schemes of using collective optomechanical interactions to increase single-photon coupling rate have been considered [40, 41, 42, 43]. More recently, there have been several proposals to achieve macroscopic quantum superpositions in the single-photon weak coupling regime via conditioned postselection in nested interferometers [44] or strong displaced Fock states [45, 46].

Here, we propose a setup in a cavity optomechanical system via periodically flip-

*Reprinted with permission from Macroscopic optomechanical superposition via periodic qubit flipping by W. Ge and M. S. Zubairy, 2015. Phys. Rev. A, vol. 91, pp. 013842, Copyright [2015] by the American Physical Society.

ping a photonic qubit to create macroscopic quantum superpositions of a mechanical mirror with large distinguishable coherent states. Our scheme relieves the requirement of $g \sim \omega_m$ with a relaxed condition in the resolved sideband regime of $g \sim \kappa$, where κ is the cavity field decay rate. The generated state can be reconstructed using quantum state reconstruction [104], such as a back-action-evading approach [105, 106, 107].

We prepare a single-photon superposition state $|\psi_c\rangle = \frac{1}{\sqrt{2}}(|0\rangle_c + |1\rangle_c)$ in a Fabry-Perot cavity with one mechanical mirror as shown in Fig. 19 (a). A coherent state $|\alpha\rangle_m$ of the mechanical mirror is entangled with the photon state as $\frac{1}{\sqrt{2}}(|0\rangle_c|\alpha\rangle_m + |1\rangle_c|\alpha + 2\beta\rangle_m)$ due to radiation pressure [26, 38], where 2β is the displacement by the single photon after certain time. To magnify the difference between its superposed mirror states, we periodically flip the cavity field states $|0\rangle_c$ and $|1\rangle_c$. This can be achieved by mapping the photonic state to a flying two-level atom, flipping the atomic state with a fast π pulse, and mapping the atomic state back to the photonic state. By using fast π pulses and flipping photon state alternatively, decoherence of the atomic state can be avoided and the effect of the cavity decay can be reversed probabilistically for null-result measurements [77]. The difference of the two coherent states of the mirror is amplified by the number of procedures performed. The superposition states of the mirror, with two possible outcomes, are obtained by a final measurement of the cavity photon in the basis of $\frac{1}{\sqrt{2}}(|0\rangle_c \pm |1\rangle_c)$. Our scheme can generate macroscopic superposition states with very large separation. A similar scheme was proposed in a coupled system of a resonator and a single qubit [108].

Our proposal requires strong coherent mapping, recycling of an atomic state, and fast atomic qubit flipping. Thanks to recent development in cavity QED, accurate manipulation of atom-field interaction [82] has been realized and the recycling may be achieved by transferring an atomic state between two cavities [109]. Ultrafast atomic

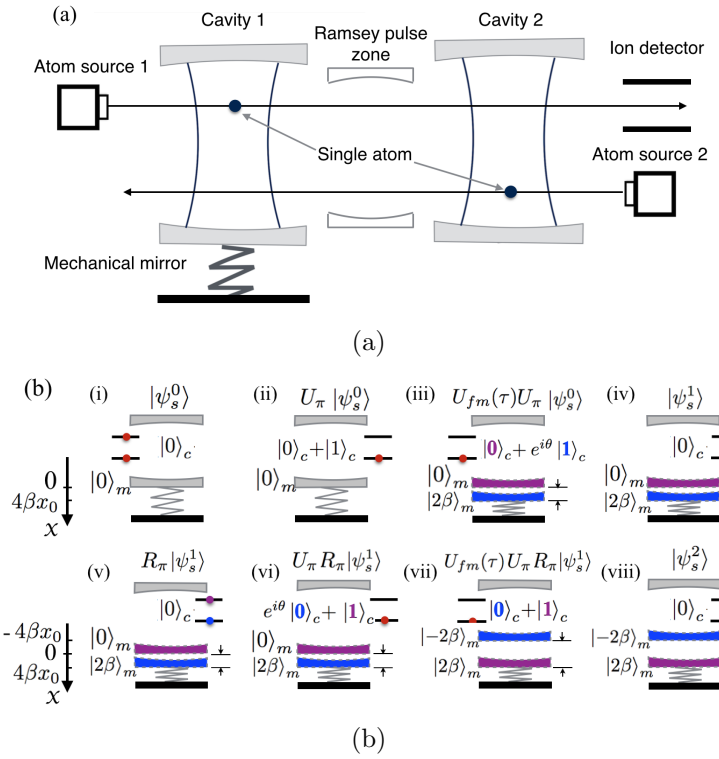

Figure 19: (a) Experimental setup for the generation of a macroscopic superposition state. Cavity 1 is an optomechanical cavity and Cavity 2 is an auxiliary cavity which serves as an atom recycling device together with Atom source 2. (b) Illustration of states of the system for the first seven unitary operations starting from $|\psi_s^0\rangle$. In each graph, the double lines represent a two-level atom, and the center dot is the state of the atom. The state of a mirror is entangled with the state of the atom or the cavity field for the same color (see text). The atom on the left of each cavity is a new atom entering the cavity and the atom on the right is recycled (discarded) if it is in a superposition state (the ground state).

qubit π pulse for less than 50 ps is also available [110]. In general, our proposal is applicable to other optomechanical platforms, such as micromechanical oscillators [24, 51, 50, 78].

IV.A The model

We consider a cavity (Cavity 1 in Fig. 19 (a)) with one mechanical mirror of mass m and mechanical frequency ω_m. The Hamiltonian of the system is described

by [65]

$$\mathcal{H}_{fm} = \hbar\omega_c c^\dagger c + \hbar\omega_m b^\dagger b - \hbar g c^\dagger c(b^\dagger + b), \tag{4.1}$$

where ω_c is the cavity photon frequency, b and c are annihilation operators of the mirror and the cavity field mode, respectively, and $g = (\omega_c/L)x_0$ is the single-photon coupling strength with L being the cavity length and $x_0 = \sqrt{\hbar/2m\omega_m}$ is the zero-point fluctuation. The unitary evolution operator of the system can be obtained exactly as [66] $U_{fm}(t) = e^{-i\omega_c t c^\dagger c} e^{i\phi(t)(c^\dagger c)^2} \mathcal{D}\left(\eta(t)c^\dagger c\right) e^{-i\omega_m t b^\dagger b}$ with $\phi(t) = \beta^2\left(\omega_m t - \sin(\omega_m t)\right)$, the displacement operator $\mathcal{D}(\alpha) = e^{\alpha b^\dagger - \alpha^* b}$, $\eta(t) = \beta(1 - e^{-i\omega_m t})$, and $\beta = g/\omega_m$ (also see Appendix A). The first and the last terms in the product are the free evolution of the field and the mirror, respectively. The second term describes a Kerr-like effect of the cavity in the single-photon strong coupling regime [63, 64]. The coupling between the mechanical mirror and the cavity field acts as the displacement operator $\mathcal{D}$ on the mirror and the strength is proportional to $\beta c^\dagger c$.

IV.B Macroscopic superposition

To understand the physical mechanism of our proposal, we plot the states of the system for the first seven steps in Fig. 19 (a) and we treat the interaction without considering the atomic decoherence and the cavity decay. We initially prepare the mirror in the ground state $|0\rangle_m$, and both cavities in the vacuum state $|0\rangle_c$. We send a two-level atom in a superposition state $|\psi_a\rangle = \frac{1}{\sqrt{2}}(|g\rangle_a + |e\rangle_a)$ into Cavity 1 interacting for a π Rabi operation U_π [82] from Atom source 1. Here $|g\rangle_a$ ($|e\rangle_a$) is the ground (excited) state of the atom. The atomic superposition state is mapped to the photonic superposition state as $U_\pi|\psi_s^0\rangle = |g\rangle_a|\psi_c\rangle|0\rangle_m$, where $|\psi_s^0\rangle = |\psi_a\rangle|0\rangle_c|0\rangle_m$ is the initial state of the system. This operation is illustrated in Fig. 19 (b) graph (ii). Here we assume the atom-field coupling strength $g_c \gg \omega_m$ so that, during the atom-field interaction, the effect of the mechanical mirror from Hamiltonian (4.1) is

negligible (see Appendix C.1).

Now the atom just leaves the cavity after the interaction and the field-mirror evolves according to U_{fm}. After a half cycle $\tau = \pi/\omega_m$ of the mirror's oscillation, the whole system will evolve as $U_{fm}(\tau)U_\pi|\psi_s^0\rangle = \frac{1}{\sqrt{2}}|g\rangle_a \left(|0\rangle_c|0\rangle_m + e^{i\theta}|1\rangle_c|2\beta\rangle_m\right)$, where $\theta = \pi\beta^2$ and the free evolution of the cavity field is omitted. This operation generates entanglement between the cavity field and the mirror as shown in Fig. 19 (b) graph (iii). We then send another atom in $|g\rangle_a$ from Atom source 1 into the cavity for another π Rabi operation in order to map the photonic state to the atomic state. The system evolves to

$$\begin{aligned} |\psi_s^1\rangle &= U_\pi U_{fm}(\tau)U_\pi|\psi_s^0\rangle \\ &= \frac{1}{\sqrt{2}}|0\rangle_c \left(|g\rangle_a|0\rangle_m - e^{i\theta}|e\rangle_a|2\beta\rangle_m\right). \end{aligned} \tag{4.2}$$

The field-mirror interaction due to radiation pressure is switched off and the mirror is entangled with the atom outside the cavity. The separation of the two superposed states of the mirror is $4\beta x_0$ (Fig. 19 (b) graph (iv)).

To magnify the separation of the superposed states, we use a Ramsey π pulse R_π and atom-field state mapping as illustrated in Fig. 19 (b) graphs (v)-(viii). We first apply a fast π pulse to flip the atomic state $R_\pi|\psi_s^1\rangle = \frac{1}{\sqrt{2}}|0\rangle_c \left(|e\rangle_a|0\rangle_m + e^{i\theta}|g\rangle_a|2\beta\rangle_m\right)$. Then we recycle the atom back into Cavity 1, mapping the atomic state to photonic state as $U_\pi R_\pi|\psi_s^1\rangle = \frac{1}{\sqrt{2}}|g\rangle_a \left(|1\rangle_c|0\rangle_m + e^{i\theta}|0\rangle_c|2\beta\rangle_m\right)$. The recycling of the atomic state can be realized by passing the atom through an auxiliary cavity Cavity 2 for a π Rabi operation and sending another atom from Atomic source 2 through Cavity 2 and Cavity 1 for a π Rabi operation, respectively. The atomic state is passed from the first atom to the second atom. After the π Rabi operation, the second atom leaves Cavity 1. Now the system is under the evolution of U_{fm} as

$U_{fm}(\tau)U_\pi R_\pi|\psi_s^1\rangle = \frac{1}{\sqrt{2}}e^{i\theta}|g\rangle_a\left(|1\rangle_c|2\beta\rangle_m + |0\rangle_c|-2\beta\rangle_m\right)$. As shown in Fig. 19 (b) graph (vii), the superposed states of the mirror are separated two-fold further than that using a single-photon only. We then send in another atom from Atom source 1 in $|g\rangle_a$ to map the photonic state back to the atom and the state of the system is represented by

$$\begin{aligned} |\psi_s^2\rangle &= U_\pi U_{fm}(\tau)U_\pi R_\pi|\psi_s^1\rangle \\ &= \frac{1}{\sqrt{2}}e^{i\theta}|0\rangle_c\left(-|e\rangle_a|2\beta\rangle_m + |g\rangle_a|-2\beta\rangle_m\right). \end{aligned} \tag{4.3}$$

We notice that the mirror is entangled with the atom similar to that of state $|\psi_s^1\rangle$, except that the separation between two superposed states is doubled (Fig. 19 (b) (viii)).

To increase the difference of the two mechanical states further, we repeat the above procedure many times. After $2N$ procedures, the state of the system is given by

$$\begin{aligned} |\psi_s^{2N}\rangle &= \left(\prod_{n=1}^{2N-1} U_\pi U_{fm}(\tau)U_\pi R_\pi\right)\left(U_\pi U_{fm}(\tau)U_\pi\right)|\psi_s^0\rangle \\ &= \frac{e^{iN\theta}}{\sqrt{2}}|0\rangle_c\left(-|e\rangle_a|2N\beta\rangle_m + |g\rangle_a|-2N\beta\rangle_m\right), \end{aligned} \tag{4.4}$$

The global phase $e^{iN\theta}$ can be neglected hereafter. We now apply a $\frac{\pi}{2}$ pulse $R_{\frac{\pi}{2}}$ to the atom, which transforms $|g\rangle_a \to (|g\rangle_a + |e\rangle_a)/\sqrt{2}$ and $|e\rangle_a \to (-|g\rangle_a + |e\rangle_a)/\sqrt{2}$, and detect the state of the atom. The mirror state collapses to

$$|\psi_{m\pm}^{2N}\rangle = \frac{1}{\sqrt{4\mathcal{P}_\pm^{2N}}}\Big(|2N\beta\rangle_m \pm |-2N\beta\rangle_m\Big). \tag{4.5}$$

Here the $+$ $(-)$ sign corresponds to the atomic detection in state $|g\rangle_a$ $(|e\rangle_a)$. The

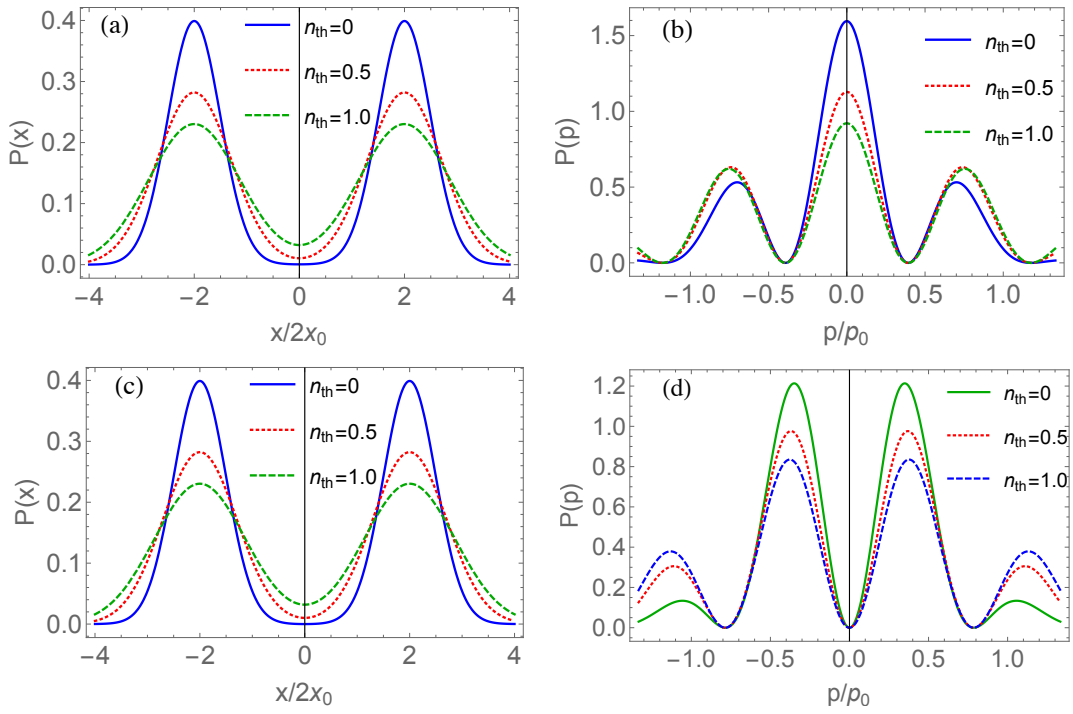

Figure 20: Quadrature distributions of the density matrix $\rho^{2N}_{m\pm}(n_{\rm th})$. (a) Position distribution and (b) momentum distribution of $\rho^{2N}_{m+}(n_{\rm th})$, and (c) position distribution and (d) momentum distribution of $\rho^{2N}_{m-}(n_{\rm th})$, at $n_{\rm th} = 0$ (blue solid curve), $n_{\rm th} = 0.5$ (red dotted curve), and $n_{\rm th} = 1.0$ (green dashed curve). $2N\beta = 2$ (for all the following figures) and $p_0 = \hbar/(2x_0)$.

macroscopic superposition state is deterministically generated, albeit the specific state is conditioned on the measurement result with probability $\mathcal{P}^{2N}_{\pm} = \left(1 \pm e^{-8N^2\beta^2}\right)/2$. The superposition state gives an average position separation between $|2N\beta\rangle_m$ and $|-2N\beta\rangle_m$ of $8N\beta x_0$. Therefore, the superposition state (4.5) is considered as a macroscopic state for $4N\beta \gtrsim 1$ and the demanding condition of a strong coupling rate [26, 38, 66] is relaxed by the number of repetitions. We note that for the largest amplitude of the mirror's coherent states obtained in this paper, the resonant cavity frequency ω_c is not affected appreciably since $x_0/L \sim 10^{-11}$ for realistic parameters.

For a finite temperature T, the mirror is initially prepared in a thermal state

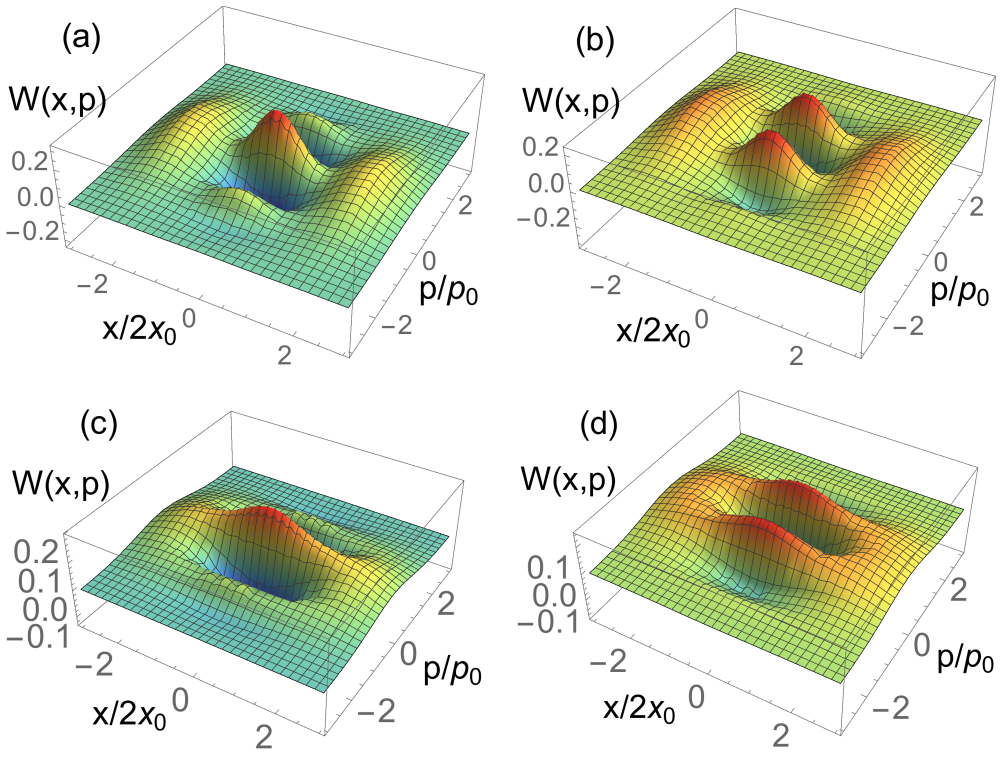

Figure 21: (Wigner distributions $W(x,p)$ of (a) $\rho^{2N}_{m+}(0)$, (b) $\rho^{2N}_{m-}(0)$, (c) $\rho^{2N}_{m+}(1.0)$, and (d) $\rho^{2N}_{m-}(1.0)$.

given by $\rho^0_m(n_{\rm th}) = \frac{1}{\pi n_{\rm th}} \int d^2\alpha e^{-|\alpha|^2/n_{\rm th}} (|\alpha\rangle\langle\alpha|)_m$ with thermal phonon number $n_{\rm th} = (e^{\hbar\omega_m/k_BT} - 1)^{-1}$ and k_B is the Boltzmann constant. After $2N$ repetitions and the final measurement as described above, the state of the mirror is given by the density operator $\rho^{2N}_{m\pm}(n_{\rm th}) = \frac{1}{\pi n_{\rm th}} \int d^2\alpha e^{-|\alpha|^2/n_{\rm th}} |\psi^{2N}_{m\pm}(\alpha)\rangle\langle\psi^{2N}_{m\pm}(\alpha)|$, where $|\psi^{2N}_{m\pm}(\alpha)\rangle = \frac{1}{\sqrt{4\mathcal{P}^{2N}_{\pm}}} \big(|\alpha + 2N\beta\rangle_m \pm |\alpha - 2N\beta\rangle_m\big)$. The final density operator $\rho^{2N}_{m\pm}(n_{\rm th})$ represents a mixed state of superposition states each with a separation of $4N\beta$. Ground-state cooling ($n_{\rm th} < 1.0$) of optomechanical mirror has been realized in recent experiments [50, 51]. For close to ground-state cooled initial state ($n_{\rm th} = 1.0$), the quadrature distributions and phase-space distributions of $\rho^{2N}_{m\pm}(n_{\rm th})$ approximate those of the pure superposition states $|\psi^{2N}_{m\pm}\rangle$ with reduced visibility and peaks (see Figs. 20 and 21).

IV.C Experimental feasibility

We now discuss the experimental feasibility of our scheme. To generate a macroscopic superposition of the mechanical mirror, fast photonic qubit flipping is required. This depends on strong coherent state mapping between an atom and a cavity field, and fast atomic π pulse. Strong atom-field coupling in cavity QED [82] and ultrafast π pulse in less than 50 ps [110] are realizable in current experiment. Fast atomic π pulse also avoids the rotation of the mirror's coherent state and the atomic state decoherence. Atomic state recycling is possible by transferring from Cavity 1 to Cavity 2 [109] and recovering it back with another atom moving from the opposite direction through both cavities. For atomic speed $\sim$ 500m/s [82], it can move a maximum of 10^{-5}m within half period of the mirror's oscillation. The experimental setup may be possible with this dimension within the near future [17].

We neglect the effect of the mechanical mirror during the atom-field interaction. By including this effect, we obtain the generated state after the same procedures as $|\bar{\psi}_s^{2N}\rangle \approx \frac{1}{\sqrt{2}}|0\rangle_c\Big(|g\rangle_a|2N\beta'\rangle_m - |e\rangle_a|-2N\beta'\rangle_m\Big)$, where $\beta' = \beta(1-e^{-i\frac{\pi}{2}\frac{\omega_m}{g_c}}) + \beta\frac{4g_c^2(1+\cos(\frac{\pi}{2}\frac{\omega_m}{g_c}))}{4g_c^2-\omega_m^2}$ (see Appendix C.1). We study this effect by considering the fidelity between $|\bar{\psi}_s^{2N}\rangle$ and $|\psi_s^{2N}\rangle$ in Eq. (4.4) and we find it negligible for large ratio of g_c/ω_m (Fig. 22 (a)). We also study the error due to imperfect timing control which results in a balance between the timing percentage error and N to retain a high fidelity (Fig. 22 (b)). The generated state under variation of the atom-field interaction time is given by $|\bar{\bar{\psi}}_s^{2N}\rangle \approx -C_1\frac{e^{iN\theta}}{\sqrt{2}}|0\rangle_c|e\rangle_a|2N\beta\rangle_m + C_2\frac{e^{iN\theta}}{\sqrt{2}}|0\rangle_c|g\rangle_a|-2N\beta\rangle_m$, where $C_j = \prod_{k=0}^{N-1}\sin(g_c\tau_{4k+2j-1})\sin(g_c\tau_{4k+2j})$ $(j=1,2)$ and τ_i is the ith atom-field interaction time (see Appendix C.2). Similar effect applies to imperfect controlled atom-field coupling rate g_c for each iteration.

In the resolved side-band regime, $\kappa \ll \omega_m$, ground-state cooling is possible and

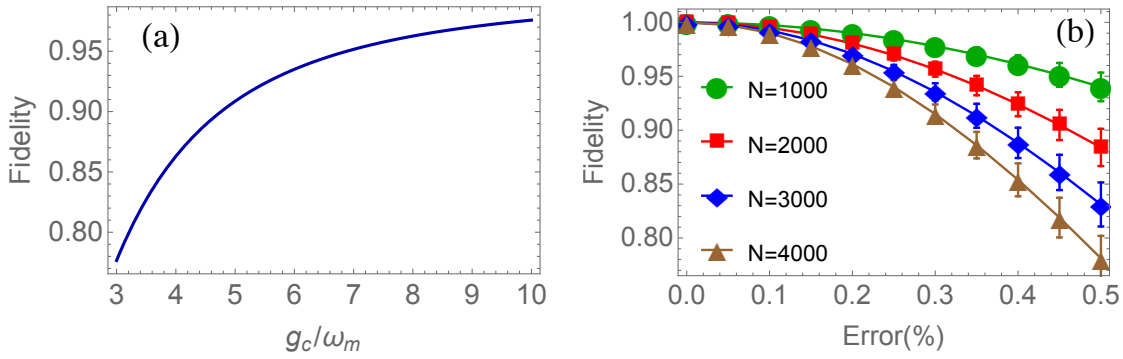

Figure 22: (a) Fidelity between the state $|\bar{\psi}_s^{2N}\rangle$and the state $|\psi_s^{2N}\rangle$ versus the ratio of g_c/ω_m. (b) Fidelity between the state $|\bar{\psi}_s^{2N}\rangle$ and the state $|\psi_s^{2N}\rangle$ versus atom-field interaction time percentage error for $N = 1000$ (green dot), $N = 2000$ (red square), $N = 3000$ (blue diamond), and $N = 4000$ (brown triangle). The fidelity is calculated at each error bar for 1000 samples of $4N$ Gaussian random numbers with mean of $\frac{\pi}{2}$ and standard deviation of the corresponding percentage error. The error bar is enlarged ten times for visual purpose.

has been realized in optomechanics recently [50, 51]. In a null-result measurement [77] when no photon leaks out of the cavity, decay of the single photon reduces the amplitude in the mechanical state that is entangled with the single photon. Since the single photon is entangled with the superposed states of the mirror alternatively in our scheme, the effect of the cavity field decay can be reversed for even number of procedures with a probability of $e^{-N\kappa\tau}$ (see Appendix C.3). For $N\beta \sim 1$, the probability $e^{-N\kappa\tau}$ is approximately equal to $e^{-\pi\kappa/g}$, therefore our proposal is feasible for $g \sim \kappa$ which is a relaxed condition compared to that of $g \sim \omega_m$ in the resolved side-band regime.

Now we consider some experimental parameters feasible within the near future. We may choose a high-Q micro-cavity with a single-atom coupling rate of $2\pi \times$ 50MHz according to Ref. [111, 112], and a mechanical mirror oscillation frequency $\omega_m \sim 0.1g_c$. Our scheme is not limited by the ratio of a single-photon coupling rate g to ω_m. We require, in order to generation a macroscopic superposition state,

$g/\kappa = Q_c \frac{x_0}{L} \sim 1$, where $Q_c = \omega_c/\kappa$ is the quality factor for the cavity field. With $L = 0.1$cm and $m = 1$ng, we estimate $Q_c \sim 10^{11}$. Ultrahigh quality factor up to 10^9 has been demonstrated in wedge-resonator on a silicon chip [113]. With improved experimental parameters, $g/\kappa \sim 1$ may be possible in the future. Another possibility is to shrink the length of the optomechanical cavity. The finesse of the cavity can be made as $F \sim 10^6$ considering the above parameters.

To measure the generated superposition state $|\psi_{m\pm}^{2N}\rangle$ of the mirror, one may consider the back-action-evading approach [105] operated in the resolved sideband regime. Measurements of sensitivity close to [106] and even below [107] the mechanical quantum zero-point fluctuation have been demonstrated recently which make the measurement of nonclassical mechanical state possible. To obtain accurate mechanical position probability distribution, one uses a two-toned driving field to avoid back-action noise [104]. By varying the phase of the probe field, the mechanical quantum state tomography can be performed using this two-toned technique.

IV.D Discussion and Conclusion

We now discuss the possibility of testing novel decoherence models with our proposal. The generated macroscopic superposition will undergo damping and decoherence according to $\dot{\rho}(t) = -\frac{i\gamma_m}{\hbar}[x, \{p, \rho(t)\}] - \frac{D}{\hbar^2}[x, [x, \rho(t)]]$ [9, 39], where γ_m is the mechanical damping rate and $D = 2m\gamma_m k_B T$ is the diffusion coefficient induced by the environment. The mechanical damping can be made negligible for mechanical mirrors with high quality factor $Q_m = \omega_m/\gamma_m \gg 1$, while the diffusion term dominates the evolution. The decoherence timescale of the off-diagonal elements in the position representation is given by $\tau_{\rm env} = \frac{\hbar^2}{D(\Delta x)^2}$ with Δx the spatial separation of a superposition state. Novel decoherence models may be testable with our scheme such that the corresponding decoherence timescale $\tau_{\rm nov}$ satisfies $\tau_{\rm pre} < \tau_{\rm nov} < \tau_{\rm env}$,

where $\tau_{\rm pre} \approx 2N\tau$ is the total preparation time. For example, the gravitationally induced collapse model [15, 16] gives a decoherence timescale $\tau_{\rm nov} \sim 2$ms with our generated superposition state $2N\beta \sim 2$, according to Ref. [114], which is less than the environment induced decoherence $\tau_{\rm env} \sim 11$ms for our scheme with $Q_m \sim 10^7$ and $T = 0.1$mK. The preparation time, $\tau_{\rm pre} \sim 0.4$ms, is smaller than $\tau_{\rm nov}$. Further more, the above parameters can be varied according to the discussed conditions to be more suitable for experimental realization.

In conclusion, we have proposed a scheme capable of creating macroscopic superposition of a mechanical oscillator without a single-photon strong coupling rate by periodically flipping the photonic qubit state. The scheme is experimentally feasible within the near future, and it may be able to test novel decoherence models.

V. SUMMARY

In this dissertation, we have discussed about several different schemes to prepare quantum states of macroscopic objects in cavity optomechanics, which may have interesting applications related to quantum information, and gravitational-wave detection, as well as fundamental importance for testing quantum mechanics.

In Chapter II, we reviewed the theory of cavity optomechanics with and without a strong external coherent driving field. We obtained the quantum Langevin equations for the field operator and the mechanical oscillator operator. We proposed a simple setup for entangling two movable end mirrors in a Fabry-Perot cavity using a single photon superposition state without coherent driving. Our proposal can generate deterministic entangled phonon states after measuring the cavity photonic state. We showed that two possible entangled states can be generated depending on the measurement outcomes. We quantified the degree of entanglement of the generated states using logarithmic negativity and derived an analytical expression of the negativity for each possible state. Our results showed that the more probable of a state to be generated the smaller the negativity of the state it will be. The experimental feasibility of our scheme is also discussed within current technology.

In Chapter III, we discussed the idea of steady-state entanglement between two end mirrors in doubly-resonant cavity with coherent driving fields. We showed that steady-state entanglement of mirrors are obtained by transferring entanglement from a correlated emission laser in the linearized optomechanical coupling regime. We reviewed the theory of a correlated emission laser as an entanglement source using two types of gain mediums. Then we considered two schemes of doubly-resonant cavity with movable end mirrors using the two types of gain mediums inside the

cavity. Due to the radiation-pressure coupling, each cavity field is coupled to its end mirror in an effective beam-splitter coupling process. Therefore, the mirrors can be cooled down close to their ground state via resolved sideband cooling. The two mirrors are effectively coupled via a down-conversion process, therefore they can be entangled. We showed that close to ground-state entanglement between two movable mirrors can be obtained with realistic experimental parameters.

In Chapter IV, we proposed a scheme to create macroscopic quantum superpositions of a mechanical mirror with large distinguishable coherent states in a cavity optomechanical system via periodically flipping a photonic qubit. Our scheme does not require single-photon strong coupling rate. We prepared a single-photon superposition state $|\psi_c\rangle = \frac{1}{\sqrt{2}}(|0\rangle_c + |1\rangle_c)$ in a Fabry-Perot cavity with one mechanical mirror. A coherent state $|\alpha\rangle_m$ of the mechanical mirror is entangled with the photon state as $\frac{1}{\sqrt{2}}(|0\rangle_c|\alpha\rangle_m + |1\rangle_c|\alpha + 2\beta\rangle_m)$ due to radiation pressure, where 2β is the displacement by the single photon after certain time. To magnify the difference between its superposed mirror states, we periodically flip the cavity field states $|0\rangle_c$ and $|1\rangle_c$. This may be achieved by mapping the photonic state to a flying two-level atom, flipping the atomic state with a fast π pulse, and mapping the atomic state back to the photonic state. By using fast π pulses and flipping photon state alternatively, decoherence of the atomic state can be avoided and the effect of the cavity decay can be reversed probabilistically for null-result measurements. The difference of the two coherent states of the mirror is amplified by the number of procedures performed. The superposition states of the mirror, with two possible outcomes, are obtained by a final measurement of the cavity photon in the basis of $\frac{1}{\sqrt{2}}(|0\rangle_c \pm |1\rangle_c)$. Our scheme can generate macroscopic superposition states with very large separation. Our proposal requires strong coherent mapping, recycling of an atomic state, and fast atomic qubit flipping, which may be possible with improved experimental tech-

nology. In general, this proposal is applicable to other optomechanical platforms, such as micromechanical oscillators in a photonic crystal cavity.

In summary, we studied three novel schemes in cavity optomechanics to generate macroscopic quantum states of mechanical objects. In the future, more attention may be paid on some other interesting quantum states, such as Fock state, and how to apply macroscopic quantum states to improve our technology.

REFERENCES

[1] Agedi N. Boto, Pieter Kok, Daniel S. Abrams, Samuel L. Braunstein, Colin P. Williams, and Jonathan P. Dowling. Quantum interferometric optical lithography: Exploiting entanglement to beat the diffraction limit. *Phys. Rev. Lett.*, 85:2733, 2000.

[2] Michael A Nielsen and Isaac L Chuang. *Quantum Computation and Quantum Information*. Cambridge University Press, 2010.

[3] Paul G. Kwiat, Klaus Mattle, Harald Weinfurter, Anton Zeilinger, Alexander V. Sergienko, and Yanhua Shih. New high-intensity source of polarization-entangled photon pairs. *Phys. Rev. Lett.*, 75:4337, 1995.

[4] C. Monroe, D. M. Meekhof, B. E. King, and D. J. Wineland. A "schrödinger cat" superposition state of an atom. *Science*, 272:1131, 1996.

[5] E. Hagley, X. Ma, G. Nogues, C. Wunderlich, M. Brune, J. M. Raimond, and S. Haroche. Generation of einstein-podolsky-rosen pairs of atoms. *Phys. Rev. Lett.*, 79:1, 1997.

[6] Q. A. Turchette, C. S. Wood, B. E. King, C. J. Myatt, D. Leibfried, W. M. Itano, C. Monroe, and D. J. Wineland. Deterministic entanglement of two trapped ions. *Phys. Rev. Lett.*, 81:3631, 1998.

[7] Markus Arndt, Olaf Nairz, Julian Vos-Andreae, Claudia Keller, Gerbrand van der Zouw, and Anton Zeilinger. Wave-particle duality of c60 molecules. *Nature*, 401:680, 1999.

[8] Stefan Gerlich, Sandra Eibenberger, Mathias Tomandl, Stefan Nimmrichter, Klaus Hornberger, Paul J Fagan, Jens Tüxen, Marcel Mayor, and Markus Arndt. Quantum interference of large organic molecules. *Nat. Commun.*, 2:263,

2011.

[9] Wojciech Hubert Zurek. Decoherence, einselection, and the quantum origins of the classical. *Rev. Mod. Phys.*, 75:715, 2003.

[10] S. Nimmrichter and K Hornberger. Ultrafast gates for single atomic qubits. *Phys. Rev. Lett.*, 110:160403, 2013.

[11] John Ellis, John S. Hagelin, D.V. Nanopoulos, and M. Srednicki. Search for violations of quantum mechanics. *Nucl. Phys. B*, 241:381, 1984.

[12] J. Ellis, S. Mohanty, and D. V. Nanopoulos. Quantum gravity and the collapse of the wavefunction. *Phys. Lett B*, 221:113, 1989.

[13] G. C. Ghirardi, A. Rimini, and T. Weber. Unified dynamics for microscopic and macroscopic systems. *Phys. Rev. D*, 34:470, 1986.

[14] Gian Carlo Ghirardi, Philip Pearle, and Alberto Rimini. Markov processes in hilbert space and continuous spontaneous localization of systems of identical particles. *Phys. Rev. A*, 42:78, 1990.

[15] L. Diósi. Models for universal reduction of macroscopic quantum fluctuations. *Phys. Rev. A*, 40:1165, 1989.

[16] R. Penrose. On gravity's role in quantum state reduction. *Gen. Relativ. Gravit*, 28:581, 1996.

[17] Markus Aspelmeyer, Tobias J Kippenberg, and Florian Marquardt. Cavity optomechanics. *Rev. Mod. Phys.*, 86:1394, 2014.

[18] J. M. Dobrindt, I. Wilson-Rae, and T. J. Kippenberg. Parametric normal-mode splitting in cavity optomechanics. *Phys. Rev. Lett.*, 101:263602, 2008.

[19] Simon Groblacher, Klemens Hammerer, Michael R. Vanner, and Markus Aspelmeyer. Observation of strong coupling between a micromechanical resonator and an optical cavity field. *Nature*, 460:724, 2009.

[20] G. S. Agarwal and Sumei Huang. Electromagnetically induced transparency

in mechanical effects of light. *Phys. Rev. A*, 81:041803, 2010.

[21] Stefan Weis, Rémi Rivière, Samuel Deléglise, Emanuel Gavartin, Olivier Arcizet, Albert Schliesser, and Tobias J Kippenberg. Optomechanically induced transparency. *Science*, 330:1520, 2010.

[22] Amir H Safavi-Naeini, TP Mayer Alegre, Jasper Chan, Matt Eichenfield, Martin Winger, Qiang Lin, Jeffrey T Hill, Darrick E Chang, and Oskar Painter. Electromagnetically induced transparency and slow light with optomechanics. *Nature*, 472:69, 2011.

[23] Daniel W. C. Brooks, Thierry Botter, Sydney Schreppler, Thomas P. Purdy, Nathan Brahms, and Dan M. Stamper-Kurn. Non-classical light generated by quantum-noise-driven cavity optomechanics. *Nature*, 488:476, 2012.

[24] Amir H. Safavi-Naeini, Simon Groblacher, Jeff T. Hill, Jasper Chan, Markus Aspelmeyer, and Oskar Painter. Squeezed light from a silicon micromechanical resonator. *Nature*, 500:185, 2013.

[25] T. P. Purdy, P.-L. Yu, R. W. Peterson, N. S. Kampel, and C. A. Regal. Strong optomechanical squeezing of light. *Phys. Rev. X*, 3:031012, 2013.

[26] William Marshall, Christoph Simon, Roger Penrose, and Dik Bouwmeester. Towards quantum superpositions of a mirror. *Phys. Rev. Lett.*, 91:130401, 2003.

[27] D. Vitali, S. Gigan, A. Ferreira, H. R. Böhm, P. Tombesi, A. Guerreiro, V. Vedral, A. Zeilinger, and M. Aspelmeyer. Optomechanical entanglement between a movable mirror and a cavity field. *Phys. Rev. Lett.*, 98:030405, 2007.

[28] C. Genes, A. Mari, P. Tombesi, and D. Vitali. Robust entanglement of a micromechanical resonator with output optical fields. *Phys. Rev. A*, 78:032316, 2008.

[29] T. A. Palomaki, J. D. Teufel, R. W. Simmonds, and K. W. Lehnert. Entangling

mechanical motion with microwave fields. *Science*, 342:710, 2013.

[30] Jing Zhang, Kunchi Peng, and Samuel L Braunstein. Quantum-state transfer from light to macroscopic oscillators. *Phys. Rev. A*, 68:013808, 2003.

[31] Michel Pinard, Aurelien Dantan, David Vitali, Olivier Arcizet, Tristan Briant, and Antoine Heidmann. Entangling movable mirrors in a double-cavity system. *Europhys. Lett.*, 72:747, 2005.

[32] David Vitali, Stefano Mancini, and Paolo Tombesi. Stationary entanglement between two movable mirrors in a classically driven fabry–perot cavity. *J. Phys. A*, 40:8055, 2007.

[33] Sumei Huang and GS Agarwal. Entangling nanomechanical oscillators in a ring cavity by feeding squeezed light. *New J. Phys.*, 11:103044, 2009.

[34] Han Xiong, Marlan O Scully, and M Suhail Zubairy. Correlated spontaneous emission laser as an entanglement amplifier. *Phys. Rev. Lett.*, 94:023601, 2005.

[35] Ling Zhou, Yan Han, Jietai Jing, and Weiping Zhang. Entanglement of nanomechanical oscillators and two-mode fields induced by atomic coherence. *Phys. Rev. A*, 83:052117, 2011.

[36] O. Romero-Isart, A. C. Pflanzer, F. Blaser, R. Kaltenbaek, N. Kiesel, M. Aspelmeyer, and J. I. Cirac. Large quantum superpositions and interference of massive nanometer-sized objects. *Phys. Rev. Lett.*, 107:020405, 2011.

[37] Zhang-qi Yin, Tongcang Li, Xiang Zhang, and L. M. Duan. Large quantum superpositions of a levitated nanodiamond through spin-optomechanical coupling. *Phys. Rev. A*, 88:033614, 2013.

[38] S. Bose, K. Jacobs, and P. L. Knight. Scheme to probe the decoherence of a macroscopic object. *Phys. Rev. A*, 59:3204, 1999.

[39] Dustin Kleckner, Igor Pikovski, Evan Jeffrey, Luuk Ament, Eric Eliel, Jeroen van den Brink, and Dirk Bouwmeester. Creating and verifying a quantum

superposition in a micro-optomechanical system. *New J. Phys.*, 10:095020, 2008.

[40] Kater W Murch, Kevin L Moore, Subhadeep Gupta, and Dan M Stamper-Kurn. Observation of quantum-measurement backaction with an ultracold atomic gas. *Nat. Phys.*, 4:561, 2008.

[41] M. Bhattacharya and P. Meystre. Multiple membrane cavity optomechanics. *Phys. Rev. A*, 78:041801, 2008.

[42] Georg Heinrich, Max Ludwig, Jiang Qian, Björn Kubala, and Florian Marquardt. Collective dynamics in optomechanical arrays. *Phys. Rev. Lett.*, 107:043603, 2011.

[43] André Xuereb, Claudiu Genes, and Aurélien Dantan. Strong coupling and long-range collective interactions in optomechanical arrays. *Phys. Rev. Lett.*, 109:223601, 2012.

[44] Brian Pepper, Roohollah Ghobadi, Evan Jeffrey, Christoph Simon, and Dirk Bouwmeester. Optomechanical superpositions via nested interferometry. *Phys. Rev. Lett.*, 109:023601, 2012.

[45] Pavel Sekatski, Markus Aspelmeyer, and Nicolas Sangouard. Macroscopic optomechanics from displaced single-photon entanglement. *Phys. Rev. Lett.*, 112:080502, 2014.

[46] R. Ghobadi, S. Kumar, B. Pepper, D. Bouwmeester, I. Lvovsky, A. and C. Simon. Optomechanical micro-macro entanglement. *Phys. Rev. Lett.*, 112:080503, 2014.

[47] Alessandra Buonanno and Yanbei Chen. Signal recycled laser-interferometer gravitational-wave detectors as optical springs. *Phys. Rev. D*, 65:042001, 2002.

[48] I. Wilson-Rae, N. Nooshi, W. Zwerger, and T. J. Kippenberg. Theory of ground state cooling of a mechanical oscillator using dynamical backaction. *Phys. Rev.*

Lett., 99:093901, 2007.

[49] Florian Marquardt, Joe P. Chen, A. A. Clerk, and S. M. Girvin. Quantum theory of cavity-assisted sideband cooling of mechanical motion. *Phys. Rev. Lett.*, 99:093902, 2007.

[50] J. D. Teufel, T. Donner, Dale Li, J. W. Harlow, M. S. Allman, K. Cicak, A. J. Sirois, J. D. Whittaker, K. W. Lehnert, and R. W. Simmonds. Sideband cooling of micromechanical motion to the quantum ground state. *Nature*, 475:359, 2011.

[51] Jasper Chan, T. P. Mayer Alegre, Amir H. Safavi-Naeini, Jeff T. Hill, Alex Krause, Simon Groblacher, Markus Aspelmeyer, and Oskar Painter. Laser cooling of a nanomechanical oscillator into its quantum ground state. *Nature*, 478:89, 2011.

[52] Stefano Mancini, Vittorio Giovannetti, David Vitali, and Paolo Tombesi. Entangling macroscopic oscillators exploiting radiation pressure. *Phys. Rev. Lett.*, 88:120401, 2002.

[53] Michael J. Hartmann and Martin B. Plenio. Steady state entanglement in the mechanical vibrations of two dielectric membranes. *Phys. Rev. Lett.*, 101:200503, 2008.

[54] Max Ludwig, K. Hammerer, and Florian Marquardt. Entanglement of mechanical oscillators coupled to a nonequilibrium environment. *Phys. Rev. A*, 82:012333, 2010.

[55] Giovanni Vacanti, Mauro Paternostro, G Massimo Palma, and Vlatko Vedral. Optomechanical to mechanical entanglement transformation. *New J. Phys.*, 10:095014, 2008.

[56] K. Børkje, A. Nunnenkamp, and S. M. Girvin. Proposal for entangling remote micromechanical oscillators via optical measurements. *Phys. Rev. Lett.*,

107:123601, 2011.

[57] Chaitanya Joshi, Jonas Larson, Mats Jonson, Erika Andersson, and P Öhberg. Entanglement of distant optomechanical systems. *Phys. Rev. A*, 85:033805, 2012.

[58] Wenchao Ge, Mohammad Al-Amri, Hyunchul Nha, and M Suhail Zubairy. Entanglement of movable mirrors in a correlated-emission laser. *Phys. Rev. A*, 88:022338, 2013.

[59] Wenchao Ge, M Al-Amri, Hyunchul Nha, and M Suhail Zubairy. Entanglement of movable mirrors in a correlated emission laser via cascade-driven coherence. *Phys. Rev. A*, 88:052301, 2013.

[60] P Rabl, C Genes, K Hammerer, and M Aspelmeyer. Phase-noise induced limitations on cooling and coherent evolution in optomechanical systems. *Phys. Rev. A*, 80:063819, 2009.

[61] Jie-Qiao Liao, Qin-Qin Wu, and Franco Nori. Entangling two macroscopic mechanical mirrors in a two-cavity optomechanical system. *Phys. Rev. A*, 89:014302, 2014.

[62] Hugo Flayac and Vincenzo Savona. Heralded preparation and readout of entangled phonons in a photonic crystal cavity. *Phys. Rev. Lett.*, 113:143603, 2014.

[63] P. Rabl. Photon blockade effect in optomechanical systems. *Phys. Rev. Lett.*, 107:063601, 2011.

[64] A. Nunnenkamp, K. Borkje, and S. M. Girvin. Single-photon optomechanics. *Phys. Rev. Lett.*, 107:063602, 2011.

[65] C. K. Law. Interaction between a moving mirror and radiation pressure: A hamiltonian formulation. *Phys. Rev. A*, 51:2537, 1995.

[66] S. Bose, K. Jacobs, and P. L. Knight. Preparation of nonclassical states in

cavities with a moving mirror. *Phys. Rev. A*, 56:4175–4186, 1997.

[67] M. O. Scully and M. S. Zubairy. *Quantum Optics*. Cambridge University Press, New York, 1997.

[68] Rafael Benguria and Mark Kac. Quantum langevin equation. *Phys. Rev. Lett.*, 46:1, 1981.

[69] M. Plenio, S. Huelga, A. Beige, and P. Knight. Cavity-loss-induced generation of entangled atoms. *Phys. Rev. A*, 59:2468, 1999.

[70] Jian Li, K. Chalapat, and G. Paraoanu. Entanglement of superconducting qubits via microwave fields: Classical and quantum regimes. *Phys. Rev. B*, 78:064503, 2008.

[71] G. Vidal and R. F. Werner. Computable measure of entanglement. *Phys. Rev. A*, 65:032314, 2002.

[72] Asher Peres. Separability criterion for density matrices. *Phys. Rev. Lett.*, 77:1413, 1996.

[73] Michał Horodecki, Paweł Horodecki, and Ryszard Horodecki. Separability of mixed states: necessary and sufficient conditions. *Phys. Lett. A*, 223:1, 1996.

[74] Lu-Ming Duan, G. Giedke, J. Cirac, and P. Zoller. Inseparability criterion for continuous variable systems. *Phys. Rev. Lett.*, 84:2722, 2000.

[75] R. Simon. Peres-horodecki separability criterion for continuous variable systems. *Phys. Rev. Lett.*, 84:2726, 2000.

[76] Mark Hillery and M. Zubairy. Entanglement conditions for two-mode states. *Phys. Rev. Lett.*, 96:050503, 2006.

[77] Qingqing Sun, Hyunchul Nha, and M. Zubairy. Entanglement criteria and nonlocality for multimode continuous-variable systems. *Phys. Rev. A*, 80:020101, 2009.

[78] J-M Pirkkalainen, SU Cho, Jian Li, GS Paraoanu, PJ Hakonen, and MA Sil-

lanpää. Hybrid circuit cavity quantum electrodynamics with a micromechanical resonator. *Nature*, 494:211, 2013.

[79] Shimon Kolkowitz, Ania C Bleszynski Jayich, Quirin P Unterreithmeier, Steven D Bennett, Peter Rabl, JGE Harris, and Mikhail D Lukin. Coherent sensing of a mechanical resonator with a single-spin qubit. *Science*, 335:1603, 2012.

[80] A. Asadian, C. Brukner, and P. Rabl. Probing macroscopic realism via ramsey correlation measurements. *Phys. Rev. Lett.*, 112:190402, 2014.

[81] Wenchao Ge and M. Suhail Zubairy. Macroscopic optomechanical superposition via periodic qubit flipping. *Phys. Rev. A*, 91:013842, 2015.

[82] J. M. Raimond, M. Brune, and S. Haroche. Manipulating quantum entanglement with atoms and photons in a cavity. *Rev. Mod. Phys.*, 73:565, 2001.

[83] E. Schrödinger. Entanglement in correlated spontaneous emission lasers. *Pro. Cambridge Philos. Soc.*, 31:555, 1935.

[84] A. Ekert D. Bouwmeester and A. Zeilinger. *The Physics of Quantum Information*. Springer, Berlin, New York, 2000.

[85] M. Kiffner, M. S. Zubairy, J. Evers, and C. H. Keitel. Two-mode single-atom laser as a source of entangled light. *Phys. Rev. A*, 75:033816, 2007.

[86] Shahid Qamar, S-Y Zhu, and MS Zubairy. Two-photon phase-sensitive amplifier via raman-driven coherence. *Opt. Commun.*, 147:274, 1998.

[87] Sajid Qamar, M. Al-Amri, and M. Suhail Zubairy. Entanglement in a bright light source via raman-driven coherence. *Phys. Rev. A*, 79:013831, 2009.

[88] Sajid Qamar, M. Al-Amri, Shahid Qamar, and M. Suhail Zubairy. Entangled radiation via a raman-driven quantum-beat laser. *Phys. Rev. A*, 80:033818, 2009.

[89] Mohammad Al-Amri, Sajid Qamar, Shahid Qamar, and M Suhail Zubairy. En-

tanglement in correlated spontaneous emission lasers. *Quantum Inf. Process.*, 8:587, 2009.

[90] Daniel Sigg. Commissioning of the ligo detectors. *Class. Quantum Grav.*, 19:1429, 2002.

[91] Marlan O. Scully. Correlated spontaneous-emission lasers: Quenching of quantum fluctuations in the relative phase angle. *Phys. Rev. Lett.*, 55:2802–2805, 1985.

[92] Nadeem A. Ansari, J. Gea-Banacloche, and M. Suhail Zubairy. Phase-sensitive amplification in a three-level atomic system. *Phys. Rev. A*, 41:5179, 1990.

[93] S. Mancini and P. Tombesi. Quantum noise reduction by radiation pressure. *Phys. Rev. A*, 49:4055, 1994.

[94] Crispin Gardiner and Peter Zoller. *Quantum noise: a handbook of Markovian and non-Markovian quantum stochastic methods with applications to quantum optics*, volume 56. Springer Science & Business Media, 2004.

[95] A Hurwitz. *Selected Papers on Mathematical Trends in Control Theory*. Dover New York, 1964.

[96] Hyunchul Nha, Su-Yong Lee, Se-Wan Ji, and M. S. Kim. Efficient entanglement criteria beyond gaussian limits using gaussian measurements. *Phys. Rev. Lett.*, 108:030503, 2012.

[97] O. Arcizet, P.-F. Cohadon, T. Briant, M. Pinard, A. Heidmann, J.-M. Mackowski, C. Michel, L. Pinard, O. Français, and L. Rousseau. High-sensitivity optical monitoring of a micromechanical resonator with a quantum-limited optomechanical sensor. *Phys. Rev. Lett.*, 97:133601, 2006.

[98] M. S. Kim, W. Son, V. Bužek, and P. L. Knight. Entanglement by a beam splitter: Nonclassicality as a prerequisite for entanglement. *Phys. Rev. A*, 65:032323, 2002.

[99] Wang Xiang-bin. Theorem for the beam-splitter entangler. *Phys. Rev. A*, 66:024303, 2002.

[100] C. Genes, D. Vitali, and P. Tombesi. Emergence of atom-light-mirror entanglement inside an optical cavity. *Phys. Rev. A*, 77:050307, 2008.

[101] Ewold Verhagen, Samuel Deléglise, Stefan Weis, Albert Schliesser, and Tobias J Kippenberg. Quantum-coherent coupling of a mechanical oscillator to an optical cavity mode. *Nature*, 482:63, 2012.

[102] A. D. O'Connell, M. Hofheinz1, M. Ansmann, R. C. Bialczak, M. Lenander, E. Lucero, M. Neeley, D. Sank, H. Wang, M. Weides, J. Wenner, J. M. Martinis, and A. N. Cleland. Quantum ground state and single-phonon control of a mechanical resonator. *Nature*, 464:697, 2010.

[103] Amir H Safavi-Naeini, Jasper Chan, Jeff T Hill, Thiago P Mayer Alegre, Alex Krause, and Oskar Painter. Observation of quantum motion of a nanomechanical resonator. *Phys. Rev. Lett.*, 108:033602, 2012.

[104] MR Vanner, I Pikovski, and MS Kim. Towards optomechanical quantum state reconstruction of mechanical motion. *arXiv preprint arXiv:1406.1013*, 2014.

[105] A. A. Clerk, F. Marquardt, and K. Jacobs. Back-action evasion and squeezing of a mechanical resonator using a cavity detector. *New J. Phys.*, 10:095010, 2008.

[106] J. B. Hertzberg, T. Rocheleau, T. Ndukum, M. Savva, A. A. Clerk, and K. C. Schwab. Back-action-evading measurements of nanomechanical motion. *Nat. Phys.*, 6:213, 2010.

[107] J. Suh, A. J. Weinstein, C. U. Lei, E. E. Wollman, S. K. Steinke, P. Meystre, A. A. Clerk, and K. C. Schwab. Mechanically detecting and avoiding the quantum fluctuations of a microwave field. *Science*, 344:1262, 2014.

[108] L. Tian. Entanglement from a nanomechanical resonator weakly coupled to a

single cooper-pair box. *Phys. Rev. B*, 72:195411, 2005.

[109] L Davidovich, N Zagury, M Brune, J. M. Raimond, and S Haroche. Teleportation of an atomic state between two cavities using nonlocal microwave fields. *Phys. Rev. A*, 50:R895, 1994.

[110] W. C. Campbell, J Mizrahi, Q Quraishi, C Senko, D Hayes, D Hucul, D. N. Matsukevich, P Maunz, and C Monroe. Ultrafast gates for single atomic qubits. *Phys. Rev. Lett.*, 105:090502, 2010.

[111] J. McKeever, A. Boca, A. D. Boozer, J. R. Buck, and H. J. Kimble. Experimental realization of a one-atom laser in the regime of strong coupling. *Nature*, 425:268, 2003.

[112] Takao Aoki, Barak Dayan, E. Wilcut, W. P. Bowen, A. S. Parkins, T. J. Kippenberg, K. J. Vahala, and H. J. Kimble. Observation of strong coupling between one atom and a monolithic microresonator. *Nature*, 443:671, 2006.

[113] Hansuek Lee, Tong Chen, Jiang Li, Ki Youl Yang, Seokmin Jeon, Oskar Painter, and Kerry J Vahala. Chemically etched ultrahigh-q wedge-resonator on a silicon chip. *Nat. Photonics*, 6:369, 2012.

[114] B. Pepper, E. Jeffrey, R. Ghobadi, C. Simon, and D. Bouwmeester. Macroscopic superpositions via nested interferometry: finite temperature and decoherence considerations. *New J. Phys.*, 14:115025, 2012.

[115] J. Restrepo, C. Ciuti, and I. Favero. Single-polariton optomechanics. *Phys. Rev. Lett.*, 112:013601, 2014.

APPENDIX A

DERIVATION OF THE UNITARY EVOLUTION OPERATOR FOR AN OPTOMECHANICAL SYSTEM

We derive in the following the unitary evolution operator for an optomechanical system of an electromagnetic field coupled to a mechanical oscillator where the system Hamiltonian is given by Eq. (2.3) as

$$\mathcal{H}_{\rm un} = \hbar\omega_c c^\dagger c + \hbar\omega_m b^\dagger b - \hbar g c^\dagger c(b^\dagger + b). \tag{A.1}$$

The unitary operator is very important for the study of undamped optomechanical system without involving a driving field. Once the unitary evolution is obtained, the dynamics of a specific system can be investigated.

We consider a different approach as compared to the unitary transformation approach used in Ref. [66]. In the interaction picture of the free Hamiltonian $\mathcal{H}_0 = \hbar\omega_c c^\dagger c + \hbar\omega_m b^\dagger b$, the interaction Hamiltonian is given by [67]

$$\begin{aligned} \mathcal{H}_I(t) &= e^{i\frac{\mathcal{H}_0}{\hbar}t}(\mathcal{H}_{\rm un} - \mathcal{H}_0)e^{-i\frac{\mathcal{H}_0}{\hbar}t} \\ &= -\hbar g c^\dagger c(b^\dagger e^{i\omega_m t} + b e^{-i\omega_m t}). \end{aligned} \tag{A.2}$$

The state vector in the interaction picture, $|\psi_I\rangle$, relates the state vector in the Shrödinger picture, $|\psi_s\rangle$, as

$$|\psi_I\rangle = e^{i\frac{\mathcal{H}_0}{\hbar}t}|\psi_s\rangle, \tag{A.3}$$

such that

$$\frac{\partial}{\partial t}|\psi_I\rangle = -\frac{i}{\hbar}\mathcal{H}_I(t)|\psi_I\rangle, \tag{A.4}$$

is satisfied. The unitary evolution operator for the state vector $|\psi_I\rangle$ is given by [67]

$$\begin{aligned} U_I(t) &= 1 - \frac{i}{\hbar}\int_0^t \mathcal{H}_I(t_1)dt_1 + (-\frac{i}{\hbar})^2 \int_o^t dt_1 \int_0^{t_1} dt_2 \mathcal{H}_I(t_1)\mathcal{H}_I(t_2) \\ &+ (-\frac{i}{\hbar})^3 \int_0^t dt_1 \int_0^{t_1} dt_2 \int_0^{t_2} dt_3 \mathcal{H}_I(t_1)\mathcal{H}_I(t_2)\mathcal{H}_I(t_3) + \cdots \end{aligned} \tag{A.5}$$

Plugging the expression $\mathcal{H}_I(t)$, we obtain

$$-\frac{i}{\hbar}\int_0^t \mathcal{H}_I(t_1)dt_1 = \frac{g}{\omega_m}c^\dagger c b^\dagger(e^{i\omega_m t} - 1) - H.c. \tag{A.6}$$

And the third term in $U_I(t)$ as

$$\begin{aligned} & (-\frac{i}{\hbar})^2 \int_0^t dt_1 \int_0^{t_1} dt_2 \mathcal{H}_I(t_1)\mathcal{H}_I(t_2) \\ = & -\frac{i}{\hbar}\int_0^t dt_1 \mathcal{H}_I(t_1)\left(\frac{g}{\omega_m}c^\dagger c b^\dagger(e^{i\omega_m t_1} - 1) - H.c.\right) \\ = & (\frac{g}{\omega_m})^2 (c^\dagger c)^2 \left(\frac{1}{2}b^{\dagger 2}(e^{i\omega_m t} - 1)^2 + H.c.\right) \\ + & (\frac{g}{\omega_m})^2 (c^\dagger c)^2 \left(bb^\dagger(e^{-i\omega_m t} - 1 + i\omega_m t) + b^\dagger b(e^{i\omega_m t} - 1 - i\omega_m t)\right) \\ = & \frac{1}{2}(\frac{g}{\omega_m})^2 (c^\dagger c)^2 \left(b^\dagger(e^{i\omega_m t} - 1) - b(e^{-i\omega_m t} - 1)\right)^2 \\ + & i(\frac{g}{\omega_m})^2 (c^\dagger c)^2 (\omega_m t - \sin\omega_m t) \end{aligned} \tag{A.7}$$

Similarly, one can find higher order terms in $U_I(t)$. By collecting them all, we find

$$U_I(t) = e^{\frac{g}{\omega_m}c^\dagger c b^\dagger(e^{i\omega_m t} - 1) - H.c.} e^{i(\frac{g}{\omega_m})^2 (c^\dagger c)^2 (\omega_m t - \sin\omega_m t)}. \tag{A.8}$$

The state vector in the interaction picture evolves as $|\psi_I(t)\rangle = U_I(t)|\psi_I(0)\rangle$ and the state vector in the Shrödinger picture evolves as

$$|\psi_s(t)\rangle = e^{-i\frac{\mathcal{H}_0}{\hbar}t}U_I(t)|\psi_s(0)\rangle. \tag{A.9}$$

Therefore, the unitary evolution operator for the state vector $|\psi_s\rangle$ in the Shrödinger picture is given by

$$\begin{aligned} U(t) &= e^{-i\frac{\mathcal{H}_0}{\hbar}t}U_I(t) \\ &= e^{-i\frac{\mathcal{H}_0}{\hbar}t}U_I(t)e^{i\frac{\mathcal{H}_0}{\hbar}t}e^{-i\frac{\mathcal{H}_0}{\hbar}t} \\ &= e^{\frac{gc^\dagger c}{\omega_m}b^\dagger(1-e^{-i\omega_m t})-H.c.}e^{i(\frac{gc^\dagger c}{\omega_m})^2(\omega_m t-\sin\omega_m t)}e^{-i\omega_c tc^\dagger c}e^{-i\omega_m tb^\dagger b}, \end{aligned} \tag{A.10}$$

which is exactly the expression used in Chapter II and Chapter IV.

APPENDIX B

THEORY OF A CORRELATED EMISSION LASER

In this appendix, we provide detailed derivations to obtain the reduced density matrix equation for a correlated emission laser. We will show how to trace the atomic subsystem to arrive at the density matrix equation for the fields only. We consider only the linear laser theory [67]. The atomic subsystem is dominated by the strong coherent driving field and its own decay process. Therefore, the atomic subsystem reaches a steady state under the influence of the coherent driving field and the fast decay. The interactions between the cavity modes and the atomic transitions are considered as perturbations to atomic state evolution. The steady state solution is then plugged into the equation of motion for the whole system to obtain the equation of motion for the field modes.

We consider the cascade three-level medium interacting with two cavity modes illustrated in Fig. 5 (a) as an example. The system is governed by the Hamiltonian [34],

$$\mathcal{H}_I^{af} = \hbar g_1(\sigma_{ab}a_1 + a_1^\dagger\sigma_{ba}) + \hbar g_2(\sigma_{bc}a_2 + a_2^\dagger\sigma_{cb}) - \hbar\frac{\Omega}{2}\left(\sigma_{ac}e^{-i\phi} + \sigma_{ca}e^{i\phi}\right). \quad \text{(B.1)}$$

The reduced density matrix equation for the cavity modes is obtained by tracing the atomic variables as

$$\begin{aligned}\dot{\rho}_f &= -\frac{i}{\hbar}\mathrm{Tr_A}[\mathcal{H}_I^{af}, \rho] \\ &= -ig_1[a_1^\dagger, \rho_{ab}] - ig_2[a_2^\dagger, \rho_{bc}] + H.c. \end{aligned} \quad \text{(B.2)}$$

where the density matrix elements ρ_{ab}, ρ_{bc} are determined by the strong coherent field and the fast decay with cavity-atom interactions considered as a perturbation. Note that the density matrix elements $\rho_{ij} = \langle i|\rho_a|j\rangle \otimes \rho_f$, where $i, j = a, b, c$. Up to the first order in g_1 and g_2, the evolution of ρ_{ba}, ρ_{bc} are given by

$$\begin{aligned}
\dot{\rho}_{ba} &= -\gamma\rho_{ba} - ig_1(a_1^\dagger\rho_{aa} - \rho_{bb}a_1^\dagger) - i\frac{\Omega}{2}e^{i\phi}\rho_{bc} - ig_2a_2\rho_{ca}, \\
\dot{\rho}_{bc} &= -\gamma\rho_{bc} - ig_2(a_2\rho_{cc} - \rho_{bb}a_2) - i\frac{\Omega}{2}e^{-i\phi}\rho_{ba} - ig_1a_1^\dagger\rho_{ac},
\end{aligned} \tag{B.3}$$

where γ is the decay rate for the atoms assumed to the same for all levels for simplicity. The evolution of density matrix elements $\rho_{aa}, \rho_{bb}, \rho_{cc}$ and ρ_{ac} are given by

$$\begin{aligned}
\dot{\rho}_{aa} &= -\gamma\rho_{aa} + i\frac{\Omega}{2}(e^{-i\phi}\rho_{ca} - e^{i\phi}\rho_{ac}), \\
\dot{\rho}_{bb} &= -\gamma\rho_{bb}, \\
\dot{\rho}_{cc} &= -\gamma\rho_{cc} - i\frac{\Omega}{2}(e^{-i\phi}\rho_{ca} - e^{i\phi}\rho_{ac}) + r_a\rho_f, \\
\dot{\rho}_{ac} &= -\gamma\rho_{ac} + i\frac{\Omega}{2}e^{-i\phi}(\rho_{aa} - \rho_{cc}),
\end{aligned} \tag{B.4}$$

where the atoms are sent into the cavity initially in the ground state $|c\rangle$ with a pumping rate r_a. Here we neglect the small perturbation due to the coupling between the atomic transitions and the cavity modes in Eq. (B.4). In the steady-state, we obtain from Eq. (B.4) by taking $\dot{\rho}_{ij} = 0$,

$$\begin{aligned}
\rho_{aa} &= \frac{r_a}{2\gamma}\frac{\Omega^2}{\Omega_2 + \gamma^2}\rho_f, \qquad \rho_{bb} = 0, \\
\rho_{cc} &= \frac{r_a}{2\gamma}\frac{\Omega^2 + 2\gamma^2}{\Omega_2 + \gamma^2}\rho_f, \qquad \rho_{ac} = \frac{r_a}{2\gamma}\frac{\Omega\gamma e^{-i\phi}}{\Omega_2 + \gamma^2}\rho_f.
\end{aligned} \tag{B.5}$$

Plugging the above results into Eq. (B.3) and applying the adiabatic approximation,

we obtain

$$\begin{aligned} -ig_2\rho_{bc} &= -\alpha_{21}^* a_1^\dagger \rho_f - \alpha_{22}^* a_2 \rho_f, \\ -ig_1\rho_{ab} &= \alpha_{12}\rho_f a_2^\dagger + \alpha_{11}\rho_f a_1, \end{aligned} \tag{B.6}$$

where

$$\alpha_{11} = \frac{g_1^2 r_a}{4} \frac{3\Omega^2}{(\Omega^2+\gamma^2)(\Omega^2/4+\gamma^2)}, \tag{B.7}$$

$$\alpha_{22} = g_2^2 r_a \frac{1}{(\Omega^2+\gamma^2)}, \tag{B.8}$$

$$\alpha_{12} = ig_1 g_2 \frac{r_a \Omega e^{-i\phi}}{\gamma(\Omega^2+\gamma^2)}, \tag{B.9}$$

$$\alpha_{21} = \frac{ig_1 g_2 r_a}{4} \frac{\Omega(\Omega^2-2\gamma^2)e^{i\phi}}{\gamma(\Omega^2+\gamma^2)(\Omega^2/4+\gamma^2)}, \tag{B.10}$$

By inserting the expressions for ρ_{bc} and ρ_{ab}, we obtain the reduced density matrix equation for the cavity fields as given in Eq. (3.3) in Chapter III. The coefficients α_{ij} recovers to those in Eq.(3.7) when we take $\phi = -\frac{\pi}{2}$.

Now we have derived the reduced density matrix equation for a correlated emission laser in a cascade three-level medium. This approach can be easily extended to derive the density matrix equation for a correlated emission laser in a gain medium with different atomic levels, such as four-level atoms discussed in Sec. C in Chapter III.

APPENDIX C

ATOM-FIELD-MIRROR INTERACTION AND ERROR ANALYSIS

C.1 Full Hamiltonian description of the atom-field-mirror system

Here we study the effect of the mechanical oscillator on the atom-field interaction. The full Hamiltonian of the tripartite system is given by [115]

$$\begin{aligned}\mathcal{H}_{afm} &= \hbar\omega_c c^\dagger c + \hbar\frac{\omega_a}{2}\sigma_z - i\hbar g_c(\sigma_+ c - c^\dagger\sigma_-) \\ &+ \hbar\omega_m b^\dagger b - \hbar g c^\dagger c(b^\dagger + b),\end{aligned} \tag{C.1}$$

where ω_a is the atomic transition frequency, g_c is the atom-field coupling strength, and σ_z, $\sigma_\pm$ are the corresponding Pauli matrices of the atomic pseudospin. In the interaction picture, the Hamiltonian can be rewritten as

$$\mathcal{H}_I = i\hbar g_c(c^\dagger\sigma_- - \sigma_+ c) + \hbar\omega_m b^\dagger b - \hbar g c^\dagger c(b^\dagger + b), \tag{C.2}$$

where we assume $\omega_a = \omega_c$ for simplicity. We perform a unitary transformation $\mathcal{T} = e^{-\beta c^\dagger c(b^\dagger - b)}$ as considered in Ref. [66] such that

$$\begin{aligned}\mathcal{H}_\mathcal{T} = \mathcal{T}\mathcal{H}_I\mathcal{T}^\dagger &= i\hbar g_c\left(c^\dagger\mathcal{D}(-\beta)\sigma_- - \sigma_+ c\mathcal{D}(\beta)\right) + \hbar\omega_m b^\dagger b \\ &\approx i\hbar g_c(c^\dagger\sigma_- - \sigma_+ c) + \hbar\omega_m b^\dagger b \\ &\quad -i\hbar\beta g_c(\sigma_+ c + c^\dagger\sigma_-)(b^\dagger - b),\end{aligned} \tag{C.3}$$

where we the displacement operator $\mathcal{D}(\beta) = e^{\beta(b^\dagger - b)} \approx 1 + \beta(b^\dagger - b)$ for $\beta \ll 1$. In the following, we limit our results up to the first order in β.

In the dressed state basis of the atom-field subsystem, $i(c^\dagger\sigma_- - \sigma_+ c)|\pm\rangle_p = \pm|\pm\rangle_p$, and $(\sigma_+ c + c^\dagger\sigma_-)|\pm\rangle_p = \pm i|\mp\rangle_p$, where $|\pm\rangle_p = \frac{1}{\sqrt{2}}(|e\rangle_a|0\rangle_c \pm i|g\rangle_a|1\rangle_c)$. We define $\sigma_z^p = i(c^\dagger\sigma_- - \sigma_+ c)$ and $\sigma_y^p = \sigma_+ c + c^\dagger\sigma_- = -i\sigma_+^p + i\sigma_-^p$. The transformed Hamiltonian is then given by

$$\mathcal{H}_\mathcal{T} \approx \mathcal{H}_0 + \mathcal{H}_1, \tag{C.4}$$

where

$$\begin{aligned} \mathcal{H}_0 &= \hbar\omega_m b^\dagger b + \hbar g_c \sigma_z^p, \\ \mathcal{H}_1 &= \hbar\beta g_c(\sigma_-^p - \sigma_+^p)(b^\dagger - b). \end{aligned} \tag{C.5}$$

In the interaction picture of $\mathcal{H}_0$, the interaction Hamiltonian is given by

$$\begin{aligned} \mathcal{V}(t) &= e^{i\frac{\mathcal{H}_0}{\hbar}t}\mathcal{H}_1 e^{-i\frac{\mathcal{H}_0}{\hbar}t} \\ &= \hbar\beta g_c \left[\sigma_-^p b^\dagger e^{-i(2g_c - \omega_m)t} + \sigma_+^p b e^{i(2g_c - \omega_m)t}\right. \\ &\quad \left. -\sigma_-^p b^\dagger e^{-i(2g_c + \omega_m)t} - \sigma_+^p b e^{i(2g_c + \omega_m)t}\right]. \end{aligned} \tag{C.6}$$

To the first order in β, the unitary operator in the interaction picture is $U_\mathcal{V}(t) \approx 1 - \frac{i}{\hbar}\int_0^t \mathcal{V}(\tau)d\tau$. According to Ref. [67], the unitary operator in the Schrödinger picture is given by $U_\mathcal{T}(t) = e^{-i\frac{\mathcal{H}_0}{\hbar}t}U_\mathcal{V}(t)$. By transforming back with $\mathcal{T}$, the unitary operator including the effect of the mechanical mirror is represented by

$$U_I(t) = \mathcal{T}^\dagger e^{-i\frac{\mathcal{H}_0}{\hbar}t}U_\mathcal{V}(t)\mathcal{T}. \tag{C.7}$$

To see the effect of the mechanical mirror during the atom-field interaction, we consider first the unitary operator acting on the states $|e\rangle_a|0\rangle_c|0\rangle_m$ and $|g\rangle_a|1\rangle_c|0\rangle_m$. Up to the first order in β,

$$\begin{aligned} & U_I(\tau_{g_c})|e\rangle_a|0\rangle_c|0\rangle_m \\ \approx\ & |g\rangle_a|1\rangle_c|0\rangle_m + \epsilon_1|g\rangle_a|1\rangle_c|1\rangle_m + \epsilon_2|e\rangle_a|0\rangle_c|1\rangle_m \\ \approx\ & \mathcal{D}(\epsilon_1)|g\rangle_a|1\rangle_c|0\rangle_m + \epsilon_2|e\rangle_a|0\rangle_c|1\rangle_m, \end{aligned} \tag{C.8}$$

and

$$\begin{aligned} & U_I(\tau_{g_c})|g\rangle_a|1\rangle_c|0\rangle_m \\ \approx\ & -|e\rangle_a|0\rangle_c|0\rangle_m + \epsilon_1^* e^{-i\omega_m\tau_{g_c}}|e\rangle_a|0\rangle_c|1\rangle_m \\ & -\epsilon_2|g\rangle_a|1\rangle_c|1\rangle_m \\ \approx\ & -\mathcal{D}(-\epsilon_1^* e^{-i\omega_m\tau_{g_c}})|e\rangle_a|0\rangle_c|0\rangle_m - \epsilon_2|g\rangle_a|1\rangle_c|1\rangle_m, \end{aligned} \tag{C.9}$$

where $\tau_{g_c} = \pi/(2g_c)$, $\epsilon_1 = \frac{2g_c^2(1-e^{-i\omega_m\tau_{g_c}})-\omega_m^2}{4g_c^2-\omega_m^2}\beta$ and $\epsilon_2 = i\frac{g_c\omega_m}{4g_c^2-\omega_m^2}(1+e^{-i\omega_m\tau_{g_c}})\beta$. For $g_c \gg \omega_m$, we have $\epsilon_i/\beta \ll 1$ and the interaction $U_I(\tau_{g_c}) \approx U_\pi$.

Next we consider the same procedures as described in the paper to obtain a macroscopic superposition state. We replace the unitary operator U_π with $U_I(\tau_{g_c})$ and vary the field-mirror interaction time. After $2N$ repetitions of the prescribed interactions, the state of the system is given by

$$\begin{aligned} |\bar{\psi}_s^{2N}\rangle \ =\ & \left(\prod_{n=1}^{2N} U_I(\tau_{g_c})U_{fm}(\tau')U_I(\tau_{g_c})R_\pi\right) \\ & \times\big(U_I(\tau_{g_c})U_{fm}(\tau')U_I(\tau_{g_c})\big)|\psi_s^0\rangle. \end{aligned} \tag{C.10}$$

We set $\tau' = \frac{\pi}{\omega_m} - 2\tau_{g_c}$ to balance the effect due to the mechanical mirror during the atom-field-mirror interaction. Using Eqs. (C.8), (C.9) and the field-mirror interaction unitary operator, we obtain the state of the system as

$$|\bar{\psi}_s^{2N}\rangle \approx \frac{1}{\sqrt{2}}|0\rangle_c\Big(|g\rangle_a|2N\beta'\rangle_m - |e\rangle_a|-2N\beta'\rangle_m\Big), \tag{C.11}$$

where $\beta' = \beta(1 - e^{-i\omega_m\tau_{g_c}}) + \beta\frac{4g_c^2(1+\cos(\omega_m\tau_{g_c}))}{4g_c^2-\omega_m^2}$ and we neglect the phase shift term $N\theta$ for simplicity. The generated state $|\bar{\psi}_s^{2N}\rangle$ under the full Hamiltonian description is similar to that of the target state $|\psi_s^{2N}\rangle$ obtained in the paper, except for different coherent states of the mirror. As can be seen from the expression of $|\bar{\psi}_s^{2N}\rangle$, it approaches to $|\psi_s^{2N}\rangle$ in the limit of $g_c/\omega_m \gg 1$, which verifies the approximation we made in the paper. For a quantitative estimation, we calculate the fidelity F_{s1} between the target state $|\psi_s^{2N}\rangle$ and the state $|\bar{\psi}_s^{2N}\rangle$ given by

$$F_{s1} = |\langle\psi_s^{2N}||\bar{\psi}_s^{2N}\rangle|^2 \approx e^{-4N^2|\beta-\beta'|^2}. \tag{C.12}$$

C.2 Error analysis on accurate timing control

Here we study in the following the fidelity of the generated state of the system under variations of the interaction time with respect to the target state $|\psi_s^{2N}\rangle$ generated with the prescribed interaction time. In the paper, we considered the atom-field interaction time $\tau_{g_c} = \pi/(2g_c)$ and the field-mirror interaction time $\tau = \pi/\omega_m$ to obtain a macroscopic superposition state. Since the timing in each step may not be accurately controlled, the generated state is affected. For the time scale $\tau_{g_c} \ll \tau$, we consider only variations of the atom-field interaction time τ_{g_c} for simplicity. After

$2N$ steps of the prescribed interactions, the state of the system is given by

$$\begin{aligned} |\bar{\bar{\psi}}_s^{2N}\rangle &= \left(\prod_{n=2}^{2N} U_{af}(\tau_{2n})U_{fm}(\tau)U_{af}(\tau_{2n-1})R_\pi\right) \\ &\quad \times U_{af}(\tau_2)U_{fm}(\tau)U_{af}(\tau_1)|\psi_s^0\rangle, \end{aligned} \tag{C.13}$$

where τ_k is the kth atom-field interaction time. According to Ref. [67], the unitary operator $U_{af}(\tau_k)$ is given by

$$\begin{aligned} U_{af}(\tau_k) &= \cos(g_c\tau_k\sqrt{cc^\dagger})(|g\rangle\langle g|)_a + \cos(g_c\tau_k\sqrt{c^\dagger c})(|e\rangle\langle e|)_a \\ &\quad + \frac{\sin(g_c\tau_k\sqrt{c^\dagger c})}{\sqrt{c^\dagger c}}c^\dagger\sigma_- - \frac{\sin(g_c\tau_k\sqrt{cc^\dagger})}{\sqrt{cc^\dagger}}c\sigma_+. \end{aligned} \tag{C.14}$$

For $g_c\tau_k = \frac{\pi}{2}$, the operation is given by $U_{af}(\tau_k) = U_\pi$ which flips the atom-field state as $U_\pi|e\rangle_a|0\rangle_c = |g\rangle_a|1\rangle_c$ and $U_\pi|g\rangle_a|1\rangle_c = -|e\rangle_a|0\rangle_c$. Here we consider $g_c\tau_k \approx \frac{\pi}{2}$ and keep up to the leading order term $\sin(g_c\tau_k)$. By carrying out the operations on $|\psi_s^0\rangle$ explicitly, we obtain

$$\begin{aligned} |\bar{\bar{\psi}}_s^{2N}\rangle &\approx -C_1\frac{e^{iN\theta}}{\sqrt{2}}|0\rangle_c|e\rangle_a|2N\beta\rangle_m \\ &\quad + C_2\frac{e^{iN\theta}}{\sqrt{2}}|0\rangle_c|g\rangle_a|-2N\beta\rangle_m, \end{aligned} \tag{C.15}$$

where $C_i = \prod_{k=0}^{N-1}\sin(g_c\tau_{4k+2i-1})\sin(g_c\tau_{4k+2i})$. Therefore, the fidelity is represented by

$$F_{s2} = |\langle\psi_s^{2N}||\bar{\bar{\psi}}_s^{2N}\rangle|^2 \approx \frac{1}{2}(C_1 + C_2). \tag{C.16}$$

The expression of fidelity F_{s2} relates to the accuracy of timing control and the number of steps one needs to perform. Therefore, to retain a high fidelity, accurate timing

control is required to some extent to balance a large number of steps.

C.3 Reversing the effect of the cavity field decay via weak measurements

We now analyze how to probabilistically reverse the effect of the cavity decay on the generation of macroscopic superposition via weak measurements. If the cavity field is continuously monitored by an ideal photon detector outside the cavity and no click event is recorded, the decay of a cavity photon results in a decrease of the amplitude in the state associated with the single photon. This is a null-result measurement and the effect of the cavity decay can be reversed probabilistically by flipping the photonic state [77].

Starting with $|\psi_s^0\rangle$, we first map the atomic superposition state to the photonic state and the effect of the cavity decay can be neglected for $\kappa\tau_{g_c} \ll 1$. During the field-mirror evolution time τ, the state $\frac{1}{\sqrt{2}}(|0\rangle_c + |1\rangle_c)|g\rangle_a|0\rangle_m$ evolves according to U_{fm} as well as the cavity decay. After interaction time τ, the state remains to be a pure state with reduced amplitude as $\frac{1}{\sqrt{2}}(|0\rangle_c|0\rangle_m + e^{i\theta}e^{-\kappa\tau/2}|1\rangle_c|2\beta\rangle_m)|g\rangle_a$ with a probability of $(1+e^{-\kappa\tau})/2$. Now we map the photonic state to the atomic state and the state of the system is then given by

$$\frac{1}{\sqrt{2}}|0\rangle_c\left(|g\rangle_a|0\rangle_m - e^{i\theta}e^{-\kappa\tau/2}|e\rangle_a|2\beta\rangle_m\right). \tag{C.17}$$

Now performing the procedure the second time, the state of the system is given by

$$\frac{1}{\sqrt{2}}e^{i\theta}e^{-\kappa\tau/2}|0\rangle_c\left(-|e\rangle_a|2\beta\rangle_m + |g\rangle_a| - 2\beta\rangle_m\right), \tag{C.18}$$

for another null-result measurement with a probability $\frac{2e^{-\kappa\tau}}{1+e^{-\kappa\tau}}$. Therefore, the probability to obtain the state (C.18) in the two steps is then $e^{-\kappa\tau}$. The state of the system is protected from the cavity decay probabilistically for even number of procedures

in such a way that both superposed states of the mirror is alternatively entangled with the single photon. After $2N$ repetitions, the target state $|\psi_s^{2N}\rangle$ can be generated faithfully with a probability of $e^{-N\kappa\tau}$. This can be realized by repeating the experiment many times.

APPENDIX D

LIST OF PUBLICATIONS

[1] Sabine Wolk, **Wenchao Ge**, and M. Suhail Zubairy, "Phase measurement with classical light", Phys. Rev. A **86**, 053833 (2012).

[2] **Wenchao Ge**, P. R. Hemmer, and M. Suhail Zubairy, "Quantum lithography with classical light", Phys. Rev. A **87**, 023818 (2013).

*[3] **Wenchao Ge**, M. Al-Amri, Hyunchul Nha, and M. Suhail Zubairy, "Entanglement of movable mirrors in a correlated-emission laser", Phys. Rev. A **88**, 022338 (2013).

*[4] **Wenchao Ge**, M. Al-Amri, Hyunchul Nha, and M. Suhail Zubairy, "Entanglement of movable mirrors in a correlated-emission laser via cascade-driven coherence", Phys. Rev. A **88**, 052301 (2013).

*[5] **Wenchao Ge** and M. Suhail Zubairy, "Macroscopic optomechanical superposition via periodic qubit flipping", Phys. Rev. A **91**, 013842 (2015).

*[6] **Wenchao Ge** and M. Suhail Zubairy, "Entanglement of two movable mirrors with a single photon superposition state", Phys. Scr. 90, 074015 (2015).

[7] Longfei Fan, **Wenchao Ge**, Hyunchul Nha, and M. Suhail Zubairy, "Tradeoff between information gain and fidelity under weak measurements", Phys. Rev. A 92, 022114 (2015).

[8] **Wenchao Ge**, Mehmet Emre Tasgin, and M. Suhail Zubairy, "Conservation of nonclassicality and entanglement of Gaussian states in a beam splitter", submitted.

*These journal publications are reproduced extensively in this dissertation.